MEDICAL ULTRASONICS: DYNAMIC FOCUSING IN DIAGNOSTIC IMAGING

by

DAVID W. PYE, B.Sc.

DOCTOR OF PHILOSOPHY
UNIVERSITY OF EDINBURGH
1983

DEDICATION

TO

MY WIFE
FRANCES

AND

MY FATHER & MOTHER
WILLIAM & DOROTHY PYE

QUOTATION

"...And make the sound a picture of the sense."

Christopher Pitt (1699-1748)
Translation of Yida's Art of Poetry

ABSTRACT

The design and implementation of an ultrasonic dynamic focusing annular array system is described. The array is designed for use as a contact transducer and for eventual incorporation into the head of a real-time mechanical scanner.

A solution for the continuous wave field of a focused thin ring array is used to examine the effects of the number of rings, ring arrangement and apodisation of the array aperture on its focal plane response. Other aspects of array design are also considered. A suitable method of array fabrication, based on printed circuit board techniques, is described.

The design and implementation of an electronic system for the generation, detection and processing of the array signals is given. Digital techniques are used to implement the dynamic delays.

The dynamic focusing capabilities of the array are confirmed experimentally. Dynamic focusing of the reception response of the array is usually combined with a fixed focus on transmission. The compromise of fixed focusing on transmission may be overcome by applying the idea of Synthetic Aperture Imaging. An effective dynamic focus is then achieved on both transmission and reception. This novel application to annular arrays is investigated experimentally, and significant advantages are confirmed, however, at the expense of a lower pulse repetition frequency.

CONTENTS

Page

Chapter 1

DYNAMIC FOCUSING: AN INTRODUCTION

A bat emits short pulses of high frequency sound and uses the reflections of these from surrounding objects to guide its path. Man uses a similar technique, SONAR (SOund NAvigation and Ranging), to detect and locate under-water objects. On a smaller scale in Non-Destructive Testing, flaws and irregularities in metalwork may be found. In Man himself, ultrasound is used as a diagnostic tool to image the internal structures of the body.

1.1 Introduction

Meire and Farrant (1982) in their text on the clinical usage of ultrasound, briefly trace its history since the discovery that sound waves above the audible exist. McDicken (1981) describes modern ultrasonic instrumentation from the users point of view and lists its advantages and attractions in a text on "Principals and Use of Instruments". The physical and technical aspects of diagnostic ultrasonics are well covered in texts by Wells (1977) and Woodcock (1979).

1.2 Present Status of Diagnostic Ultrasonic Instrumentation

Since its inception, diagnostic ultrasonic imaging has developed considerably, aided primarily by the parallel development of modern electronic and associated devices. Exceptionally, one area has been relatively neglected until recently, the ultrasonic transducer. It is ultimately the quality of the ultrasound beam itself, used to interrogate the interior of the body which determines the quality of the image produced.

Improvement in beam shape is achieved by manipulation of the transducer aperture and the signals associated with it. The first

attempts to improve beam quality involved the use of acoustic lenses or bowl shaped transducers. These focus the ultrasound beam at a particular depth. Compared to the unfocused beam, the focused beam produces better images, but only over a limited range about the focus. Outside this range the beam is of poorer quality than the original unfocused beam (figure 1.1). (Note: figures and tables will normally be found on the page succeeding that on which reference is made to them). The problem of achieving a suitable compromise has been addressed by Kossoff (1963).

Ideally, a focused response is sought at all depths within the image. The development of "Axicon" devices, which produce a line focus in place of a point focus, has been one approach, Burckhardt et al.(1975), Patterson and Foster (1978). A second approach has been to have a "moveable" focus which can be made to track the point from which echoes are returning at a given moment. This technique is variously referred to as "Dynamic", "Swept" or "Electronic" Focusing.

1.3 Dynamic Focusing

Consider a plane arbitrarily shaped transducer receiving echoes from a depth z_1 (figure 1.2). Echoes returning to the central region of the transducer arrive before those to the outer areas because of their shorter path. They may arrive out of phase thereby reducing their combined output from the transducer. If an acoustic lens is introduced, signals arriving at the centre may be delayed relative to those to the outer edge if the lens is chosen to have a lower acoustic velocity than the surrounding medium, (figure 1.3). Echoes returning from a particular depth z_f, will now arrive at the transducer face in phase if the lens is appropriately shaped.

A similar effect may be achieved using electronic delays if the

Figure 1.1: Beam-shape of an ultrasonic transducer (schematic).

(a) unfocused

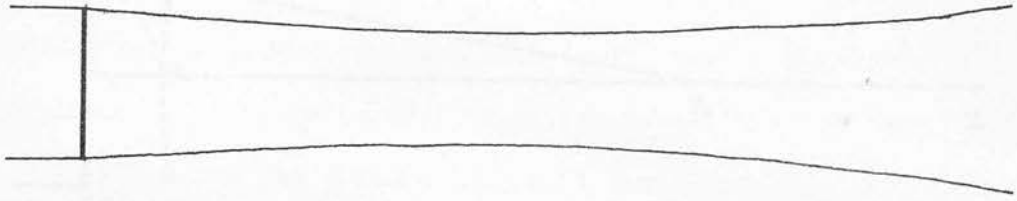

(b) focused

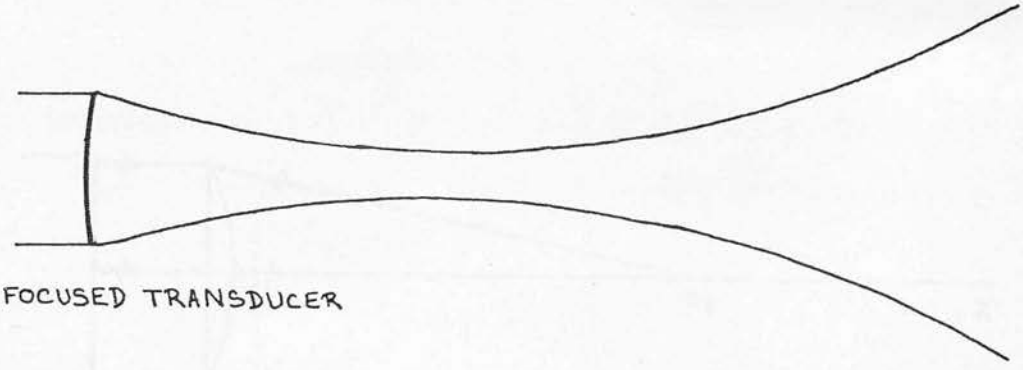

Figure 1.2: Echoes received from an on-axis point by a plane transducer

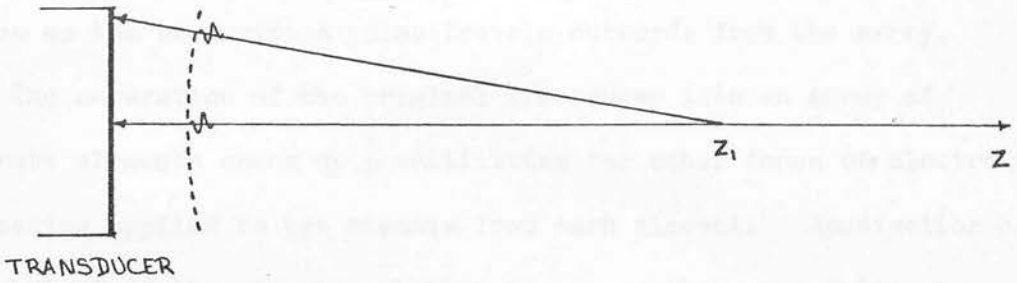

Figure 1.3: Echoes received via a lens, from its focus

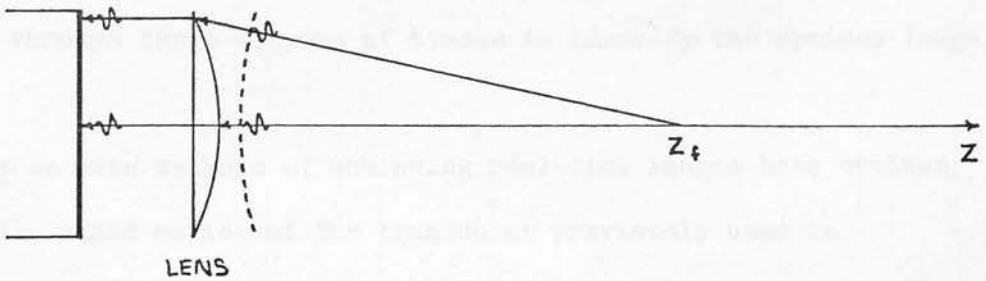

transducer is split into isolated regions, see figure 1.4. The path difference to each element of the transducer array is a function of depth and so of time. The replacement of the fixed delays in figure 1.4 by time variable delays enables compensation for path difference at all depths. This technique enables a focused response to be maintained throughout the range of interest. The focal point tracks the returning echoes as the transmitted pulse travels outwards from the array.

The separation of the original transducer into an array of separate elements opens up possibilities for other forms of electronic processing applied to the signals from each element. Apodisation or "weighting" of the signals relative to one another or non-linear amplification are two such possibilities.

1.4 Real-time Imaging

Early imaging techniques required the transducer to be scanned manually across the surface of the body. The resulting image was static. Rapidly moving tissue within the image area introduced artifacts. In order to adequately observe tissue motion, for example in the heart, an image must be produced approximately 30 or more times per second. An equally important aspect of real-time imaging is the ability to rapidly search through large volumes of tissue to identify the optimum image plane.

Three main methods of achieving real-time images have evolved:

(1) rapid motion of the transducer previously used in static image production by a suitably driven mechanical device - mechanical real-time scanner;

(2) an array of small transducers, operating in parallel, each creating a separate line in the image - linear array scanner;

Figure 1.4: Focusing using an array and delay lines

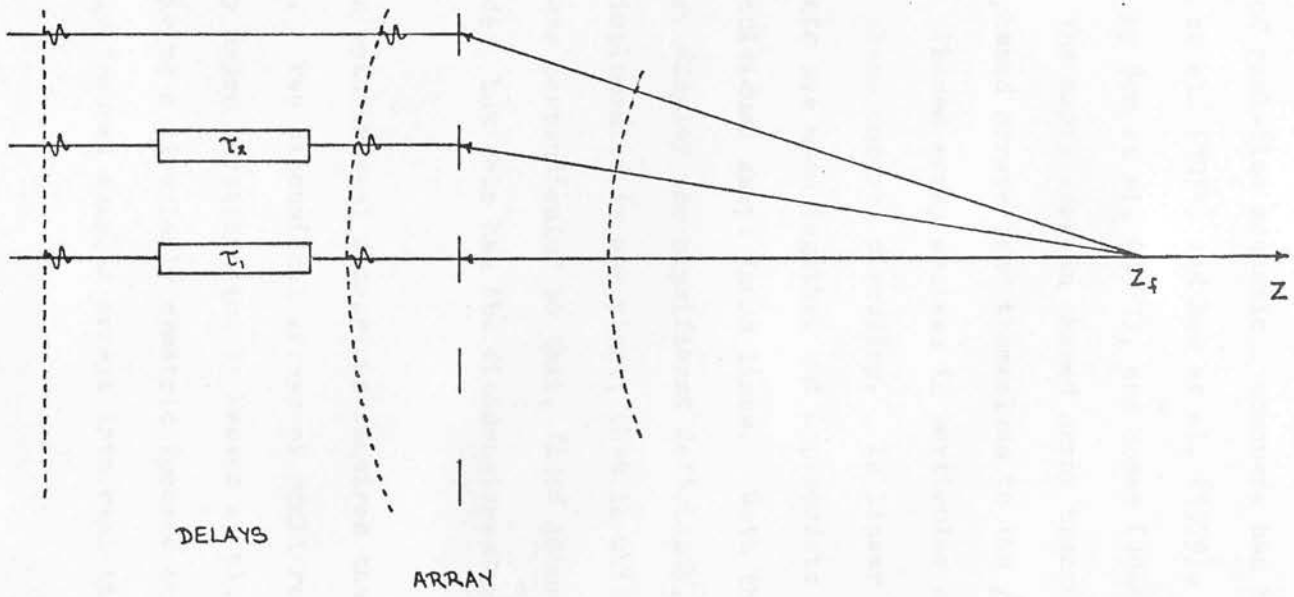

(3) an array of a few small transducers, the signals from which are variably phased relative to one another to steer the beam through a sector of tissue - phased array scanner.

The development of real-time mechanical scanners has been described by McDicken et al. (1974) and Bow et al. (1979). Linear arrays were pioneered by Bom et al. (1971), and Somer (1968) is credited with much of the early work on phased array transducers.

Both linear and phased arrays lend themselves to the provision of dynamic focusing. Phased array systems in particular already contain the necessary phase control circuitry. In linear arrays, small groups of elements are used together and appropriate delays added, to implement individual swept focus lines. Both these types of transducer, however, display one significant deficiency. Dynamic focusing can only be implemented in one plane, that in which the image lies. In a plane perpendicular to this, fixed geometrical focusing may be provided, but this has the disadvantages described in Section 1.2.

Swept focusing in both lateral dimensions requires the use of a two dimensional array. Two dimensional arrays of small rectangular elements are currently under investigation by Beaver et al. (1975). A simpler solution, giving a circularly symetric focused beam, is to incorporate dynamically focused annular arrays into real-time mechanical scanners.

1.5 Review of Annular Array Technology

The first description of an annular array dynamic focusing system is given in a British patent applied for by Brown and Haslett in 1959. The proposed system was for use in flaw detection in Non-Destructive Testing (NDT).

1.5.1 Array Design

Melton and Thurstone (1978) present a general procedure for the design of annular arrays as contact or water bath transducers. A specific design for a water bath transducer is given. Dietz et al. (1979) discuss the design of an "expanding aperture" array for use as a contact B-scan transducer.

The available literature to date, on the various aspects of annular array design is reviewed in the following paragraphs.

1.5.1.1 Number of Rings

Melton and Thurstone, and Hubelbank and Tretiak (1970), present computer simulations on the effects of the number of rings on focal response. 3 rings appear to produce a good response (Melton and Thurstone), with 5 rings producing a response similar to that of a completely filled aperture. Arrays of 5 - 15 rings are considered by Hubelbank and Tretiak, whose results suggest a similar conclusion.

Experimental systems of between 5 and 12 rings are reported by Dietz et al., Conner et al. (1975), Bernardi et al. (1976), Melton (1979) and Melton and Thurstone.

1.5.1.2 Ring Width

The effects of ring width have been considered by Dietz et al., Melton and Thurstone, and Conner et al. It is concluded that focusing should take place in the far-fields of the rings. Dietz et al. indicate the desirability of relatively large elements giving lower cross talk, less coupling of energy into radial modes of vibration and a higher signal-to-noise ratio.

1.5.1.3

Hubelbank and Tretiak, in their computer simulations, study two

different ring arrangements, equal spacing and "Fresnel" pattern spacing. The latter gives a narrower main lobe in the focal region, and is that generally adopted by other workers, Dietz et al., Melton and Thurstone, and Bernardi et al.

1.5.1.4 Apodisation

Dietz et al. (1978, 1979), report theoretical and experimental results. A weighting function tapered towards the outer edge of the array results in lower side lobe levels, but an increased beam width. Conversely, tapering the function towards the array centre may be used to improve resolution without grossly affecting side lobe levels.

Melton identifies a Gaussian function as the optimum of a series of functions tested on an experimental imaging system.

1.5.2 Signal Compression

The echo video signal is often compressed before being fed to a display. This helps to match the dynamic range of the signal to that of the display and prevents the "loss" of low level echoes. Unfortunately, it effectively raises side lobe levels and increases beam width. Ligtvoet et al. (1977) applied signal compression prior to the combination of signals from elements of a dynamic focusing linear array and found that this reduced the undesirable effects while maintaining the required compression. Melton and Thurstone found from beam simulations that side lobe levels are reduced and the resolution of low level reflectors close to high level ones is improved. Melton further investigated various compression ratios to find an optimum. Corl et al. (1978) and Dietz et al. (1979) also report the use of signal compression.

1.5.3 Resolution and Side Lobe Levels

Bernardi et al., Dietz et al. (1979) and Melton and Thurstone, all

report close to diffraction limited resolution over an extended depth obtained with experimental dynamic focusing systems.

Dietz et al. report side lobes between 20 and 40 dB below the main lobe depending on depth and apodisation.

1.6 Proposed Project

McDicken et al. (1974) describe a scanner which used a single crystal oscillating about a point on its front face to provide real-time sector scans. Bow et al. (1979) report the development of a mechanical real-time scanner for routine investigation of the heart. This scanner used four plane, unfocused transducers mounted around the circumference of a spinning "wheel", to obtain real-time images. Image quality was later improved in this system by the use of fixed focus transducers. The limitations of fixed focusing are discussed in Section 1.3. Deficiencies in the focusing action of other real-time scanners has been discussed in Section 1.4. The incorporation of dynamically focused annular array transducers into the head of a mechanical real-time scanner presented itself as a logical step towards further improvement of real-time image quality.

It was proposed that as a first step towards putting an annular array into a mechanical scanner a prototype system should be designed and built which could be used with a contact B-scanner. The annular array and associated electronics would replace the standard transducer and couple into the B-scanner at its scan converter input.

At the start of this project in 1977, the available literature on annular array technology was relatively sparse and generally oriented towards the design of water bath rather than hand held contact transducers. It was decided, therefore, that the project should follow both theoretical and experimental lines of investigation.

1.6.1 Theoretical Approach

This was to present a coherent investigation of the effects of all aspects of array design on the quality of the focused beam. The effects of parameters such as aperture size and frequency are well known. Those of number of rings, ring arrangement, ring width and apodisation are less well documented, even now, in the literature. This particularly applies to the former two.

1.6.2 Experimental Approach

The proposed prototype system was to be designed based on the available literature and early theoretical results. Such a system would allow an experimental assessment of the feasibility and focusing capabilities of contact annular array transducers. Confirmation of the theoretical results would be sought with a view to their application in future designs.

In general, an annular array system will be dynamically focused on reception and have a fixed point or line focus on transmission. Some means of extending the focus on transmission, as has been done on reception, is desirable.

1.6.2.1 Synthetic Aperture Imaging

Synthetic aperture imaging is a technique whereby each region of an aperture is sampled independently and successively, often by a single transducer. The echo information from each region is stored and then suitably combined to form the final image after the complete aperture has been sampled. In this way a large aperture is synthesised yielding higher resolution than would be possible with the small sampling transducer alone. The following description is given by Lancée and Bom (1977).

> "Practically all developments in the medical ultrasound area are induced by preceding investigations in either Sonar, Radar or NDT techniques. One of such techniques is the synthetic aperture system (SAS) used in airborne Radar applications.....SAS enables high resolution mapping of areas. Instead of a lateral trajectory of one antenna accomplished by motion a similar effect can be obtained by using a linear array. By subsequent scanning from each position within the array and storage of the echo signals in a fast memory, high resolution imaging can be achieved. In this way parallel processing at many elements in a large aperture is replaced by repeated processing of one element followed by fast combinational scanning of the memory content. The development of such techniques may provide a new powerful diagnostic instrument to the medical profession."

Corl et al. describe the technique applied to an NDT system. Individual elements of a linear array are used to scan the aperture.

The techniques may also be implemented with an annular array system. Successive annuli are pulsed on successive transmit-receive cycles until an echo line has been received and stored from each element of the array. Compensation is then possible for the varying echo path lengths to each element on both transmission and reception. The array is effectively dynamically focused on both transmission and reception.

Unlike linear array synthetic aperture systems, in which the final image is similar in width to the length of the array, a synthetic aperture annular array system must still be scanned mechanically across the region of interest to achieve a two dimensional image.

Earlier remarks (Section 1.4) on the limited resolution of linear arrays in one lateral dimension also apply here.

The application of the synthetic aperture concept to annular array technology is considered to be a novel idea. It was, therefore, proposed to investigate the possibilities of synthetic aperture annular array imaging as a further part of the investigations intended with the prototype dynamic focusing system. The modifications required to

perform this further investigation were minimal (Section 4.2.1).

1.7 Format of Thesis

The main body of the thesis consists of four chapters. Chapter 2 reviews the acoustic theory used in the development of computer beam-simulation programs. These are described and results from them used to analyse the effects of number of rings, ring arrangement and apodisation of the array. The following chapter covers other aspects of array design and the actual fabrication techniques developed. Chapter 4 describes the design and construction of the associated dynamic focusing electronics. Chapter 5 presents experimental results obtained using the prototype system. The experimental and theoretical performance of the array are compared. Pulse-echo beam plots and phantom images are presented and discussed. The final chapter summarises conclusions drawn from the results of both theoretical and experimental approaches. Further development of the system is considered.

Chapter 2

THEORETICAL ANALYSIS OF THE ULTRASONIC FIELD

Theoretical analysis offers a means of prediction and explanation of experimental observations.

2.1 Introduction

In ultrasonic imaging theoretical analysis can identify the sources of features of the ultrasonic field; these may or may not be desirable and may be inherent in the design or simply a result of manufacturing errors. Theory may also be used to predict the field shapes of designs not yet put into practice. Design parameters may be varied to optimise the desirable features and minimise the undesirable. In this way the costly production of a large number of prototypes to investigate the effects of varying a given parameter is eliminated. Artifacts introduced by manufacturing variations and indistinguishable from the real effects of variations in the parameter of interest are also obviated.

It is difficult to take into account all possible influences on the ultrasonic field which may occur in real life. It is not so difficult to produce a simplified model which does not try to take account of all influences, but which will still produce a useful result. Such an approximate model has been used, with the aim of:

(1) attaining a better understanding of the way in which the transducer affects the beam shape;

(2) having a flexible, economical method of transducer design.

In pursuing the second of these aims it has been necessary to develop a series of computer programs to solve the equations which define the beam shape for a given transducer. The output of these programs is

subject to various approximations and limitations and is, therefore, not readily comparable to, for example, pulse-echo beam plots derived experimentally. However, it is sufficiently realistic to allow intercomparison of the theoretical plots for different transducers with the knowledge that the optimum from these will represent the optimum transducer design in practice. The results which will be presented are intended for intercomparison as an aid to design rather than quantitative prediction of experimental results. Experimental verification of the theory used is available in the literature, see Section 2.4.1.2. Qualitative comparison of theoretical and experimental results is performed in Section 5.5, as a confirmation of the reasonable use of the theory.

2.2 Format of Chapter

The theory of sonic fields is well documented in the literature. By way of introduction a brief review of the relevant publications will be given. As the derivation of the basic equations governing sound propagation is given in a number of publications it will not be repeated here. Only the results and conditions on them will be quoted, with the appropriate references.

The program suite and the facilities it offers will be introduced. Use has been made of both continuous wave (CW) and pulsed wave (PW) theories, although the majority of imaging transducers operate in pulsed mode. The reasons for using CW theory are explained in Section 2.5. The results presented in this chapter are those derived for CW fields. The PW results are presented along with the experimental pulse-echo results in Chapter 5. Because it has proved useful to use results derived for CW fields, careful consideration is given to their applicability to pulsed fields.

2.3 Review of Acoustic Theory

Radiation from plane piston radiators and the propagation of acoustic waves in lossless homogeneous media have been widely discussed in the literature on theoretical acoustics and scalar diffraction theory. (Kinsler and Frey (1962), Morse and Ingard (1968), Strutt Lord Rayleigh (1945)). With the increasing use of ultrasound in recent years, in a number of technological disciplines, there has been renewed interest in the solution of related theoretical problems. The general solution for the radiation propagated from radiators of arbitrary shape has been known for many years, see Rayleigh's treatise on sound, published in 1896. These general solutions have been in the form of integral equations for which no closed form analytic solutions could be found. Approximate methods have been used to obtain solutions for specific cases under limited conditions and have yielded useful insights. It was not until recently, with the advent of high speed digital computers, that it has been possible to obtain exact solutions for a large variety of cases, numerically.

The radiation pattern produced by a given form of radiator is a problem in Scalar Diffraction Theory and is usually approached via Green's equation (Goodman 1968). Green's equation is solved for a particular Green's function which conforms to the boundary conditions set by the radiator configuration and surrounding medium (Archer-Hall and Gee 1980). The solution used here is one commonly found in the literature and uses a Green's function corresponding to a plane rigid piston situated in an infinite rigid planar baffle. The piston is assumed to radiate into a semi-infinite lossless homogeneous medium to one side of the baffle. Other Green's functions have been identified (Archer-Hall and Gee) corresponding to different boundary conditions. The Green's function most

closely corresponding to an actual ultrasonic transducer used for medical diagnosis is a subject for some discussion. However, the three solutions arrived at by Archer-Hall and Gee, of which one corresponds to the one used here, all converge to similar values beyond the penultimate axial maximum of a plane circular piston transducer. Only the near-fields differ, the closer to the transducer the more dramatic the difference. However, as will be seen later, it is only beyond or just prior to, the near-field/far-field transition distance, which is of interest when considering individual rings of an annular array, and so any of the solutions may be used.

2.4 Transient and Stationary Fields of a Plane Piston Radiator

Since detailed discussions of the derivation of both transient (PW) and stationary (CW) responses of plane piston radiators exist in the literature, they will not be repeated here. Derivations may be found in Kinsler and Frey (CW response) and Goodman (CW and PW response). Strutt, Lord Rayleigh (CW and PW response) published one of the original treatises on the theory of sound propagation in 1896. Excellent reviews of the literature have been published by Freedman (1970) and more recently by Harris (1981).

2.4.1 The Transient Field

The approach used to compute the transient response of a plane piston radiator follows that of Beaver (1974) who cites Rayleigh as the originator of this solution. Beaver solves the integral equation representing the transient response numerically in the time domain. The time domain approach is simpler to interpret physically, although possibly slower to compute, than others which utilise a frequency domain approach where the power and speed of numerical Fast Fourier Transform algorithms may be implemented.

The transient pressure in the sonic field of a plane piston radiator in an infinite planar baffle, radiating into a lossless isotropic medium is given by:

$$\frac{p}{c\rho_o} = \left[\int_o^{\tau_p} \frac{\theta(\eta)}{2\pi} \cdot \frac{\partial v_n(\eta)}{\partial \eta} \cdot d\eta\right]_{\text{PISTON SURFACE}} \qquad ---2.1$$

where p is pressure
c is velocity of sound propagation in the medium
ρ_o is equilibrium density of the medium
v_n is normal velocity of the piston surface
τ_p is length of the excitation pulse
η is "departure time" = t - r/c
t is time measured from some arbitrary zero

It is understood that the integral covers only elements on the piston surface for which $o < \eta < \tau_p$. A suitable choice of co-ordinate system has allowed the two dimensional surface integral derived by Rayleigh to be expressed as a one dimensional integral over the departure time, η . The co-ordinate system used is illustrated in figure 2.1.

The field point P_c, has co-ordinates z, along the axis and x, off the axis (the system is circularly symetric) and the distance between it and a general point P_b, on the piston surface is r. $\theta(\eta)$ is the angle subtended by the edges of the piston at the foot of the perpendicular P_a, from the field point P_c, to the plane of the piston, for a particular r. The arc so defined represents an arc of equal phase for the wave arriving at P_c.

A numerical algorithm has been used to compute the exact solution for the quantity $\frac{p}{c\rho_o}$ as a function of t, x and z. In future, "pressure" or "relative pressure" will be used to refer to the quantity $\frac{p}{c\rho_o}$ for transient radiation.

Figure 2.1: Co-ordinate system used in Section 2.4.1.

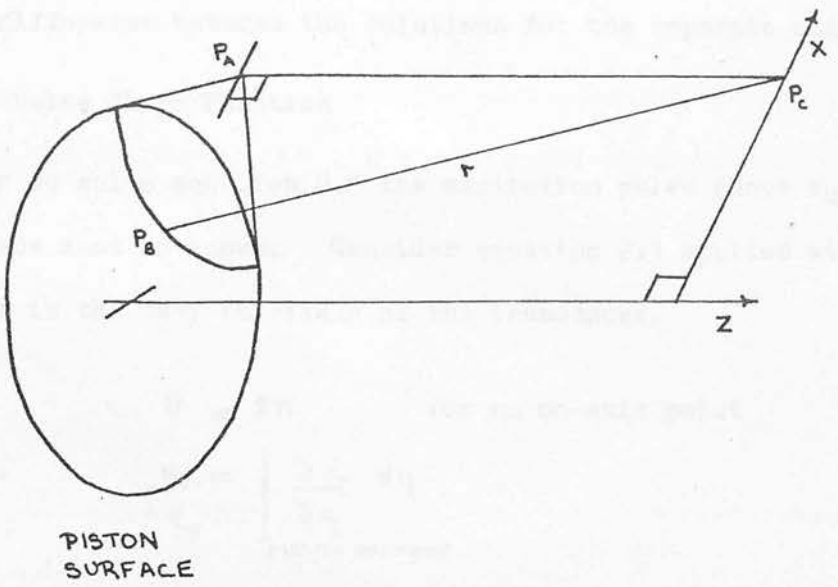

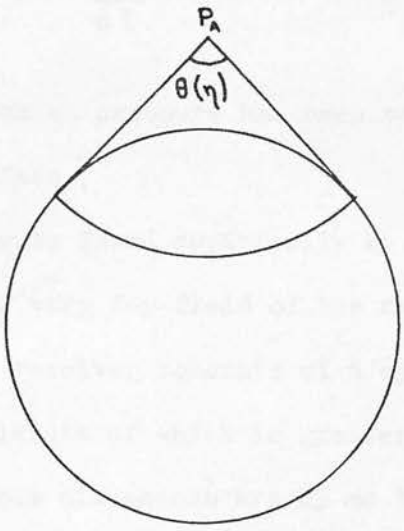

The aforementioned solution is for a plane disc radiator. The response for an annulus may be found using the Principle of Superposition. An annulus of radii a_1 and a_2, may be generated by removal from a disc of radius a_2, a concentric disc of radius a_1, the solution for the annulus is then the difference between the solutions for the separate discs.

2.4.1.1 The Pulse Shape Function

In order to solve equation 2.1 the excitation pulse shape v_n, at the transducer face must be known. Consider equation 2.1 applied at an on-axis point in the very far-field of the transducer.

$$\theta = 2\pi \qquad \text{for an on-axis point}$$

$$\therefore \quad \frac{p}{c\rho_0} = \int_{\text{PISTON SURFACE}} \frac{\partial v_n}{\partial \eta}\, d\eta$$

$$r \simeq z \qquad \text{for all points on the transducer face, from the far-field}$$

$$\therefore \quad \eta = t - \frac{z}{c}$$

$$\text{hence} \quad p(t) \propto \frac{d v_n}{d t}(t - z/c) \qquad \text{---2.2}$$

that is, the far-field axial pressure has been related to the normal velocity of the piston face.

The pressure p, may be found empirically by observing the transmitted pulse in the very far-field of the radiator using a "thick" crystal receiver. The receiver consists of a cylinder of piezo-electric material, the length of which is greater than that of the pulse in the crystal. Suitable dimensions are 25 mm long x 10 mm diameter. If a low impedance load (e.g. 47Ω) is connected across it, the voltage developed across this load is proportional to the incident pressure and represents a true replica of the impinging transmitted pulse (Foster and Hunt 1978). By recording this pulse shape and approximating to it by a

suitable mathematical function, an analytic description of p, and hence $\frac{\partial v_n}{\partial t}$ is obtained. An example of such a recording is given in figure 2.2(a). This was approximated mathematically by a 1.5 cycle sine wave with a 0.5 cycle sine envelope which is shown in figure 2.2(b). The tail of the pulse is partly because of poor matching of the cable impedance to the transmitting electronics and as such has been ignored. A closer fit using a more complex mathematical representation could be found. However, a more complex mathematical formula considerably increases the computation time, which is undesirable.

2.4.1.2 Assumptions and Limitations on Equation 2.1

Certain assumptions and limitations are associated with equation 2.1 and are summarised below.

(1) The validity of the equation is limited to those regions where the "obliquity factor" may be ignored (Arditi et al. 1981 p.39). In practice it is invalid closer to the radiator than a few wavelengths.

(2) Sound wave propagation is assumed to be linear and to occur in a non-attenuating isotropic medium. Only small amplitude oscillations fulfil the linearity condition. A suitable medium for observing the beam is water.

(3) The radiator surface acts as a piston, i.e. all points on it move in phase. In practice this is not strictly true, particularly where the piezo-electric crystal used to generate the sound waves is supported around its edges. Dekker et al. (1974) investigated theoretically the implications for the response of

Figure 2.2: Transmitted pulse shape from an ultrasonic transducer.

(a) observed

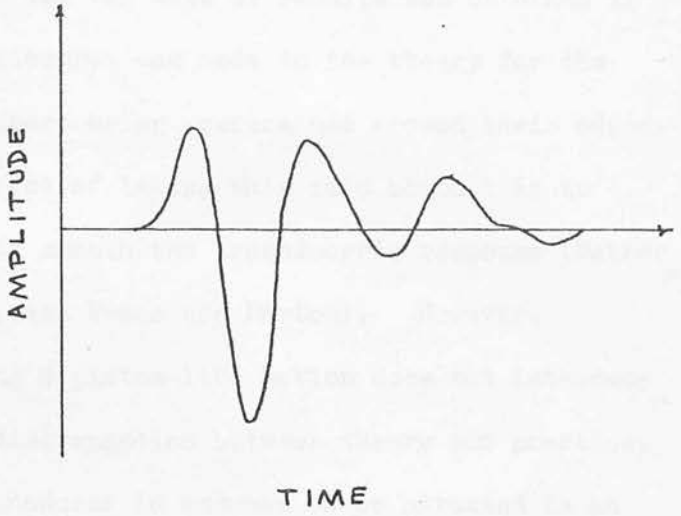

(b) analytic approximation (A_o.sin wt. sin wt/3).

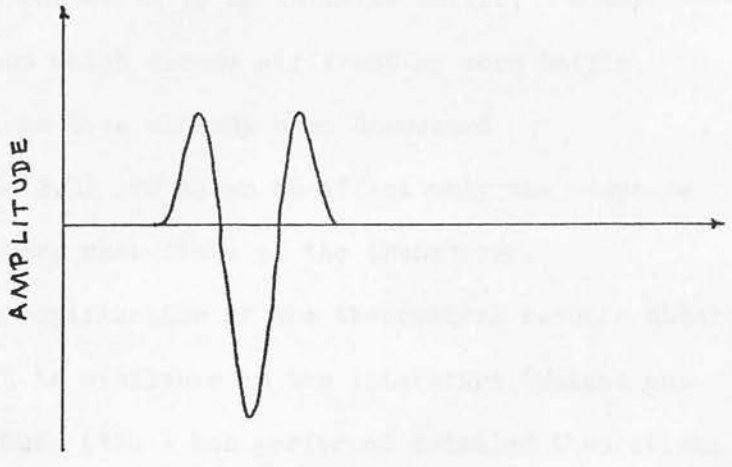

having the transducer edges bound. Evans and Parton (1981), while considering the fields of Doppler transducers both experimentally and theoretically, found that better correlation between the two sets of results was obtained if some allowance was made in the theory for the transducers being constrained around their edges. The effect of taking this into account is to slightly smooth the transducer's response (Dekker et al., and Evans and Parton). However, assuming a piston-like motion does not introduce gross discrepancies between theory and practice.

(4) The transducer is assumed to be situated in an infinite planar baffle. In the case of medical transducers this depends mainly on the extent of the casing in the plane of the transducer. Where this extends for a number of wavelengths, this approximates to an infinite baffle. Other solutions which assume different or zero baffle conditions have already been discussed (Section 2.3) and shown to affect only the response in the very near-field of the transducer.

Experimental verification of the theoretical results obtained using equation 2.1 is available in the literature (Weight and Hayman, 1978). Duck (1981) has performed detailed theoretical and experimental investigations on pulsed fields and has obtained close agreement between the two.

2.4.1.3 Pulse-Echo Response

Equation 2.1 represents the pressure at points in the sonic field of a particular radiator, i.e. it represents the transmission characteristics of a given transducer. A medical imaging ultrasonic transducer normally operates in pulse-echo mode where both transmission and reception responses influence the effective field shape. It is possible to relate the reception sensitivity of a radiator towards any given point in the reception field, to the relative amplitude of its transmission response at that point. If the reception response at a particular field point is defined as the relative response of the transducer to a spherical wave diverging from that point and with a pulse shape similar to that defined for use in computing the transmission field, then the reception and transmission fields will be identical. It might then be assumed that the pulse-echo response would be formed by a simple multiplication of the two responses. Unfortunately, this is only true for CW radiation. The transmitted pulse in a pulsed system is distorted by diffraction, particularly in the near-field. The wave scattered from a point reflector does not have the temporal shape of that transmitted. In general, the pulse-echo response of a transducer may not be found by squaring its transmission response. In particular regions of the pulsed field, such as in the region of a focus and in the very far-field, the pulse shape at a given point is similar to that transmitted. Squaring the transmission response will then yield a good approximation to the pulse-echo response.

In this work only one way processes have been considered, i.e. only separate transmission or reception responses, as the results have been intended mainly for intercomparison. An exception to this is Section 5.5 where theoretical and experimental results are compared.

2.4.2 The Stationary Field

Equation 2.1 may be solved for monochromatic radiation under limited conditions. Dietz et al. (1978) (who ascribe the result to Goodman) quote the following as the response of an infinitesimally narrow annulus in the far-field or at the focus, if the annulus is considered to be part of a focused system. Continuous wave excitation is assumed.

$$R(x,z,\lambda,r) = \frac{2\pi}{\lambda z} \cdot r \cdot \exp j\left[\frac{2\pi}{\lambda}\left(z - \frac{x^2}{2z}\right) - \frac{\pi}{\lambda}\right] \cdot J_0\left(\frac{2\pi x r}{\lambda z}\right) \quad \text{---2.3}$$

where $J_0(.)$ is the zero'th order Bessel function
x is off-axis distance
z is axial distance
λ is wavelength
r is the radius of the annulus
j is $\sqrt{-1}$

Similar limitations and assumptions apply to this result as to equation 2.1, Section 2.4.1.2, along with the additional ones given above. The above response is applicable in the focal plane of a focused radiator. A swept focus transducer is, ideally, always focused in the plane of interest during reception (Section 1.3). Its response throughout the reception field is a focal plane response. For further discussion of the reasons for using this expression and its applicability to pulsed wave fields see Section 2.5.

Writing

$$\frac{2\pi}{\lambda z} \cdot r = \omega \quad \text{---2.4}$$

and

$$\exp j\left[\frac{2\pi}{\lambda}\left(z - \frac{x^2}{2z}\right) - \frac{\pi}{\lambda}\right] = e^{j\phi} \quad \text{---2.5}$$

equation 2.3 can be expressed as

$$R_{ANNULUS} = \omega \cdot e^{j\phi} \cdot J_0\left(\frac{2\pi x r}{\lambda z}\right) \quad \text{---2.6}$$

$e^{j\phi}$ represents the phase of the wavefront, expressed as a complex number, at the point P(x,z). It is independent of r, and so the response of the array at P, may be found without reference to the relative phases of the contributions from each ring.

ω appears as a weighting or scaling factor on the off-axis response shape $J_0(.)$. The response for an array is given by the sum of the responses of the individual rings.

Hence:- $$R_{ARRAY} = \sum_{i=1}^{n} R_i$$

$$= e^{j\phi} \sum_{i=1}^{n} \omega_i \cdot J_0\left(\frac{2\pi x r_i}{\lambda z}\right) \quad ---2.7$$

where n is the total number of rings. Although ω has been defined as $\frac{2\pi}{\lambda z} r$, in practice it may be influenced electronically by the amplitude of excitation or receiver gain. Hence, it may be varied from one ring to another.

2.5 Comparison of Transient and Stationary Fields

Equation 2.1 represents the exact solution for the sonic field of a transiently excited transducer. Its solution may be performed numerically on a computer. A suite of programs to do this has been developed and is discussed in more detail in Section 2.6. Ideally, to obtain the optimum design of transducer the effects of varying its design parameters should be investigated as each is incremented. This was discovered to be impracticable with the programs described and the computer available, (a DEC PDP-12 Mini-Computer with 32K of core memory and a floating point processor) because of the time required to produce the data. One to four hours were required for a cross-sectional plot of the beam, midfield, of a four ring annular array. Hence, it was decided to make use of the solution for monochromatic radiation. This has the advantage, as described in Section 2.4.2, that an analytic solution

(equation 2.7) is available. The Bessel function part of the solution still requires evaluation by computer. However, a cross section using this method takes only seconds, compared to hours for the exact PW solution. Data from the analytic solution is fed into the program suite for display and analysis. The rest of this section is a comparison of CW and PW fields with a view to identifying the CW field features common to PW fields.

2.5.1 Direct and Edge Waves in Transient and Stationary Fields

CW or monochromatic excitation is a continuous sinusoidal wave (figure 2.3). Pulsed radiation is produced by shock excitation of the transducer giving a short burst of roughly sinusoidal oscillations with a smooth envelope (figure 2.4). Pulses may vary from approximately one to ten cycles in length. A pulse may be considered as a "temporally-apodised" version of the monochromatic radiation.

Schoch (1941) has identified two major components of the sonic field. The more recent article by Duck also discusses these features which are illustrated for a single cycle pulse at a particular time in figure 2.5. A hemi-toroidal (in three dimensions) wave is associated with the edge of the transducer and appears as the two semi-circular edge waves in the figure. It is inverted with respect to the plane wave which propagates as a geometrical projection of the source. Interference of the "edge" and "direct" waves results in maxima and minima. The CW field may be looked at in the same way, figure 2.6. However, the degree of interference between components is much greater because of their "infinite" temporal, and hence spatial, extent. The field of a focused radiator is built up in a similar manner. The direct wave is no longer plane but is a projection of the radiator, which converges onto and then diverges from, the focus. This is illustrated in figure 2.7.

Figure 2.3: Continuous sinusoid (monochromatic radiation).

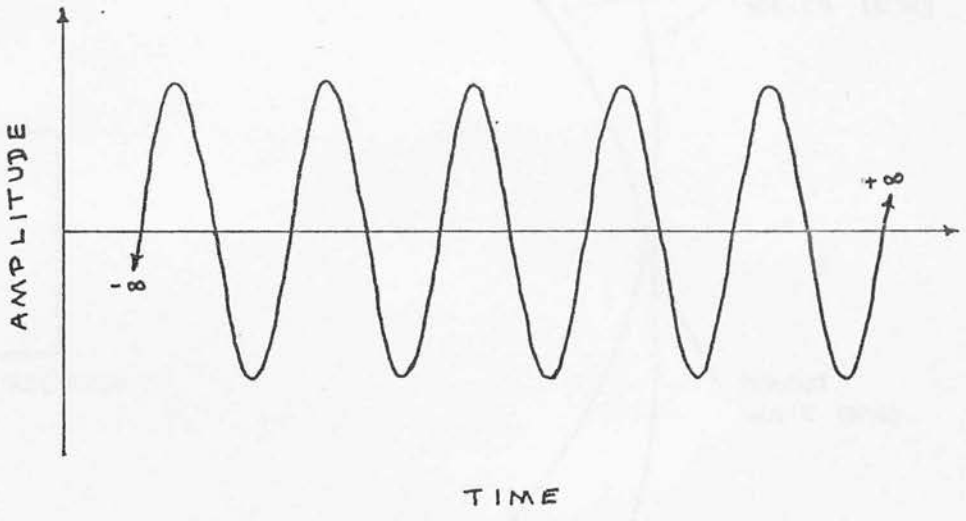

Figure 2.4: Short pulse (broad band radiation).

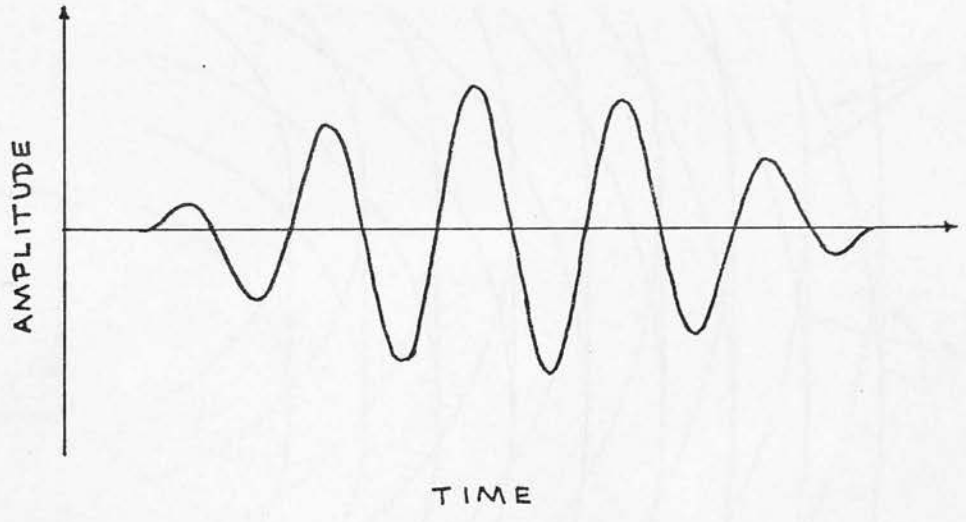

Figure 2.5: Direct and edge waves, single cycle pulsed radiation, plane radiator (note: the edge waves are generated in anti-phase with the direct wave).

Figure 2.6: As above, continuous wave radiation.

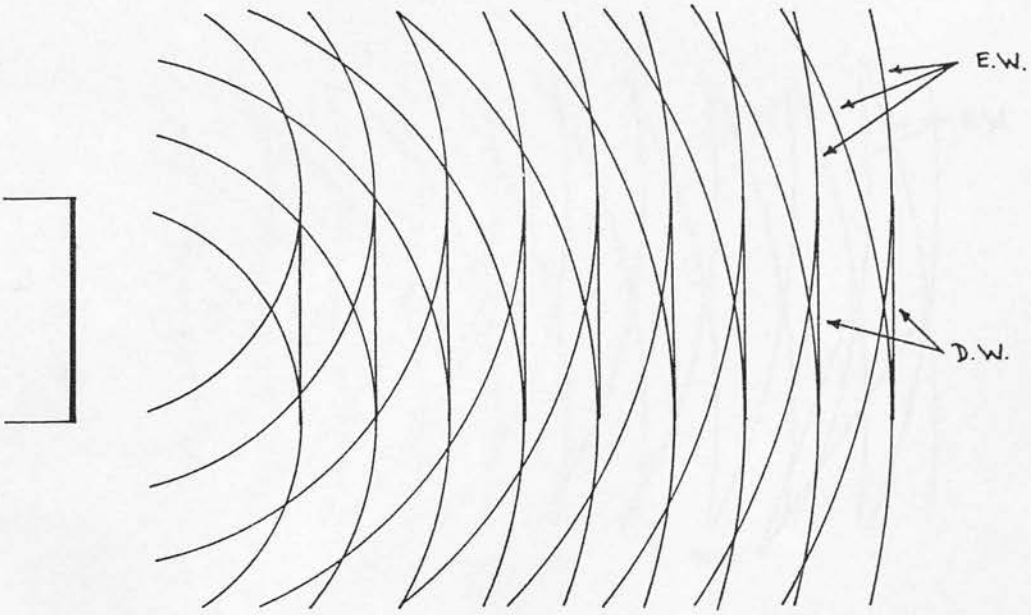

Figure 2.7: Direct and edge waves, focused radiator.

(a) single cycle pulsed radiation

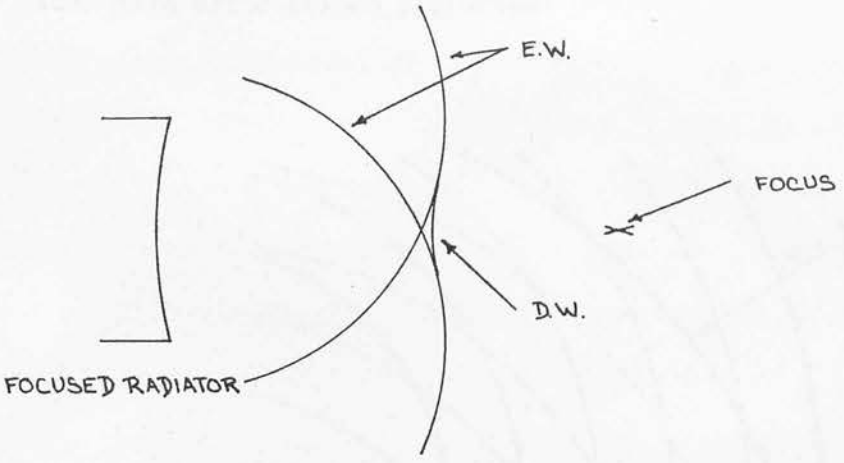

(b) continuous wave radiation

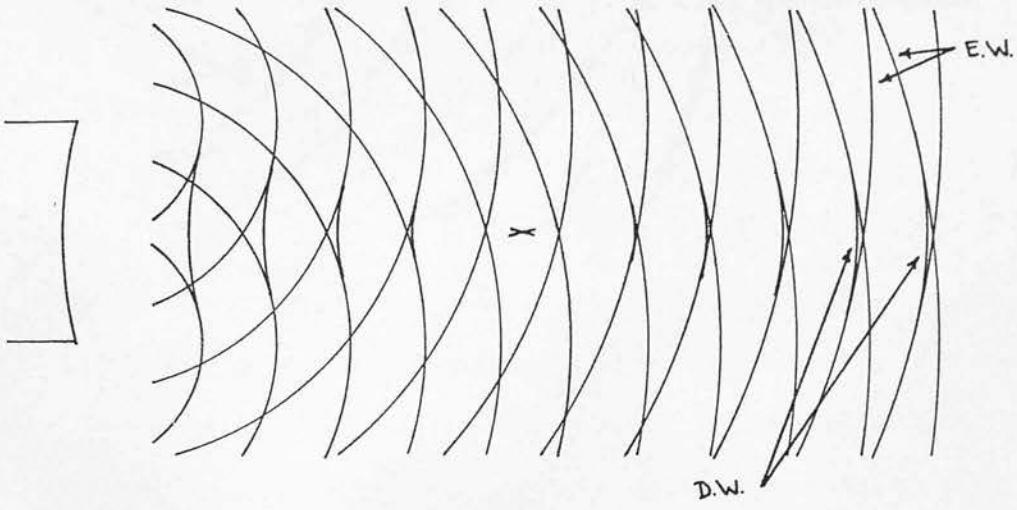

Figure 2.7: Direct and edge waves, focused radiator.

(c) five cycle pulsed radiation

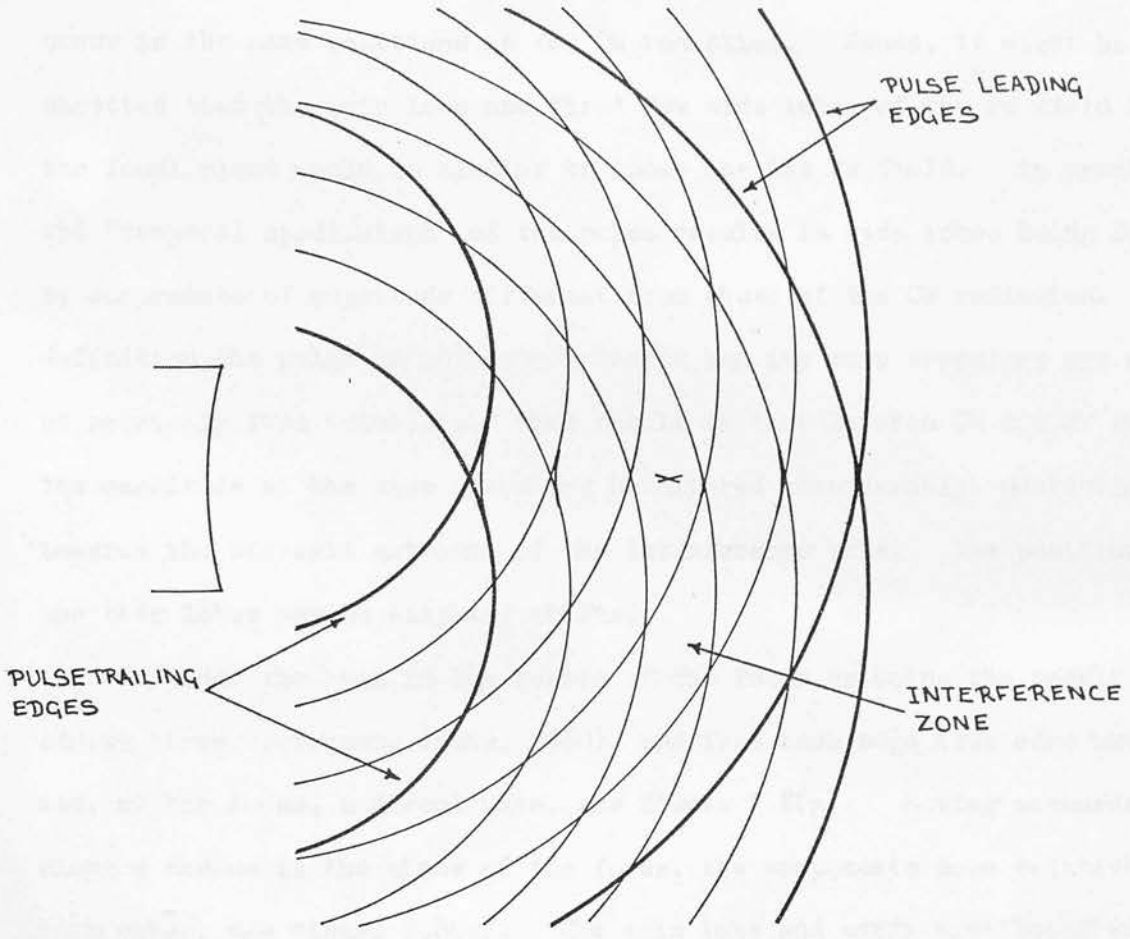

From figures 2.7(a) and (b) it is obvious that for a very short pulse (one cycle) CW and PW fields will only show any similarity in a region immediately about the axis. Off-axis, the edge waves no longer interfere and so the response falls off smoothly as the edge wave amplitude decreases with distance. For a pulse length typical of that used in diagnostic imaging (about five cycles) there is an area of interference defined mainly by the leading and trailing edges of the two edge waves. From figure 2.7(c) it can be seen that maxima and minima occur in the same positions as for CW radiation. Hence, it might be expected that the main lobe and first few side lobes of the PW field in the focal plane would be similar to those for the CW field. In practice, the "temporal apodisation" of the pulse results in side lobes being formed by components of magnitude different from those of the CW radiation. By definition the pulse is not monochromatic and its zero crossings are not at precisely even intervals. The result is that between CW and PW fields, the magnitude of the side lobes may be altered considerably, particularly towards the off-axis extremes of the interference zone. The position of the side lobes may be slightly shifted.

Consider the beam in the region of the focus as being the result of adding three components (Dehn, 1960), one from each edge (the edge waves) and, at the focus, a direct wave, see figure 2.8(a). Moving outwards along a radius in the plane of the focus, the components move relative to each other, see figure 2.8(b). The main lobe and early side lobes will be similar to those for CW radiation so long as there are relatively even-amplitude sinusoidal cycles within the pulses to interfere with each other. For a pulse with four cycles in the centre of roughly even amplitude, it would be expected that the main lobe and first three side lobes be similar to those of the CW case.

Figure 2.8: Three component construction for transmitted wave (Dehn).

(a) on-axis, at a focus

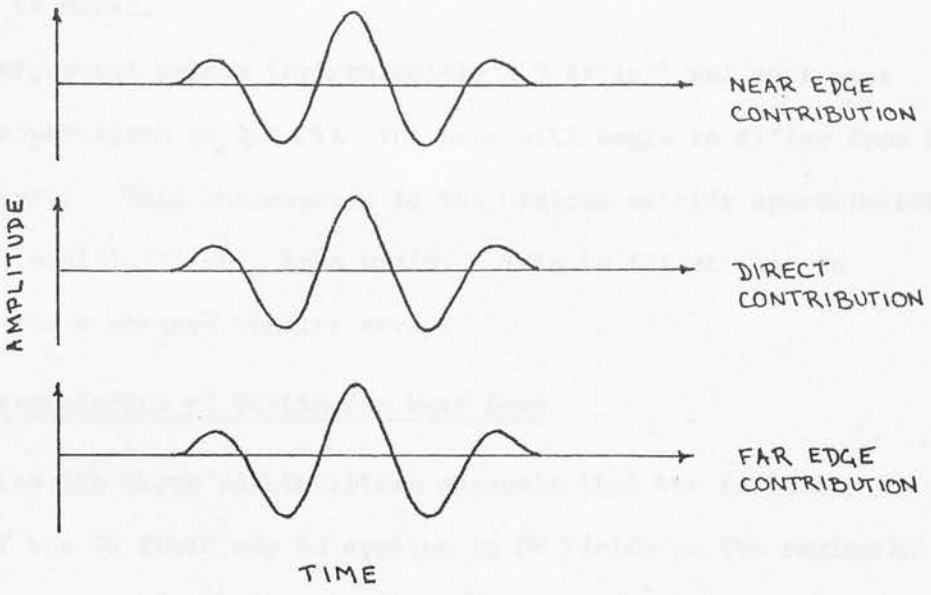

(b) slightly off-axis, in the focal plane

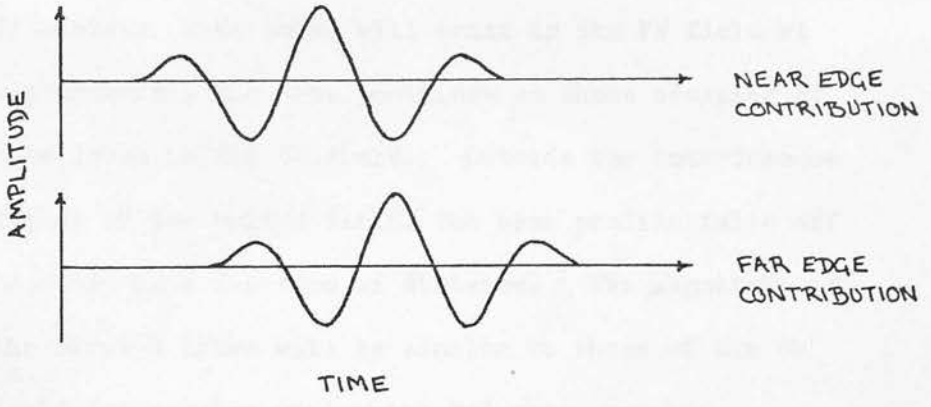

Dietz et al. (1978) when considering the effect of bandwidth on beam shape, claim that the -20 dB beam width is unaffected by bandwidth for pulses up to a bandwidth of at least 100% (equivalent to a pulse of ~3 cycles or more).

For very short pulses (approximately 1.5 cycles) and edge wave component separations of $\geq 0.25\lambda$ the beam will begin to differ from its CW counterpart. This corresponds to the regions outside approximately the -10 dB (amplitude) main lobe width. This is illustrated in figure 2.9 for a focused annular array.

2.5.2 Interpretation of Continuous Wave Data

Studying the above constructions suggests that the following features of the CW field may be applied to PW fields in the region of a focus.

(1) Mainlobe: the shape and size of the main lobe will be very similar in both cases (excepting for very short pulses (one to two cycles) which will cause marked broadening of the main lobe;

(2) Sidelobes: side lobes will exist in the PW field at approximately the same positions as those occupied by side lobes in the CW field. Outside the interference region of the pulsed field, the beam profile falls off smoothly as a function of distance. The magnitude of the first N lobes will be similar to those of the CW field for a pulse containing N+1 even, maximum amplitude cycles.

Results which will be quoted for CW fields are, therefore, -15 dB mainlobe half-width, first side lobe level and maximum side lobe level.

Figure 2.9: Focal plane response of an array.

(a) continuous wave radiation

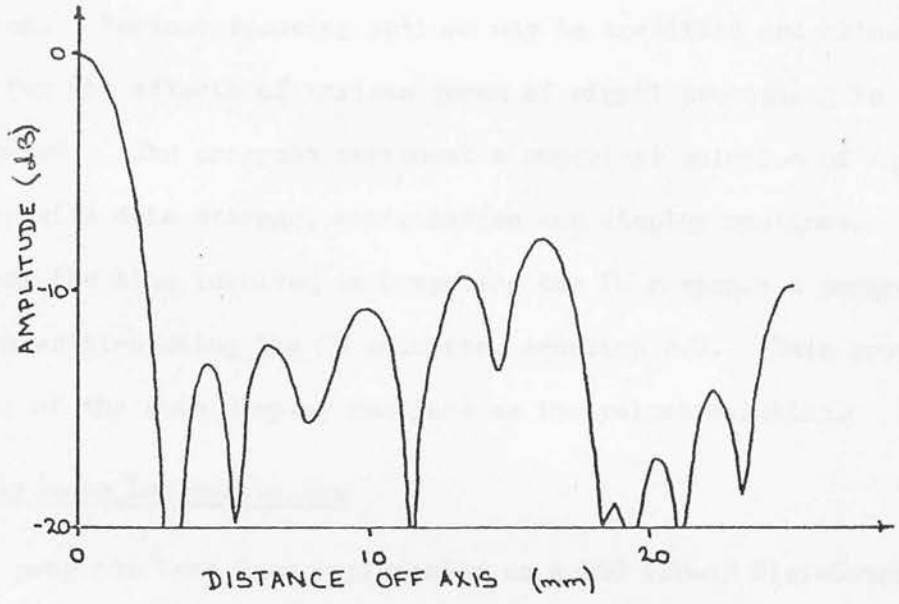

(b) two cycle pulsed radiation

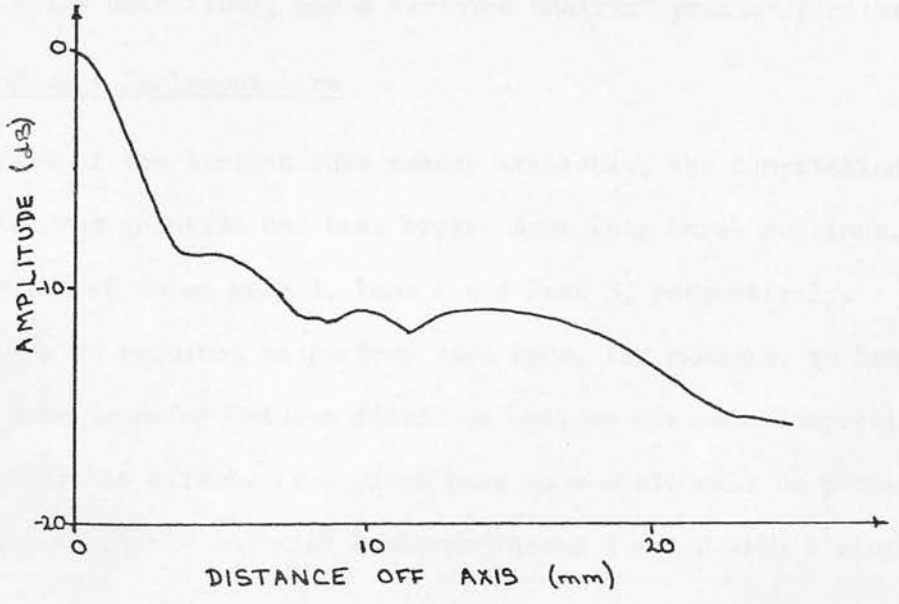

2.6 Beam Simulation Programs

A suite of interactive FORTRAN programs has been written to simulate the action of a swept focus annular array transducer. The transmission or reception response (Section 2.4.1.3) of a given array geometry is computed at specified field points for a given pulsed excitation. Various focusing options may be specified and allowance is made for the effects of various forms of signal processing to be investigated. The programs represent a numerical solution of equation 2.1 along with data storage, manipulation and display routines. Because of the time involved in computing the PW response a program has also been written using the CW solution, equation 2.7. This program makes use of the same display routines as the pulsed solution.

2.6.1 Hardware Implementation

The programs have been implemented on a DEC PDP-12 Mini-Computer with 32k of core memory and incorporating a floating point processor. High speed back-up memory and bulk storage is provided by magnetic cartridge diskettes. Peripheral devices supported include teletype (TTY), visual display unit (VDU), and a Versatec "Matrix" printer/plotter.

2.6.2 Software Implementation

Because of the limited core memory available, the computation for the pulsed wave solution has been broken down into three sections. These will be referred to as Pass 1, Pass 2 and Pass 3, respectively. Several programs may be required to perform each Pass, for example, to handle data input or data transfer between files, as well as the main computation. However, only the effects of a given pass as a whole will be presented. Computation of the CW solution replaces Passes 1 and 2 with a single program.

2.6.2.1 Pass 1

Pass 1 accepts as input, details of the annular array. For example, number of rings and frequency, the grid of points at which the ultrasonic field is to be computed, and the excitation pulse shape to be used.

An automatic adaptive quadrature subroutine is used to perform the numerical integration("QUANC8", Forsythe et al., 1977).

The integral of equation 2.1 is well behaved throughout most of the field. However, there are certain field points particularly associated with the geometrical projection of the array, where the integrand contains severe discontinuities. These may result in false convergence in the integration routine which may pass undetected. Such points occur only occasionally and are easily detected in the final plot by inspection. A more sophisticated technique to correctly handle the discontinuities could be used (for the general procedure see Arditi et al., p 49) but was not considered worthwhile in the time available.

The output from Pass 1 is the pressure pulse from each ring as a function of time at each field point and is stored in a data file on the bulk storage device.

2.6.2.2 Pass 2

Pass 2 simulates focusing and signal processing. It combines the 'component' pulses from each ring, at a given field point, to form the resultant pulse from the whole array. Input is in the form of fixed delays, for a fixed focus at a single depth, or the specification of an appropriate delay function to simulate a swept focus. Various forms of signal processing may be implemented by loading different subroutine subprograms with the main program before running it. Signal processing can be performed either before or after the component pulses are combined.

After the resultant pulse has been computed its amplitude at any given field point is found and stored. This characterises the field at that point. Other techniques may be used to simulate the rectification and smoothing of the pulse which occurs in a real system but were not considered of any benefit here.

2.6.2.3 Pass 3

Pass 3 is a flexible display and data analysis program which takes the output of Pass 2 as input. Pass 3 is highly interactive to allow the most suitable display of a given data set to be obtained. The desired plot is arrived at while the data is viewed on the VDU. It may then be hard-copied on the electrostatic printer/plotter. Two examples of plotter output are shown in figures 2.10 and 2.11. One is drawn on a logarithmic and the other on a linear scale.

Other possibilities include the provision for loading a data processing subroutine with the main program. This allows automatic calculation of such details as the -15 dB beam width of a given cross section, for example.

Another program available, which does not fall directly in the main Pass 1-2-3 stream, performs the same data manipulations as Pass 2 but also allows component and resultant pulses to be displayed at each stage of the processing. Like Pass 3 this is a highly interactive program allowing the details of pulse shape at a given field point to be viewed and a hard copy to be made if so desired (figure 2.12).

2.6.2.4 Continuous Wave Simulation Program

This program replaces Passes 1 and 2 above. It uses a standard algorithm to compute the zero'th order Bessel function in equation 2.7. All the appropriate input parameters, numbers of rings, ring radii, frequency, may be entered by the user. The output, which is directly

Figure 2.10: Example plotter output, beam cross-section, log.vertical scale.

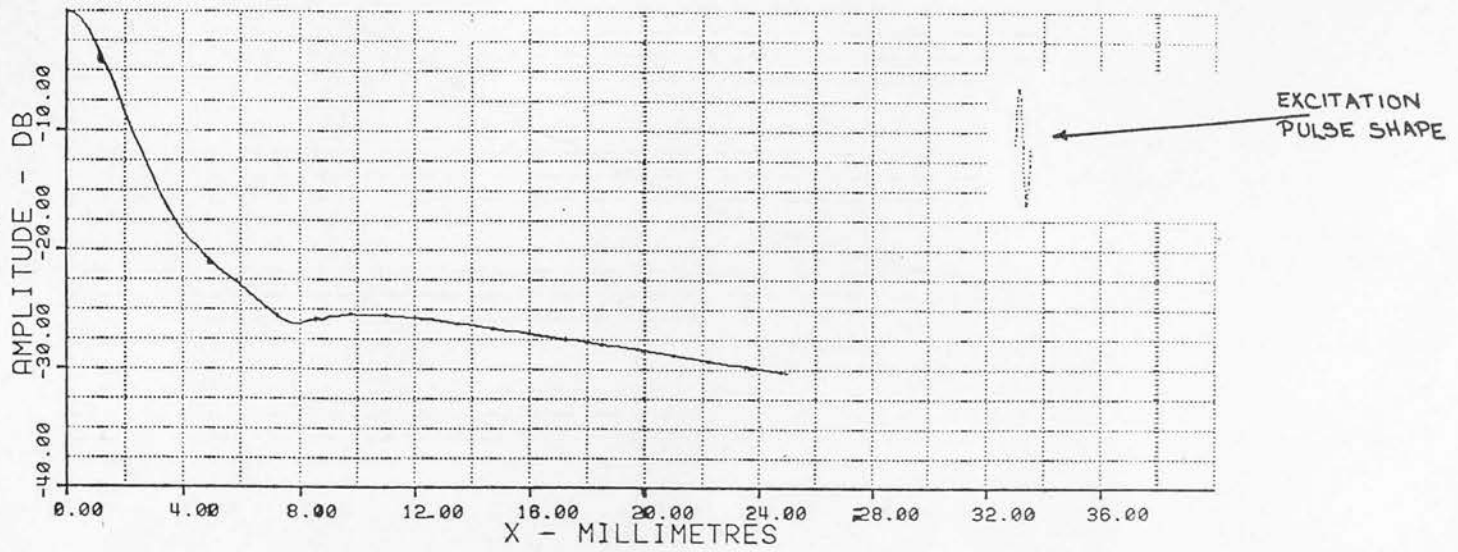

BEAM CROSS SECTION OF AN ULTRASONIC TRANSDUCER:

AMPLITUDE REFERENCE LEVEL (ZERO DB LEVEL) : 3.0992 :

SYSTEM SPECIFICATION:

FREQUENCY	3.5	MHZ	:	FIELD LINE COORDINATES:			
VEL. OF SOUND	1540.0	M/SEC	:	DISTANCE OFF AXIS (X)	0.0	TO 25.0	MM
NO. OF ANNULI	4		:	DISTANCE FROM TRANSDUCER FACE (Z)	100.0		MM

RADII (MM) 2.38 - 3.38 : 5.25 - 6.25 : 8.12 - 9.12 : 11.00 - 12.00:
DELAY (MICRO SEC) :0.402 :0.318 :0.180 :0.000 :

COMMENT: IDENT: A06AC.DA
EXCITATION: PULSE (#3)
A0607 :(PRA1): WIEGHTED TO GIVE EVEN ON AXIS RESPONSE
(PRBCW0,PRB1): FOCUSED AT 100.0 MM (DELAYS IN MU)

Figure 2.11: Example plotter output, beam axis, lin.vertical scale.

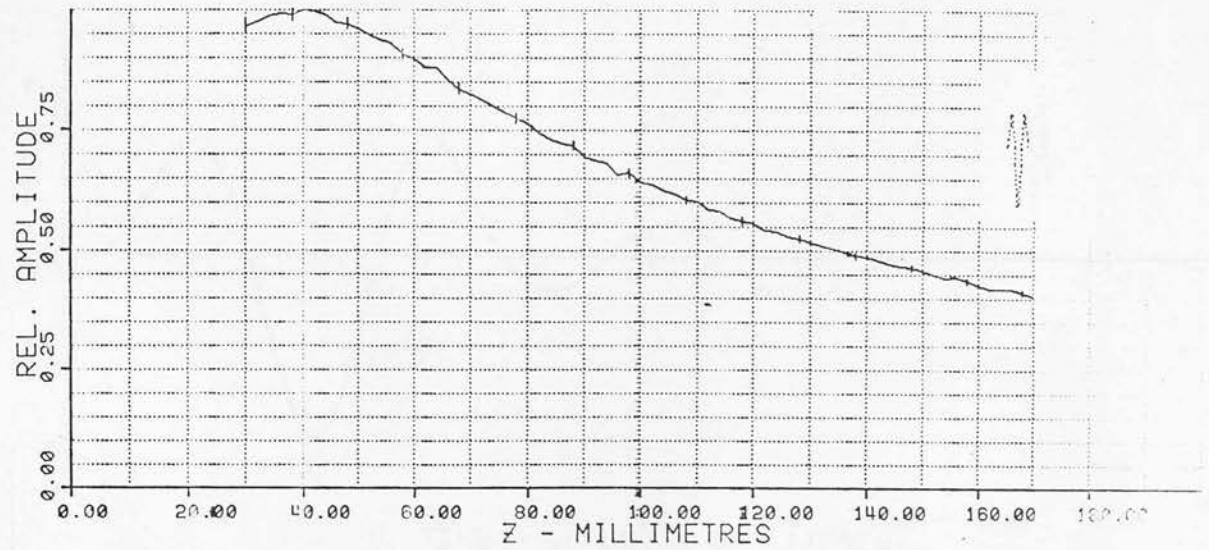

BEAM AXIS OF AN ULTRASONIC TRANSDUCER:

AMPLITUDE REFERENCE LEVEL (ZERO DB LEVEL) : 0.891 :

SYSTEM SPECIFICATION:
FREQUENCY 3.5 MHZ :
VEL. OF SOUND 1540.0 M/SEC :
NO. OF ANNULI 4 :

FIELD LINE COORDINATES:
DISTANCE OFF AXIS (X) 0.0
DISTANCE FROM TRANSDUCER FACE (Z) 30.0 TO

RADII (MM) 2.34 - 3.32 : 5.28 - 6.26 : 8.16 - 9.13 : 11.05 - 12.06:
DELAY (MICRO SEC) :0.000 :0.000 :0.000 :0.000 :

COMMENT: IDENT: A02C1.DA
EXCITATION: PULSE (*8) 1.5 CYCLES
A02C02:(FRA2): SWEPT FOCUS, WIEGHTING PROP. TO RING RADII
(PRBCW0,PRB1):

Figure 2.12: Example plotter output, pulse shape as a function of time at a point in the beam.

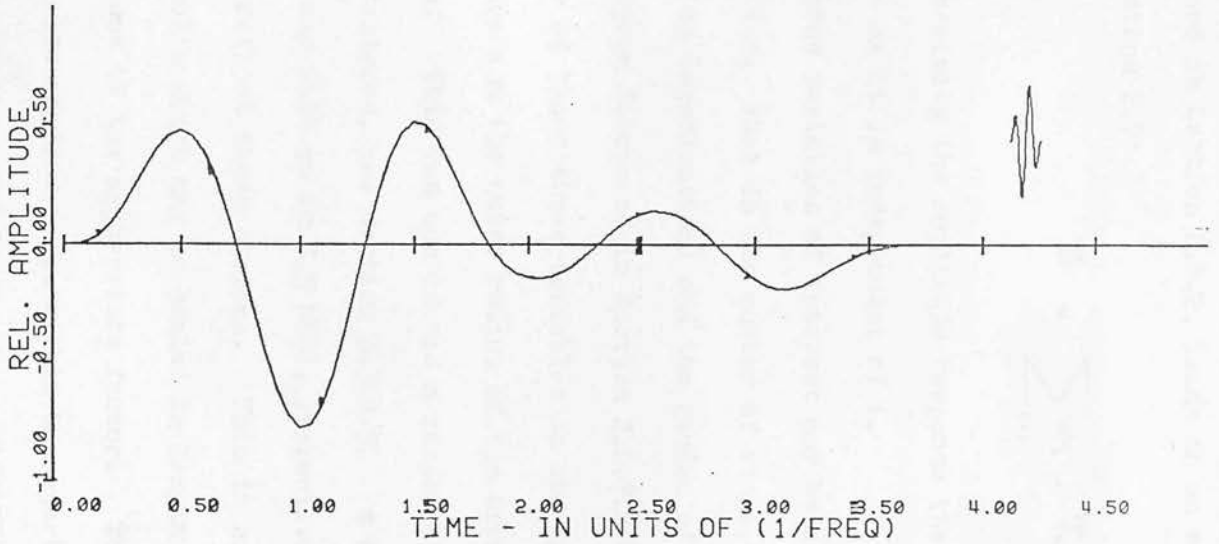

PULSE SHAPE FROM AN ULTRASONIC TRANSDUCER:

AMPLITUDE REFERENCE LEVEL (ZERO DB LEVEL) : 1.000 :
TIME AXIS ZERO OFFSET (MICRO SEC) : 9.648 :

SYSTEM SPECIFICATION:

FREQUENCY	3.5	MHZ :	FIELD POINT COORDINATES:		
VEL. OF SOUND	1540.0	M/SEC :	DISTANCE OFF AXIS (X) :	0.0	MM
RING NUMBER	0	:	DISTANCE FROM TRANSDUCE FACE (Z) :	10.0	MM

RADII (MM) 2.32 - 3.34 : 5.23 - 6.23 : 8.11 - 9.11 : 10.99 - 11.99:
DELAY (MICRO SEC) :2.981 :2.321 :1.287 :0.000 :

COMMENT: IDENT: A04D_DA
EXCITATION: PULSE (#1)

compatible with that of Pass 2, represents the CW focal plane response of an array of ideally narrow concentric annuli.

2.7 Discussion of Continuous Wave Simulation Results

The model for the focal plane transmission response of an array, discussed in Section 2.4.2, leads to an expression for the response given by equation 2.7:

$$R = \sum_{i=1}^{n} \omega_i \cdot J_0\left(\frac{2\pi \times r_i}{\lambda z}\right)$$

In determining the amplitude response the phase term $e^{j\phi}$ has been omitted as it is independent of i.

Three variables of interest may be identified from the above equation, n, ω_i and r_i, that is the number of rings, the weighting factor applied to each ring (apodisation) and the radius of each ring (ring arrangement). The program discussed in Section 2.6.2.4 has been used to investigate the effects of these three variables on the array response. During the investigation the outer radius of the array r_n, has been kept constant at 11.5 mm. This was considered a reasonable value for the type of array being designed, see Section 3.3.1.5. z and λ were also held constant at 100 mm and 0.44 mm ($\equiv$ 3.5 MHZ), respectively. The spatial scales on the graphs reflect these choices. This in no way reduces the generality of the results which may be scaled in length to apply to other r_n, x, or z, by the use of the appropriate factor. The factor ω_i has also been chosen so that its maximum value within the aperture is unity.

In practice, array rings are of finite width. Considering relative widths, two specific cases of interest may be identified:

(1) where the rings are of equal area; and

(2) where they are of equal width.

These two cases are modelled in the above equation by choosing the following forms for ω_i:

(1) equal area - $\omega_i = 1.0 \times \alpha_i$

(2) equal width - $\omega_i = (r_i / r_n) \times \alpha_i$

where α_i represents an apodising function applied electronically. When no electronic apodisation is applied (α_i=1.0) rings of equal area have a constant 'natural' weight. For rings of equal width the weight is directly proportional to the position of the ring within the array aperture. In reality the relative weight of a finite width ring varies with depth, the above approximations being most realistic in the far-field or at a focus.

2.7.1 Effects of Number of Rings

The effect of number of rings n, on beam quality is considered for an array of evenly spaced rings. The results are presented in figures 2.13 and 2.14. As the number of rings increases the array response asymptotically approaches a limiting value. A small number of rings (<15) achieves a response similar to that of a filled aperture. The change in array response is slower for arrays of equal area rings than for those of equal width. The main features as n increases are as follows:

(1) An increase in the width of the main lobe. Rings are added nearer the centre of the array, whose energy is less well localised about the central axis.

(2) A steady decrease in the height of the maximum side lobe. As more rings are added this occurs further and further off-axis. Consequently, there is less energy in the diverging wave which forms it.

(3) The first side lobe also decreases monotonically for equal width rings. For equal area rings a sharp

Figure 2.13: Effect of number of rings on array focal plane response (equal area rings).

(a) -15dB main lobe half width vs. number of rings.

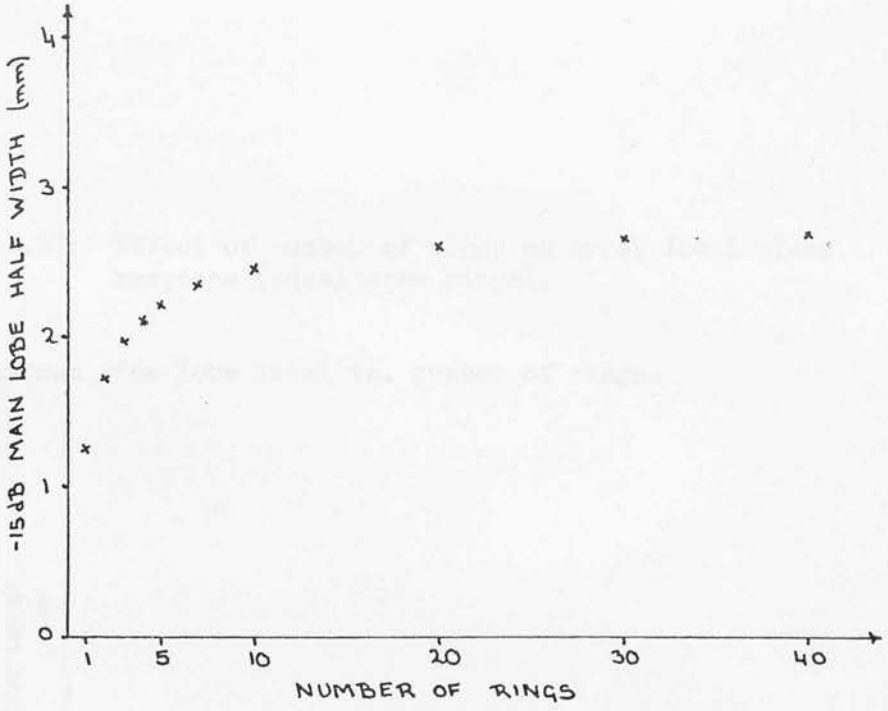

(b) 1st side lobe level vs. number of rings.

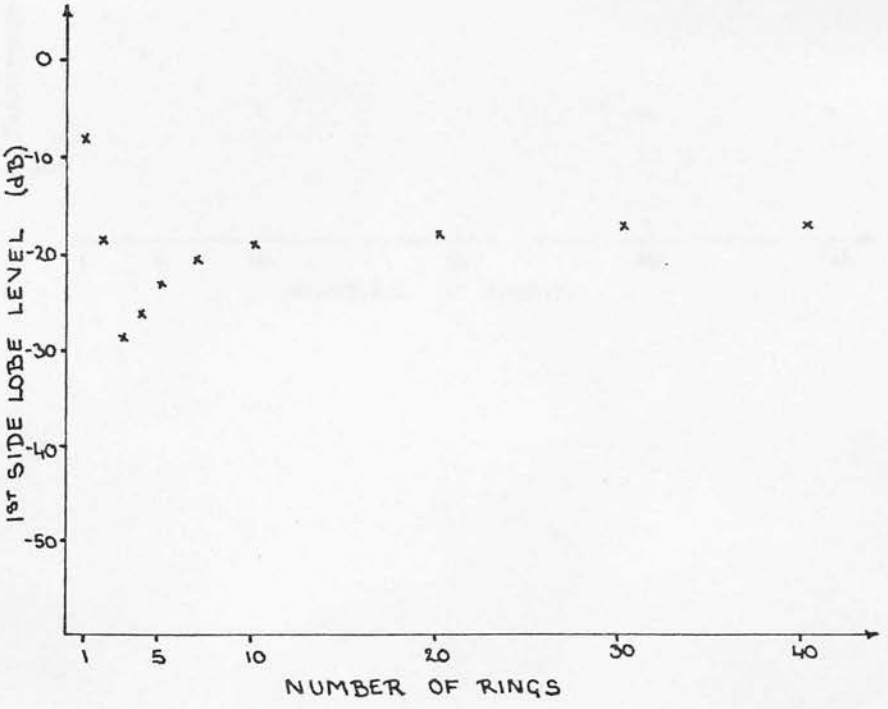

Figure 2.13: Effect of number of rings on array focal plane response (equal area rings).

(c) maximum side lobe level vs. number of rings.

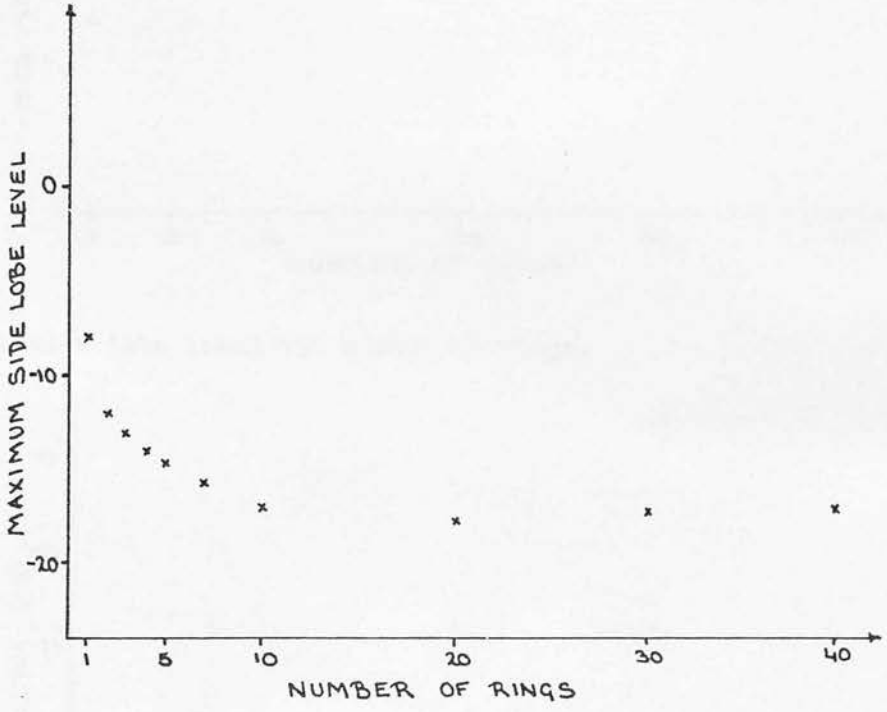

Figure 2.14: Effect of number of rings on array focal plane response (equal width rings).

(a) -15 dB main lobe half width vs. number of rings.

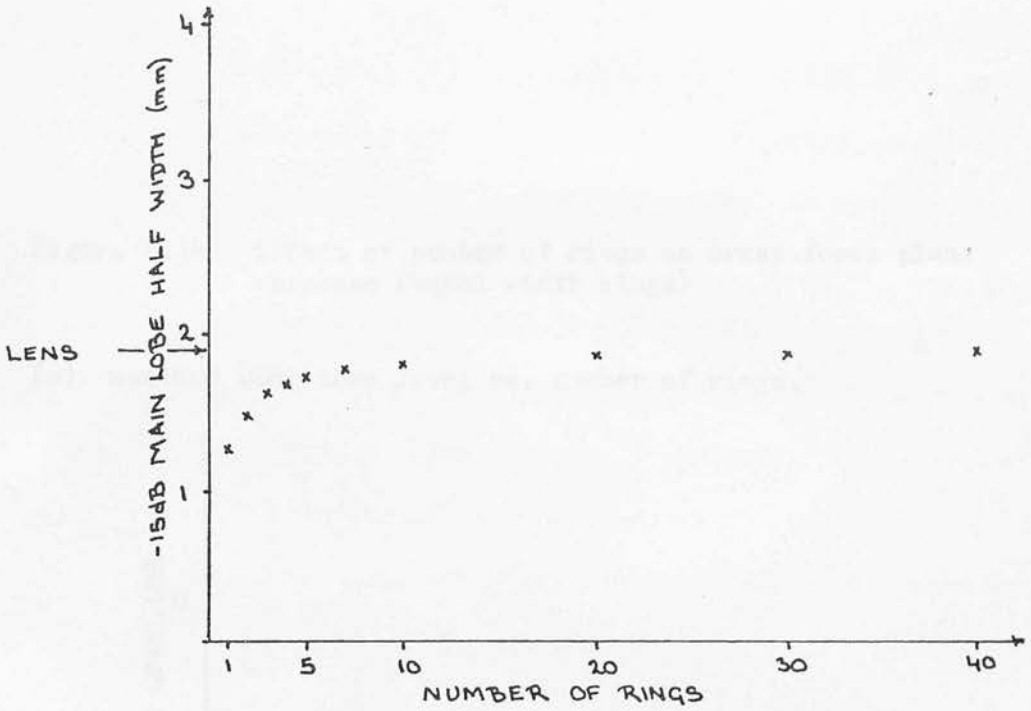

(b) 1st side lobe level vs. number of rings.

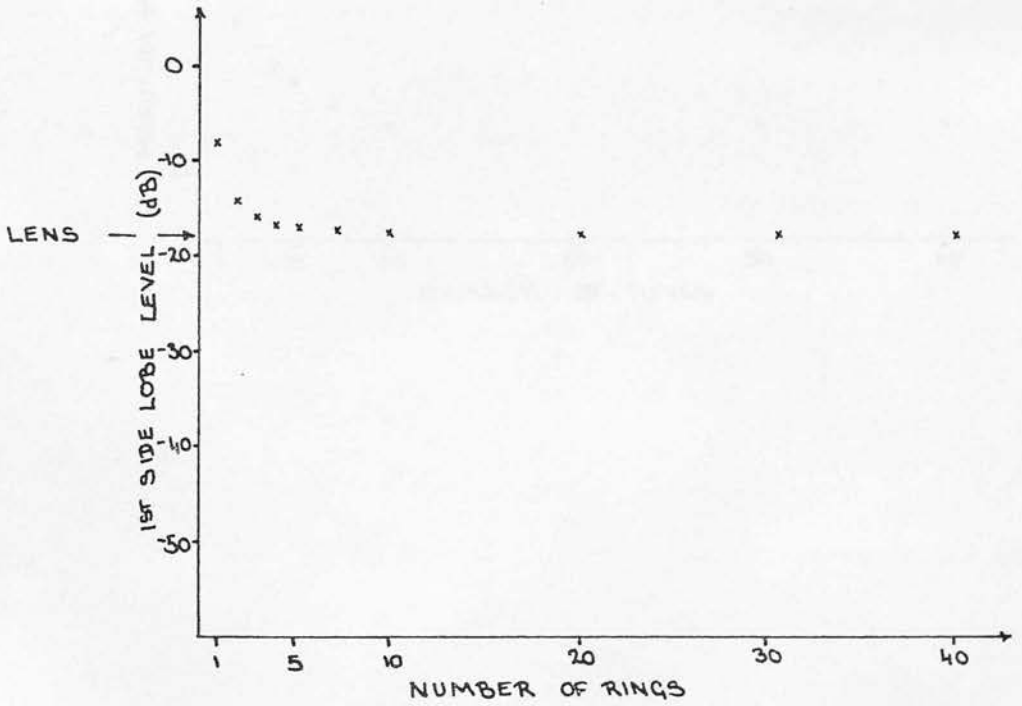

Figure 2.14: Effect of number of rings on array focal plane response (equal width rings)

(c) maximum side lobe level vs. number of rings.

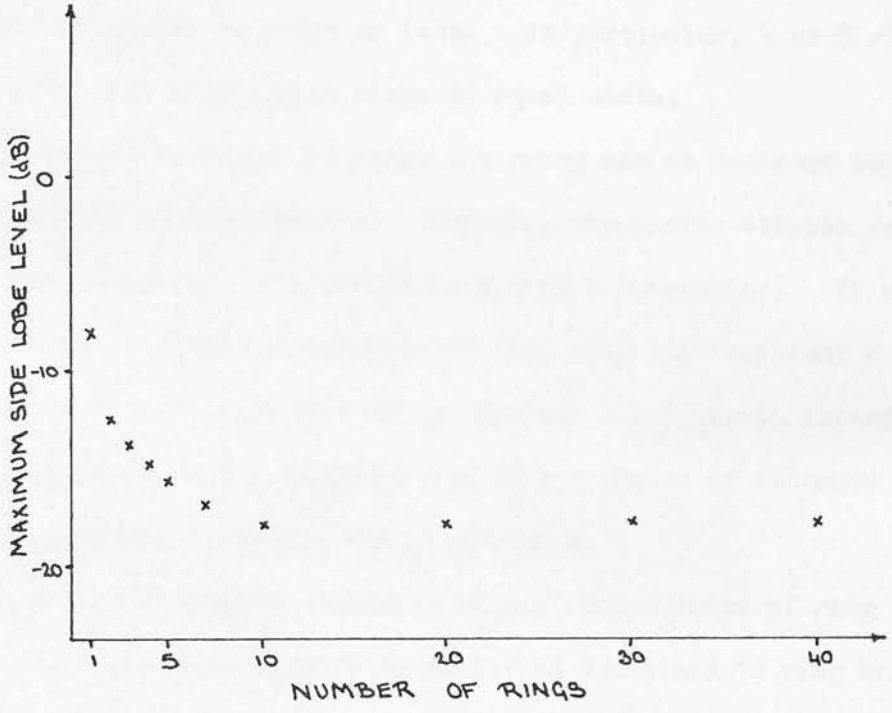

minimum at 3 rings is observed after which the level increases towards its final value.

The values of the beam quality parameters for a filled aperture focused at the same depth as the array are indicated on both sets of figures. They represent the limiting values to which an array of equal width rings approaches. This is to be expected as the areas of the equal width rings are proportional to radius, as is the area at any given radius, in a filled aperture.

In the context of array design these results suggest that an array may be fabricated having a focal plane response similar to that of a filled aperture, with 10 rings or less. In particular, 4 or 5 rings are sufficient for arrays with rings of equal width.

By altering the number of rings the array may be designed to optimise some particular feature. However, the choice between optimum side lobe level and main lobe width is always a compromise. It should also be remembered that the addition of each ring can represent a marked increase in cost and complexity of the system. For arrays intended for use with signal processing techniques a larger number of returned signals is probably required to obtain optimum results.

Based on these results, investigation of the effects of ring arrangement and apodisation will be performed for 4 and 10 ring arrays. These represent an array similar to the one envisaged as a prototype in the actual system and one well into the limiting region of response shape.

2.7.2 Effects of Ring Arrangement

The alteration of the position of the rings relative to one another within the aperture has a pronounced effect on beam quality. The individual Bessel function responses are expanded or contracted as the rings are made smaller or larger in radius, respectively. The degree

of constructive and destructive interference amongst the side lobes and the width of the main lobe are varied.

To investigate the effects of ring arrangement, the ring radii have been chosen to follow two (arbitrary) functions containing a single parameter which defines a particular ring arrangement. Evenly spaced rings are defined as the norm and variations are referred to the results for this case.

Four variations have been performed:

(1) with the rings concentrated towards $r = r_n$

(2) with the rings concentrated towards $r = 0$

(3) with the rings concentrated towards $r = 0.5r_n$

(4) with the rings concentrated away from $r = 0.5r_n$

Two functions are used to produce these variations. Variation of β in equations 2.8 and 2.9 produces the desired ring arrangement:

types 1 and 2

$$r_i = \left(\frac{i}{n}\right)^{\beta} r_n \qquad \text{---2.8}$$

$\beta = 1.0$ corresponds to evenly spaced rings;

types 3 and 4

$$r_i = (2\beta - 0.5)\left(\frac{i}{n}\right)^3 + (-3\beta + 0.75)\left(\frac{i}{n}\right)^2 + (\beta + 0.75)\left(\frac{i}{n}\right) \qquad \text{---2.9}$$

$\beta = 0.25$ corresponds to evenly spaced rings.

The choice of a specific function out of the many which would produce similar variations was arbitrary. Extreme values for these functions are shown in figures 2.15 and 2.16 along with the variations in beam quality factors. The results of varying ring arrangement are presented for arrays of equal area rings in figures 2.17 and 2.19 and equal width rings in figures 2.18 and 2.20.

2.7.2.1 Major Features of the Results

The beam quality factors of equal area ring arrays show a marked

Figure 2.15: Normalised ring radius (r_i/r_n) vs. relative position (i/n) for extreme values of β in equation 2.8:

(a) β = 0.2, (b) β = 1.0, (c) β = 2.0.

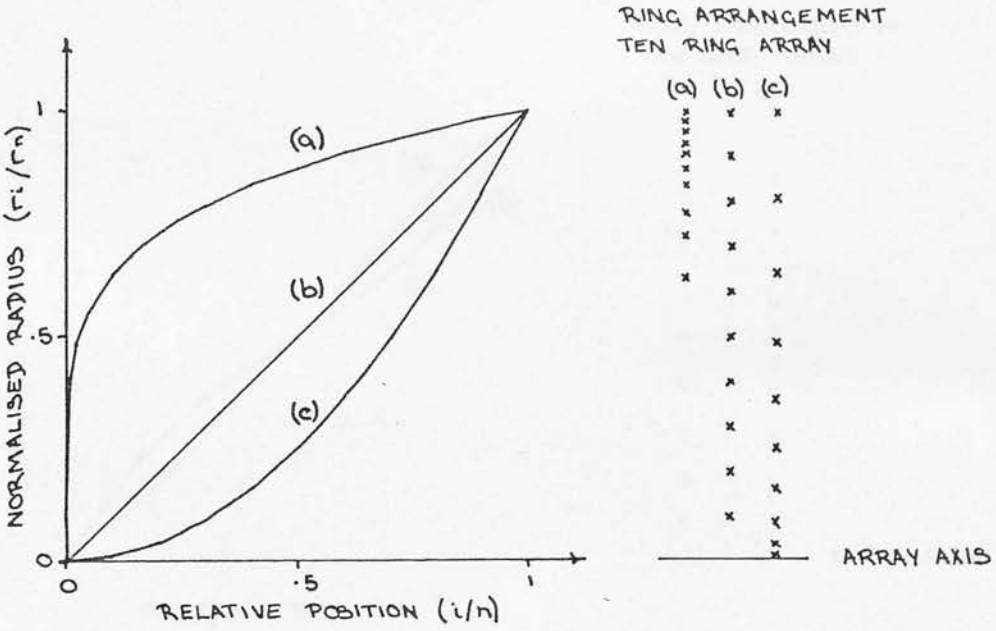

Figure 2.16: Normalised ring radius (r_i/r_n) vs. relative position (i/n) for extreme values of β in equation 2.9:

(a) β = 0.0, (b) β = 0.25, (c) β = 1.0.

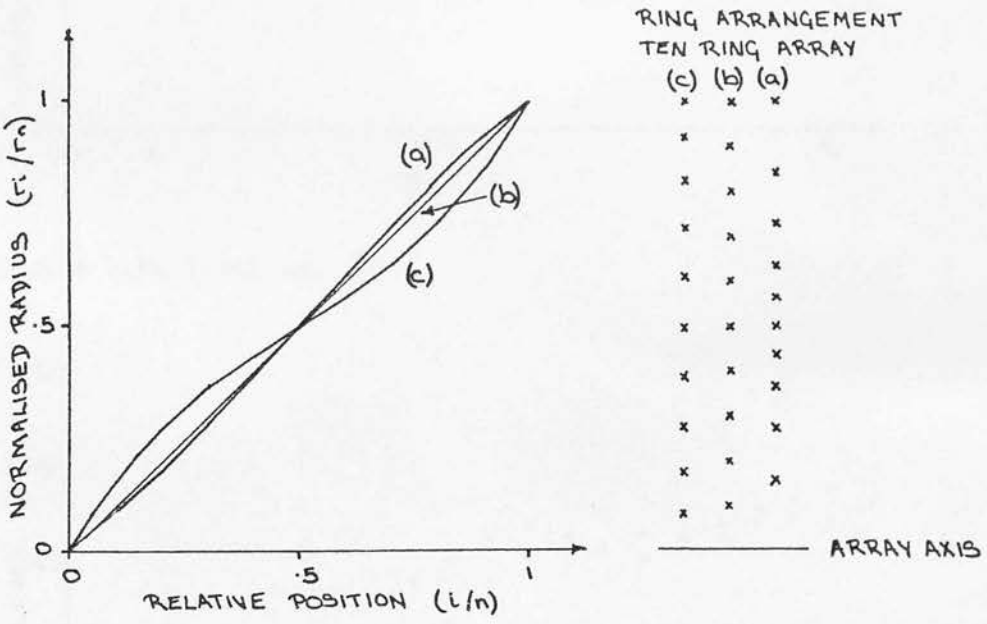

Figure 2.17: Effect of ring arrangement on array focal plane response (equal area rings; equation 2.8).

(a) -15dB main lobe half width vs. β ,

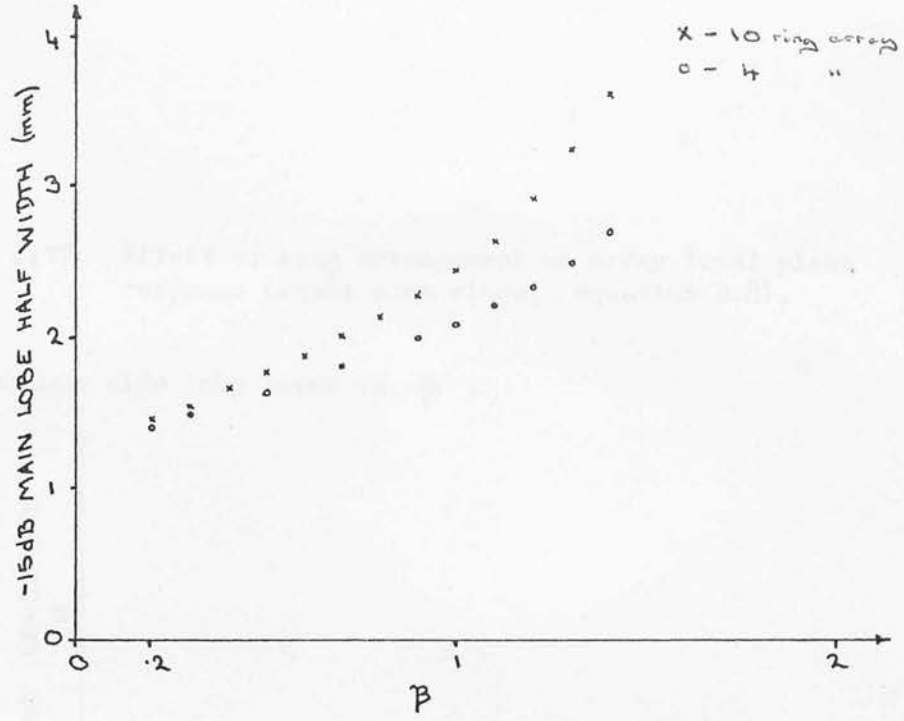

(b) 1st side lobe level vs. β .

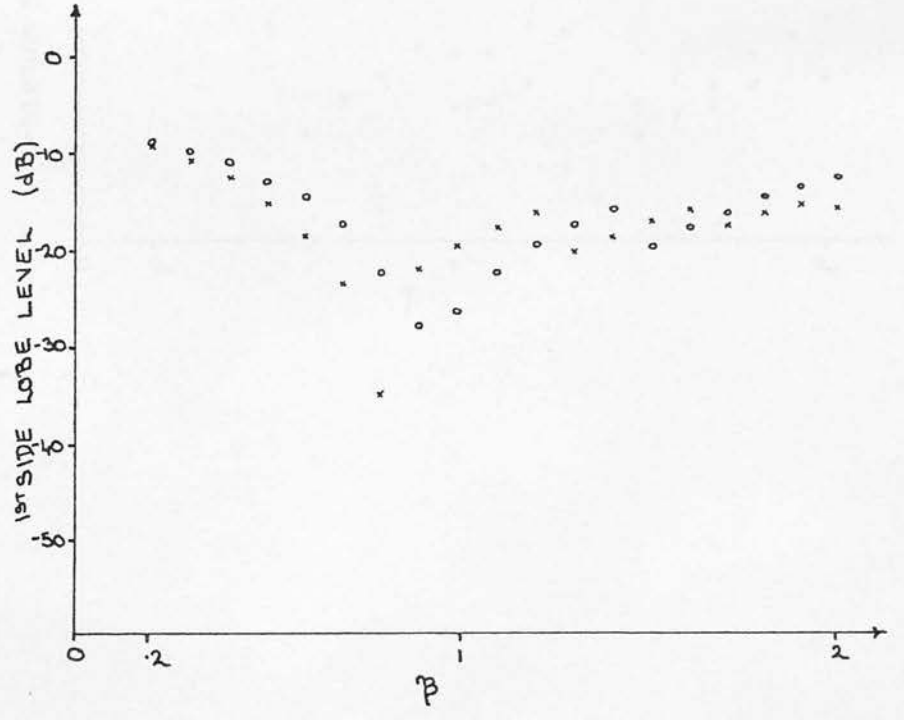

Figure 2.17: Effect of ring arrangement on array focal plane response (equal area rings; equation 2.8).

(c) maximum side lobe level vs. β .

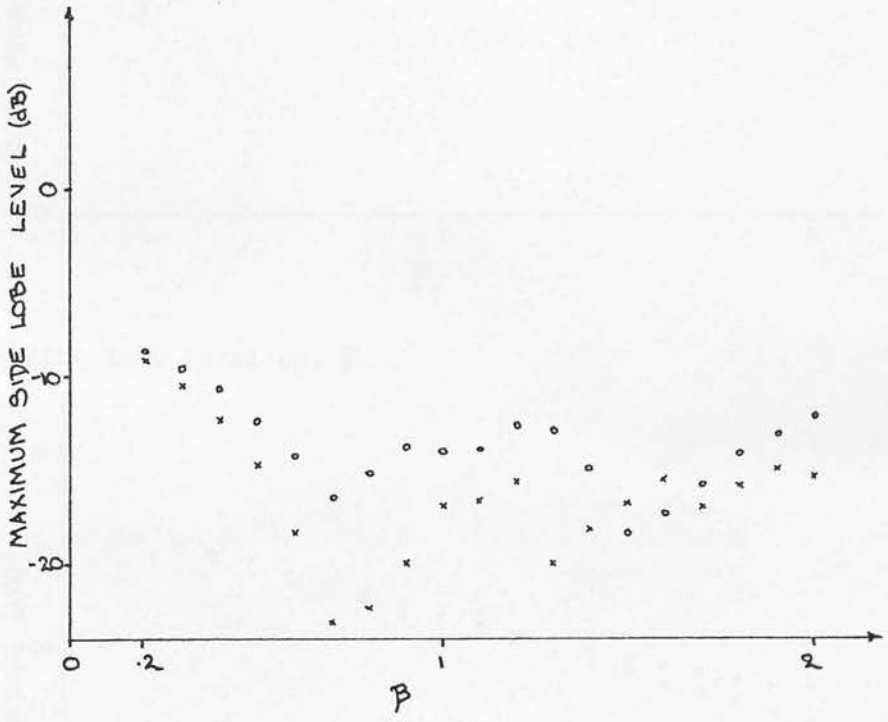

Figure 2.18: Effect of ring arrangement on array focal plane response (equal width rings; equation 2.8).

(a) -15dB main lobe half width vs. β .

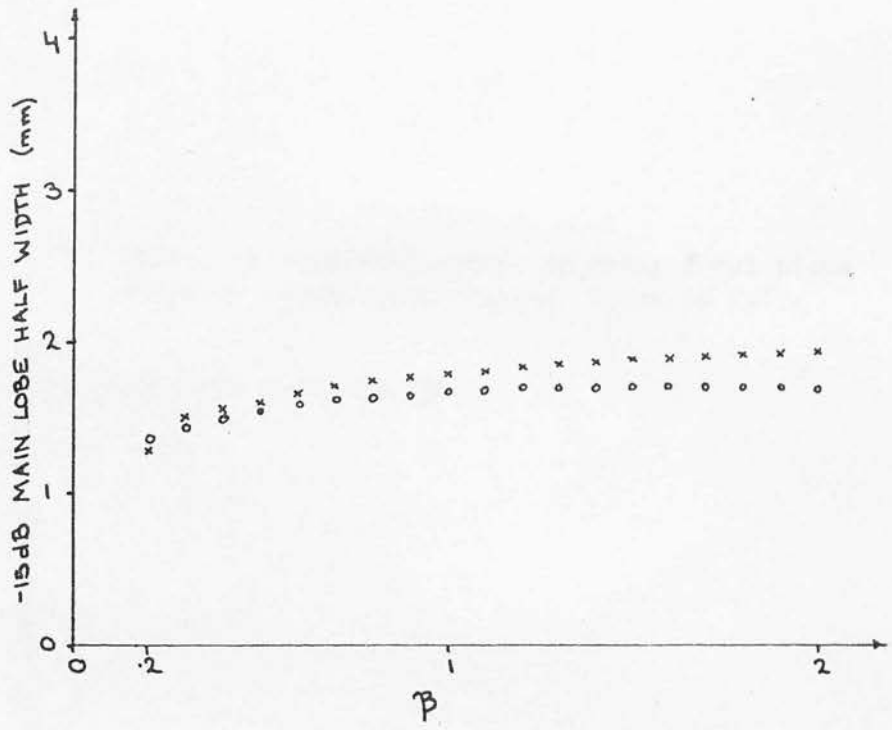

(b) 1st side lobe level vs. β .

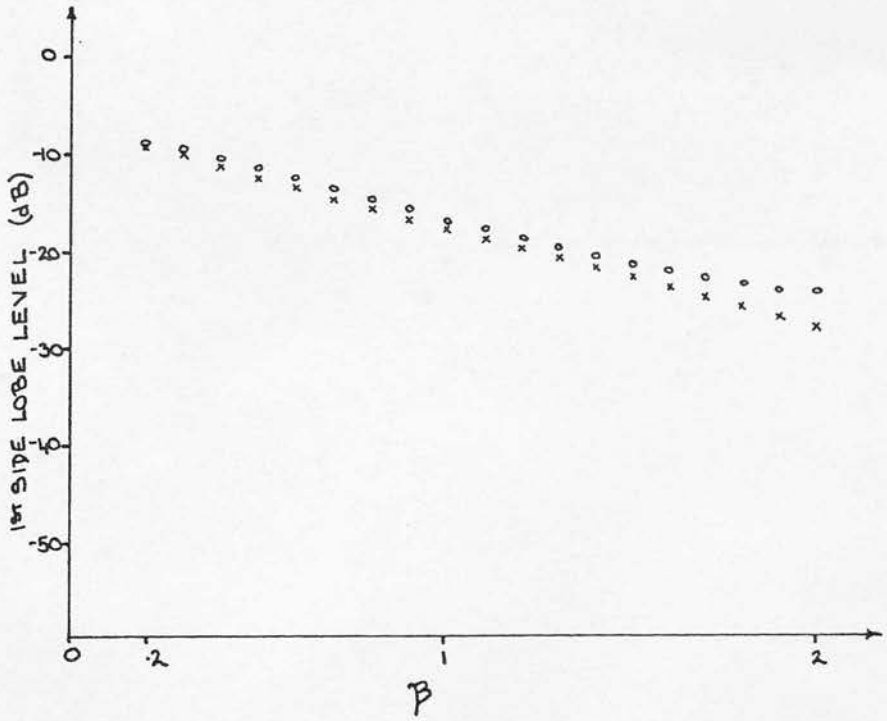

Figure 2.18: Effect of ring arrangement on array focal plane response (equal width rings; equation 2.8).

(c) maximum side lobe level vs. β .

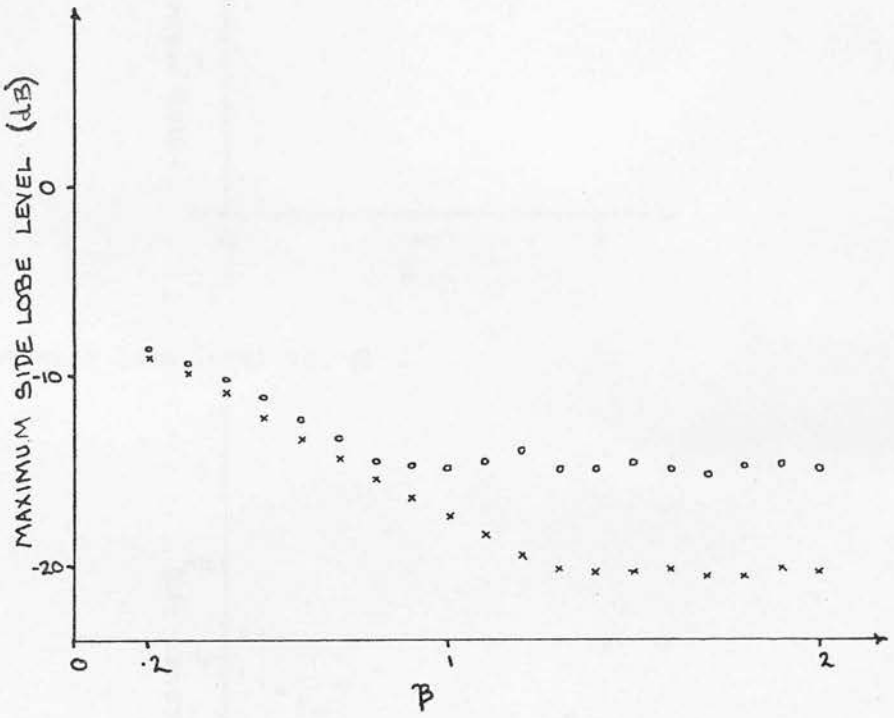

Figure 2.19: Effect of ring arrangement on array focal plane response (equal area rings; equation 2.19).

(a) -15dB main lobe half width vs. β .

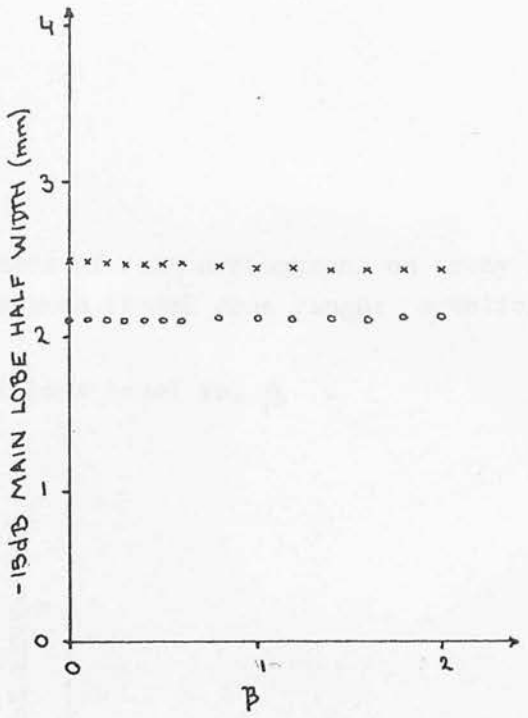

(b) 1st side lobe level vs. β .

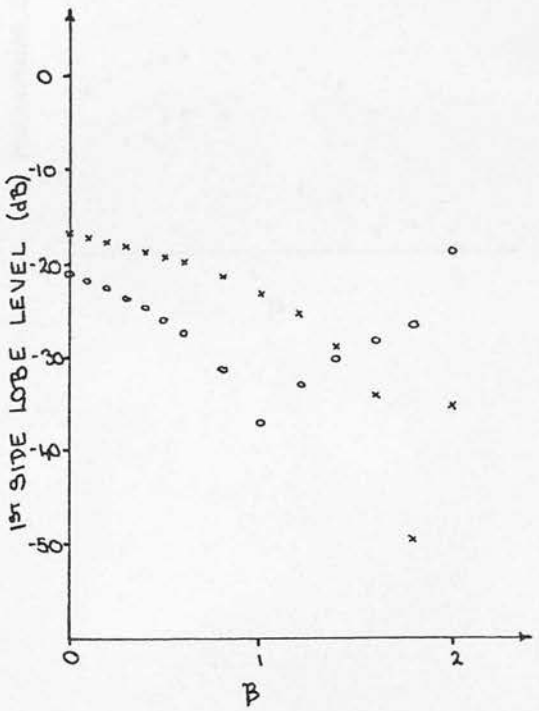

Figure 2.19: Effect of ring arrangement on array focal plane response (equal area rings; equation 2.19).

(c) maximum side lobe level vs. β .

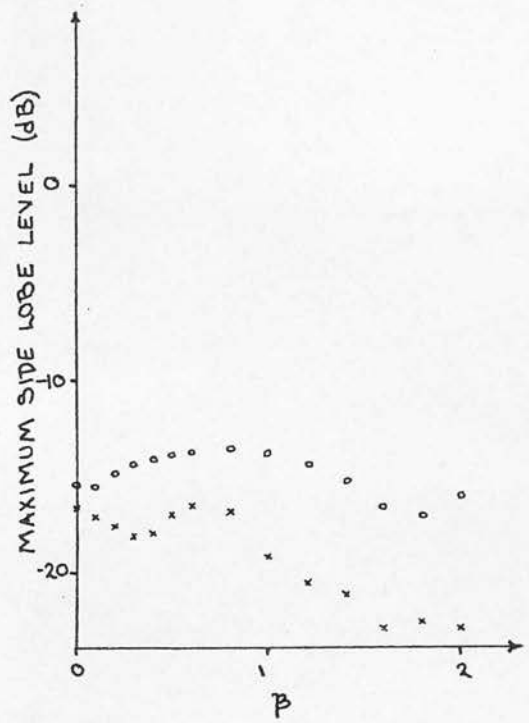

Figure 2.20: Effect of ring arrangement on array focal plane response (equal width rings; equation 2.19).

(a) -15dB main lobe half width vs. β .

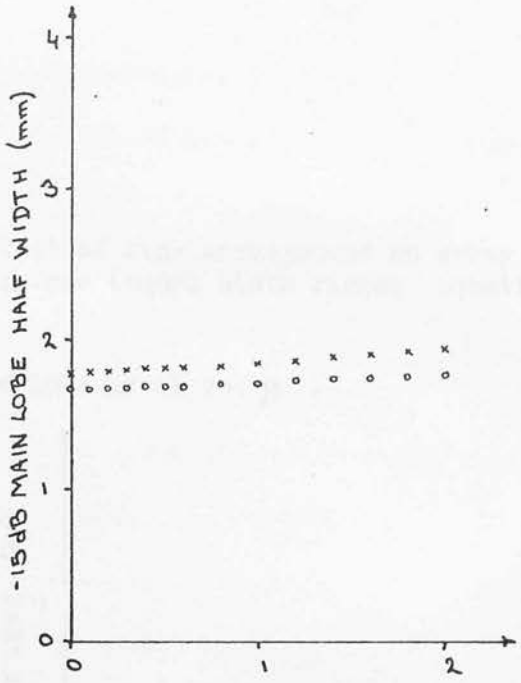

(b) 1st side lobe level vs. β .

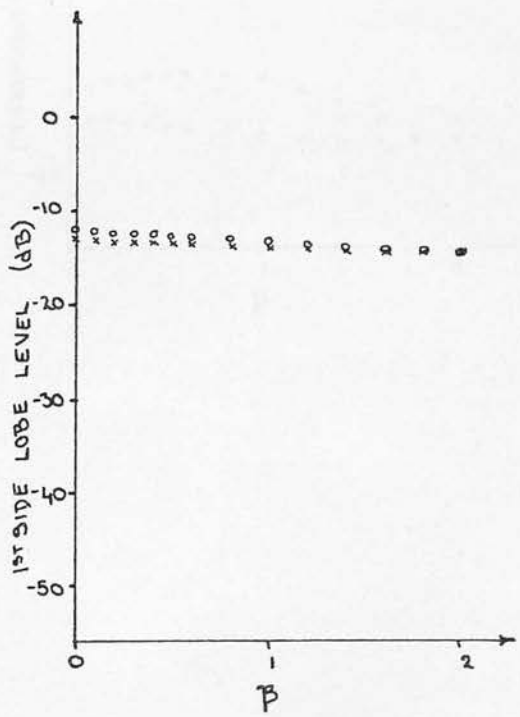

Figure 2.20: Effect of ring arrangement on array focal plane response (equal width rings; equation 2.19).

(c) maximum side lobe level vs. β .

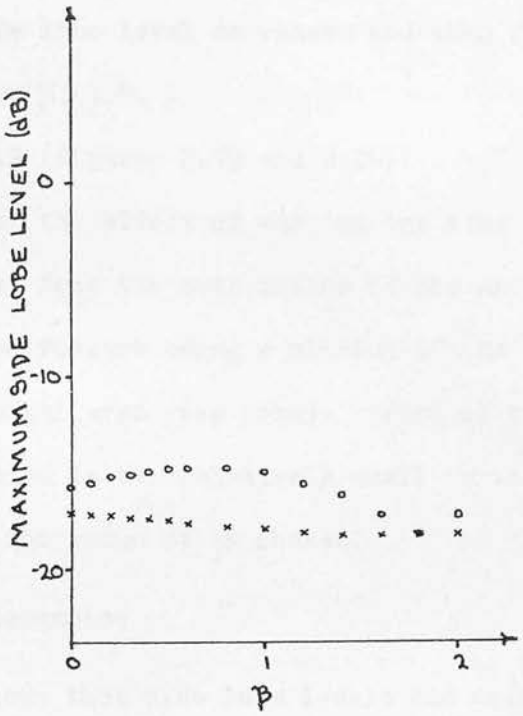

dependence on β. By comparison the variations for equal width ring arrays are less marked and more regular.

Variation of beam quality factors with increasing β

(a) In equation 2.8, for equal area ring arrays, (figure 2.17):

1) main lobe width increases;

2) side lobe levels pass through a series of maxima and minima;

for equal width ring arrays, (figure 2.18):

1) main lobe width increases;

2) first side lobe level decreases;

3) maximum side lobe level decreases and then remains constant for $\beta > 1.4$.

(b) In equation 2.9 (figures 2.19 and 2.20):

In general the effect of varying the ring arrangement towards or away from the mean radius of the array is only slight. The only marked feature being a minimum of the first side lobe level of the equal area ring array. Part of the reason for this lack of variation is the relatively small variations of the function over the range of β chosen.

2.7.2.2 General Discussion

It has been shown that side lobe levels and main lobe width are sensitive to ring arrangement. Any arrangement which tends to place a preponderance of rings towards the centre of the array tends to widen the main lobe, because the energy from these rings is less well localised about the central axis (figures 2.17(a) and 2.18 (a)). The reverse is true where rings are concentrated towards the outer edge. The response of each ring consists of a main lobe and a series of positive and negative going side lobes (the J_0 Bessel function), the

width of these lobes increases with decreasing ring radius. Hence, as radii are gradually increased or decreased with respect to one another interference maxima and minima are observed at any given point in the response and while observing particular side lobes (figures 2.17 - 2.20, (b) and (c)).

When the responses from each ring have the same on-axis magnitude independent of radius (equal area rings, $\omega_i = 1.0$) there are pronounced interference effects in the definition of the side lobes (e.g. figures 2.17(b) and (c)). The responses of the inner rings dominate the width of the main lobe (e.g. figure 2.17(a)). Hence, larger variations in beam quality factors are observed. Particular values of β suggest the possibility of marked improvements in side lobe response without major sacrifice of main lobe width. However, the variability of the response and the speed with which it changes in the region of minima indicates a strong dependence on ring radius, and suggests poor tolerance of manufacturing errors. With the model used to arrive at these results, rings are free to move within the aperture. In practice this is not true because of the finite width of the rings. Whatever radius is chosen to represent a ring, may only be brought as close to the next ring as slightly greater than the ring width, see Section 3.3.1.8. This constraint is more severe for equal area rings, where in order to maintain an equal area, rings towards the centre of the array must increase their width at a rate somewhat greater than their rate of decrease of radius.

For equal width rings the variations in response are smoother and generally monotonic, (e.g. figure 2.18). The outer ring has the highest on axis response. The response of rings closer to the centre decreases with decreasing radius. The decrease in response from rings as they move towards the centre is responsible for the smooth variation in beam

characteristics with varying β . As a ring is moved closer and closer to the centre, its contribution to the response gets less and less. Hence, limiting values are approached. The more even variation of response with β suggests greater tolerance of manufacturing errors. As all the rings have equal width, they have greater freedom, particularly towards the centre of the aperture, than equal area rings.

The functions chosen to control variation of ring arrangement have been arbitrary, within the constraint that the four general variations outlined in Section 2.7.2 be achieved. Variations of ring arrangement with similar general characteristics could be obtained with many other functions. The general features of the beam quality parameters would be similar whatever the function, but specific features would not.

All the figures indicate that the responses of 4 and 10 ring arrays are very similar, although particular features (e.g. the minimum in figure 2.19(b)) occur at different values of β . The variation of array response with number of rings has only been considered for evenly spaced rings. The effect of number of rings for some other ring arrangement has not been investigated, but is assumed to be similar. The fact that this is only partially true is indicated by figures 2.17(c) and 2.18(a) where the 4 and 10 ring responses cross at various points. This suggests that some other parameters such as minimum or maximum ring spacing may be of more fundamental significance than either number of rings or ring arrangement, both of which vary these quantities.

2.7.2.3 Implications for Array Design

The implications of this section for array design must be read in conjunction with similar sections for the effects on array response of number of rings, apodisation and practical construction techniques, (Sections 2.7.1, 2.7.3.3 and Chapter 3).

The control of side lobe levels and main lobe width by altering the relative positions of the annuli within the aperture of an array has been illustrated. Specific arrangements of rings have been shown to be particularly advantageous, for example, for an array of equal area rings, the ring arrangement given by equation 2.8 with $0.7 < \beta < 1.0$ reduces first and maximum side lobes and main lobe width (the total energy in the side lobes is probably increased with respect to that in the main lobe, but is more evenly distributed between lobes). An array of equal width rings has been shown to have a more predictable response.

2.7.3 Effects of Apodisation

The effects of apodising the array aperture for a number of different apodising functions are shown in figures 2.21 - 2.25. These functions have been applied to arrays of 4 and 10 evenly spaced rings, and both equal area and equal width ring arrays have been investigated. The apodising functions as applied to equal area rings are:

(1) $\omega_i = \delta \frac{r_i}{r_n} + 1 \qquad -1 \leq \delta \leq 0$

(2) $\omega_i = \delta\left(\frac{r_i}{r_n} - 1\right) + 1 \qquad 0 \leq \delta \leq +1$

(3) $\omega_i = \exp\left[-\delta\left(\frac{r_i}{r_n}\right)^2\right] \qquad 0 \leq \delta \leq 2$

(4) $\omega_i = \exp\left[-\delta\left(\frac{r_i}{r_n} - 0.5\right)^2\right] \qquad 0 \leq \delta \leq 4$

The parameter δ is used to vary the function over an arbitrary range (cf β for defining ring arrangement). The functions are illustrated for extreme values of δ in the figures for the corresponding quality parameter variations. In order to apply the above functions to arrays of equal width rings the factor r_i/r_n is introduced, for example, type (1)

Figure 2.21: Effect of apodisation on array focal plane response (equal area rings; types 1 and 2).

(a) -15dB main lobe half width vs. δ .

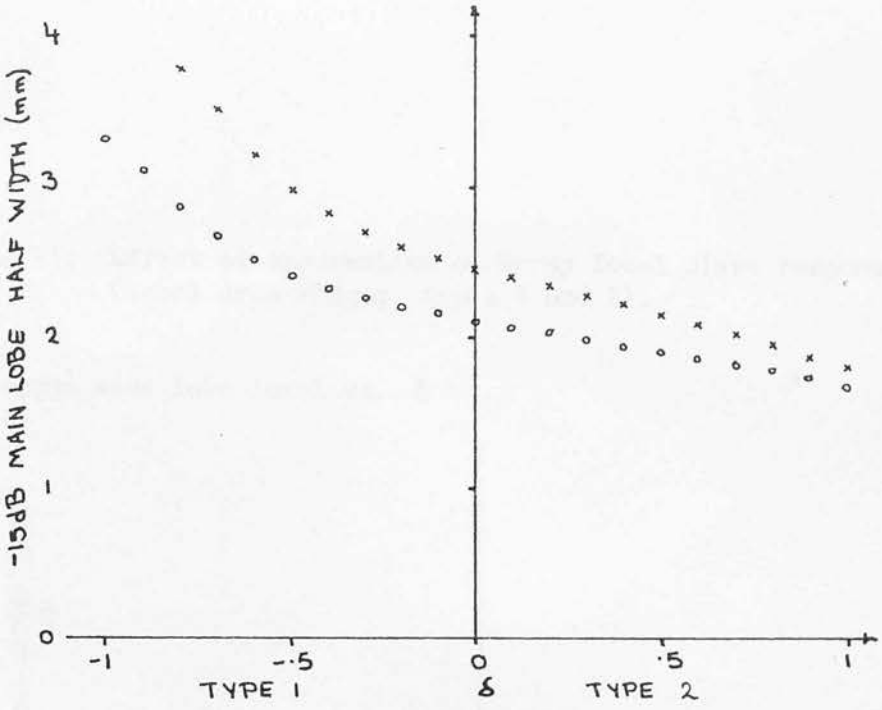

(b) 1st side lobe level vs. δ .

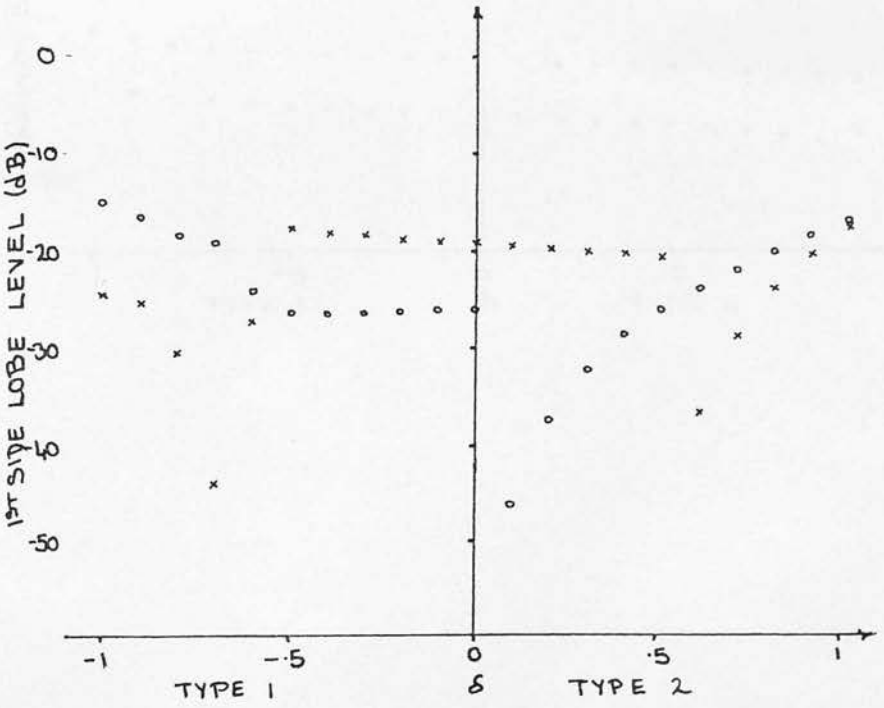

Figure 2.21: Effect of apodisation on array focal plane response (equal area rings; types 1 and 2).

(c) maximum side lobe level vs. δ .

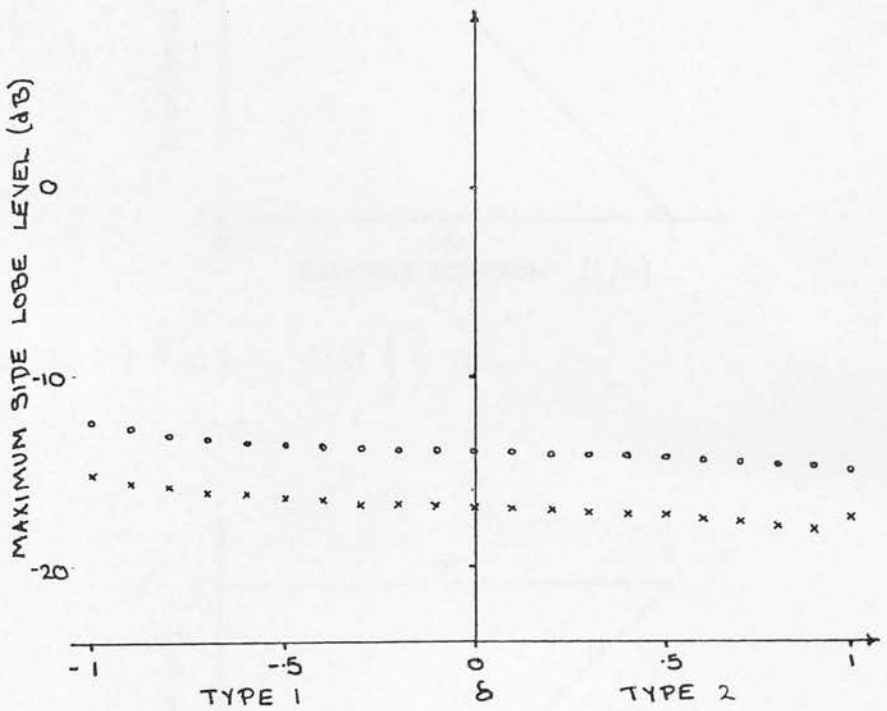

Figure 2.21: Apodisation (ω_i) vs. relative position (i/n) for extreme values of δ (equal area rings).

(d) Type 1, (i) δ = 0.0, (ii) δ = -1.0,

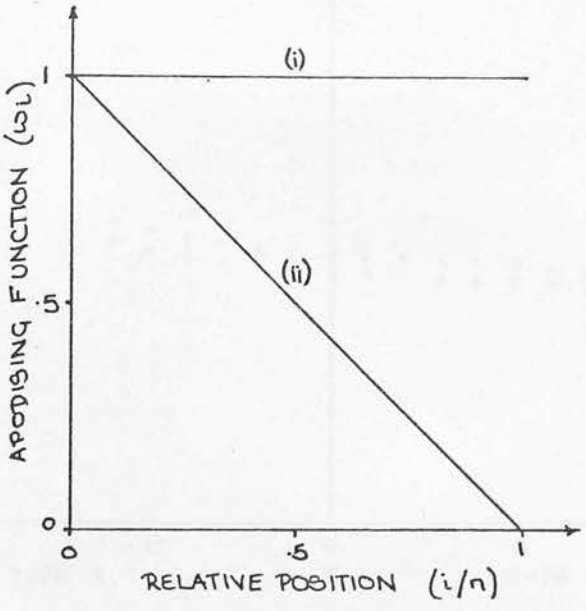

(e) Type 2, (i) δ = 0.0, (ii) δ = 1.0.

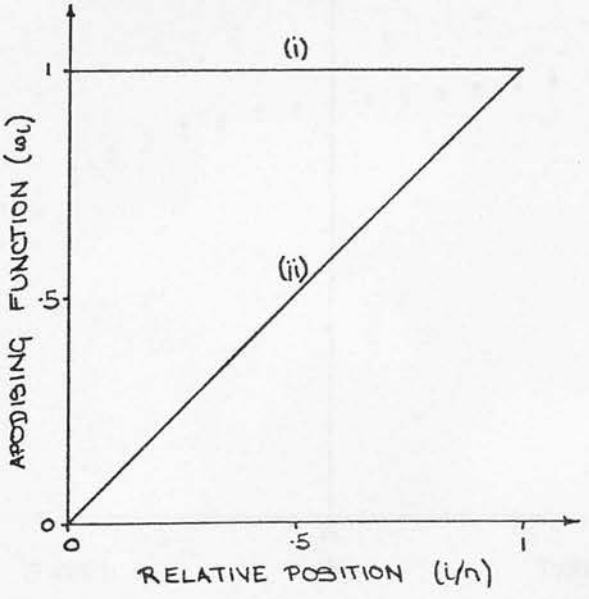

Figure 2.22: Effect of apodisation on array focal plane response (equal width rings; types 1 and 2).

(a) -15dB main lobe half width vs. δ .

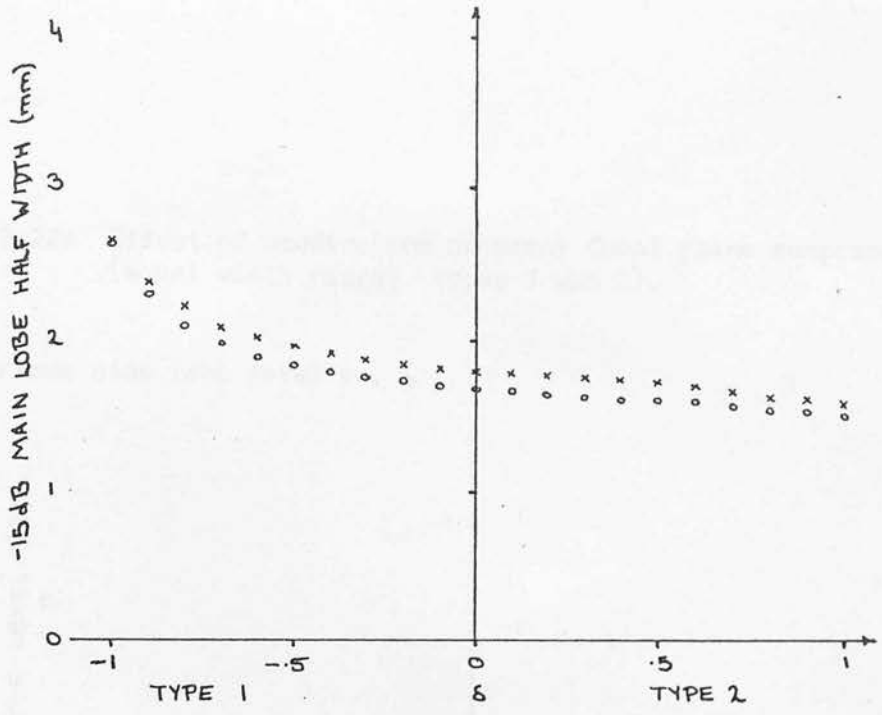

(b) 1st side lobe level vs. δ .

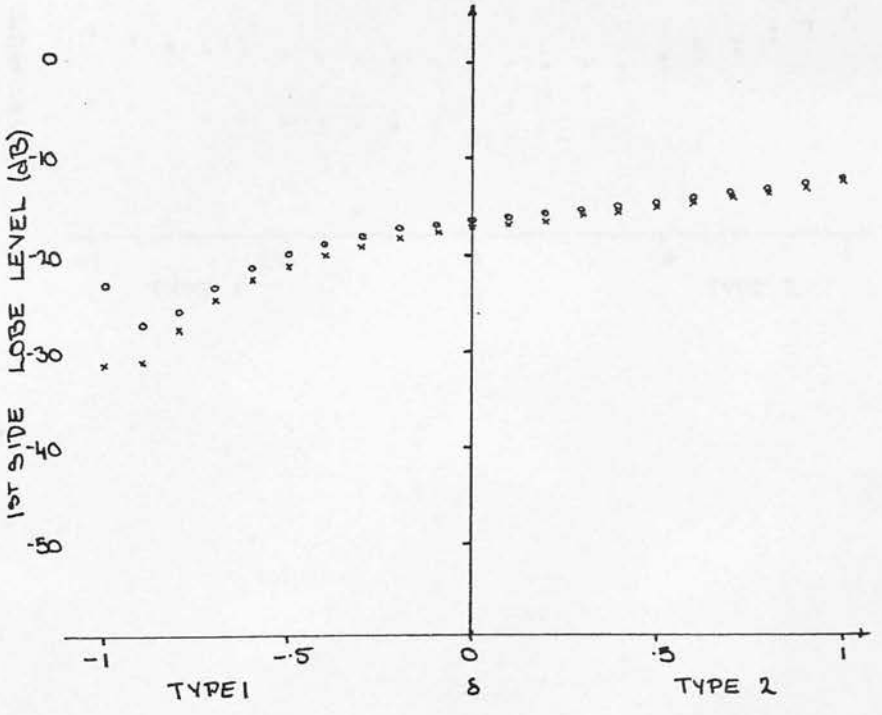

Figure 2.22: Effect of apodisation on array focal plane response (equal width rings; types 1 and 2).

(c) maximum side lobe level vs. δ .

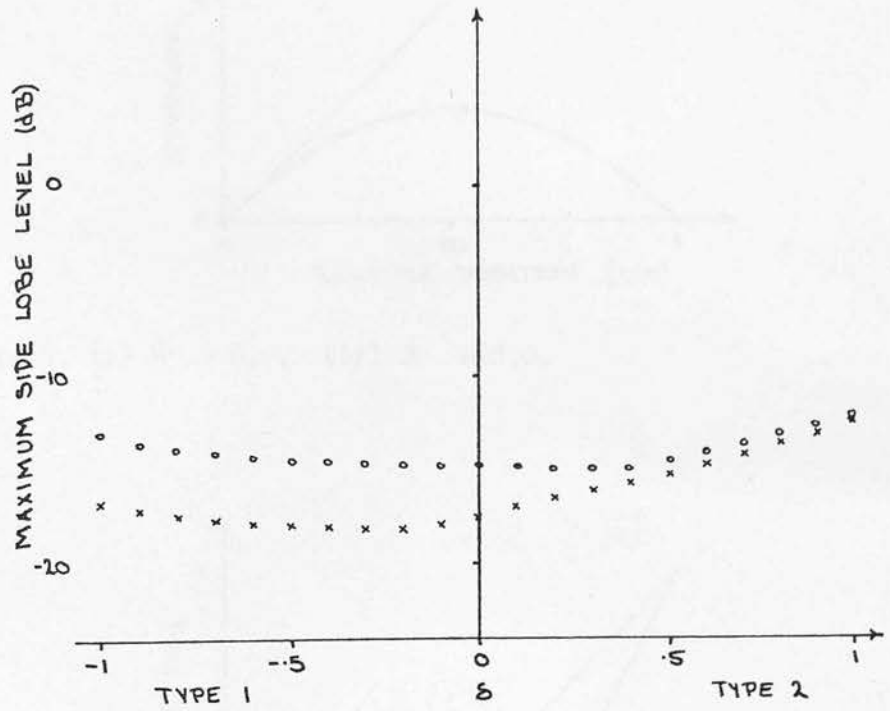

Figure 2.22: Apodisation (ω_i) vs. relative position (i/n) for extreme values of δ (equal width rings).

(d) Type 1, (i) δ = 0.0, (ii) δ = -1.0,

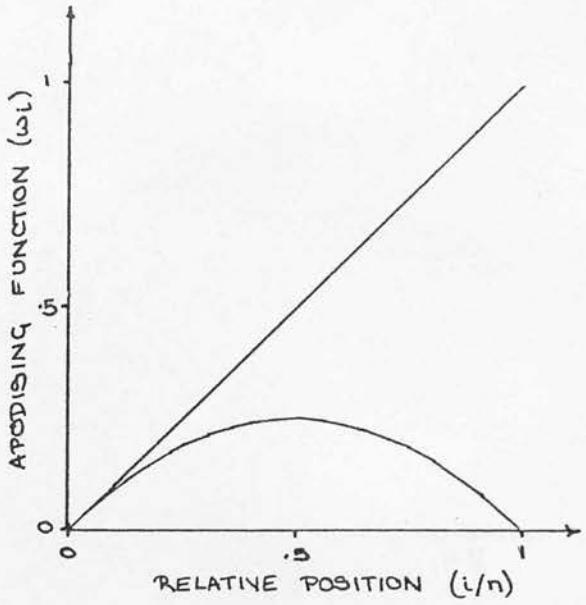

(e) Type 2, (i) δ = 0.0, (ii) δ = 1.0.

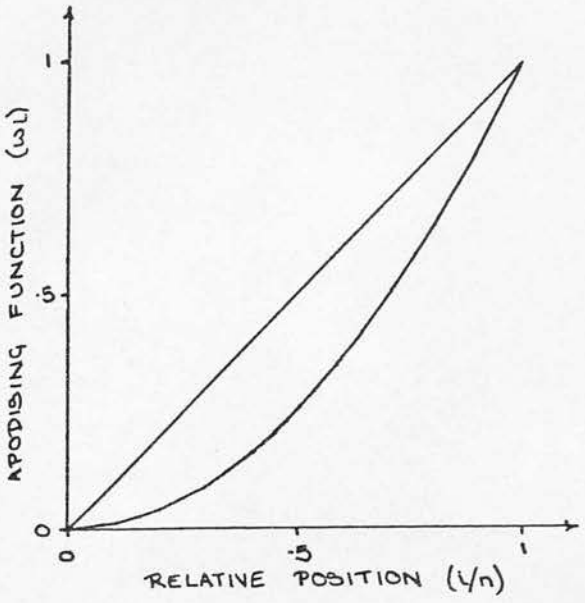

Figure 2.23: Effect of apodisation on array focal plane response (equal area rings; type 3).

(a) -15dB main lobe half width vs. δ .

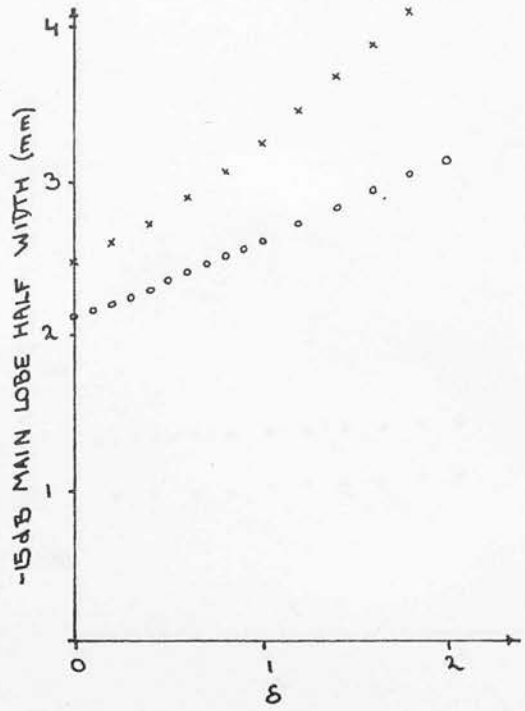

(b) 1st side lobe level vs. δ .

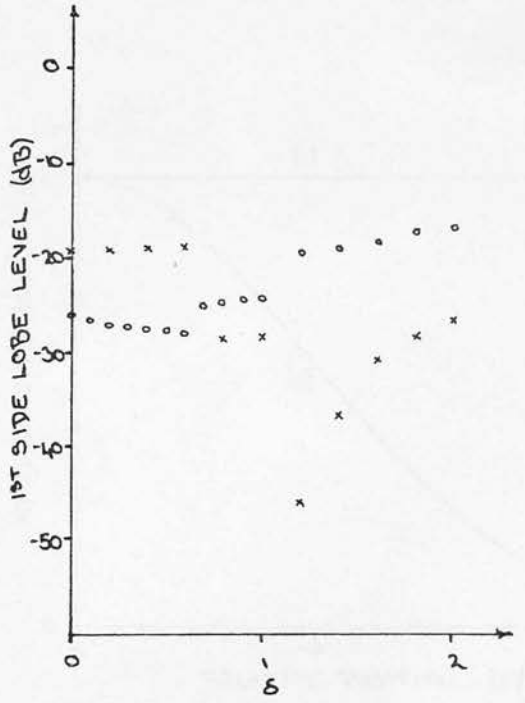

Figure 2.23: Effect of apodisation on array focal plane response (equal area rings; type 3).

(c) maximum side lobe level vs. δ .

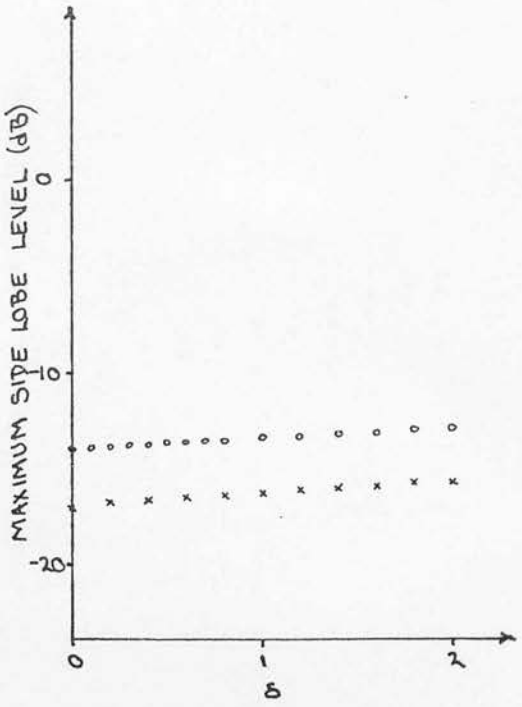

(d) apodisation (ω_i) vs. relative position (i/n) for extreme values of δ , (1) δ = 0.0, (ii) δ = 2.0.

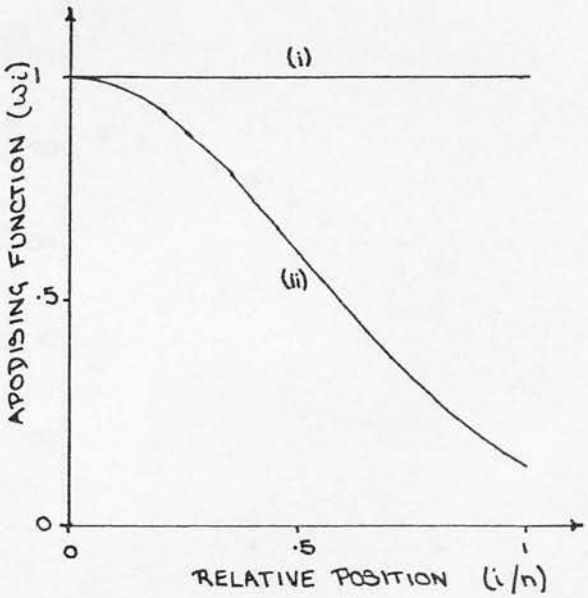

Figure 2.24: Effect of apodisation on array focal plane response (equal width rings; type 3).

(a) -15dB main lobe half width vs. δ .

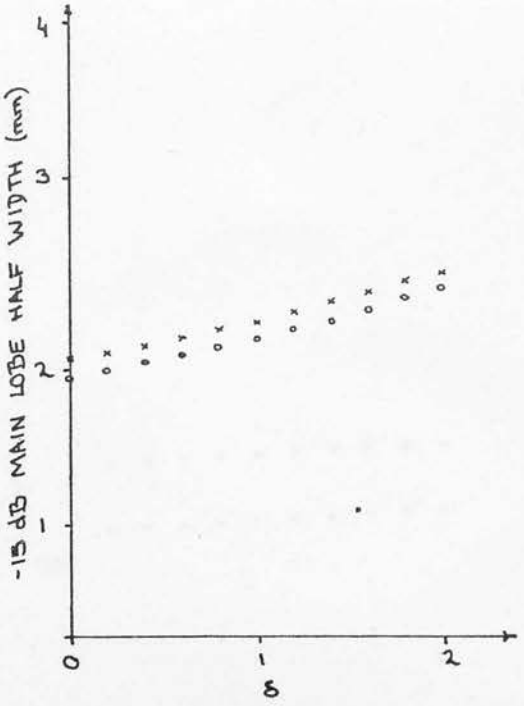

(b) 1st side lobe level vs. δ .

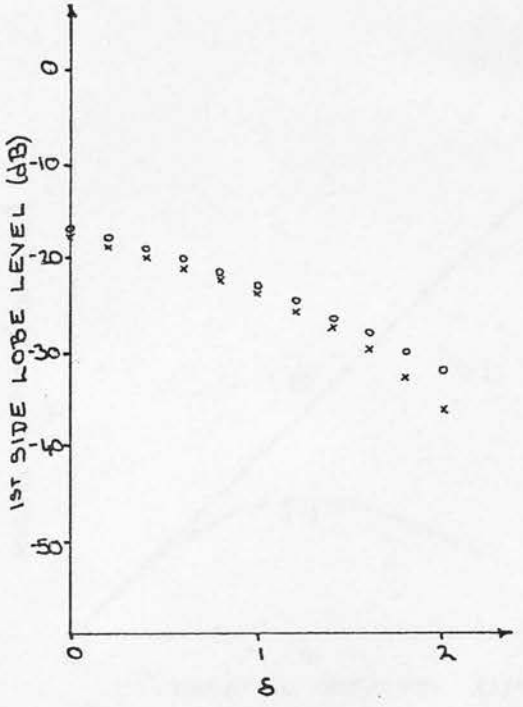

Figure 2.24: Effect of apodisation on array focal plane response (equal width rings; type 3).

(c) maximum side lobe level vs. δ .

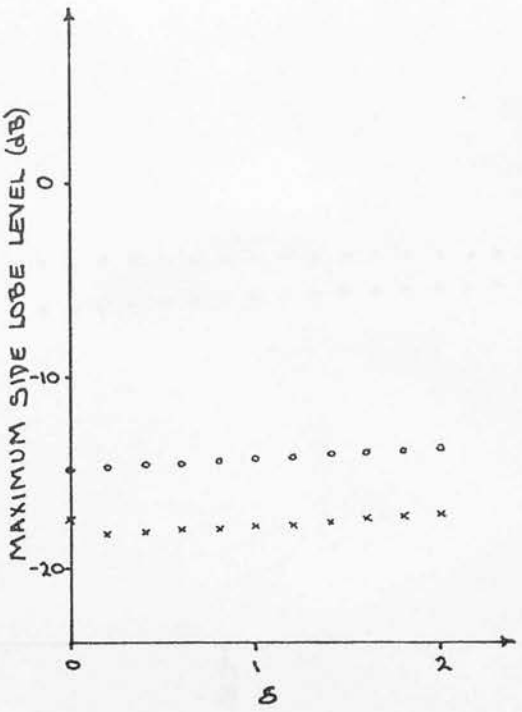

(d) apodisation (ω_i) vs. relative position (i/n) for extreme values of δ . (i) δ = 0.0, (ii) δ = 2.0.

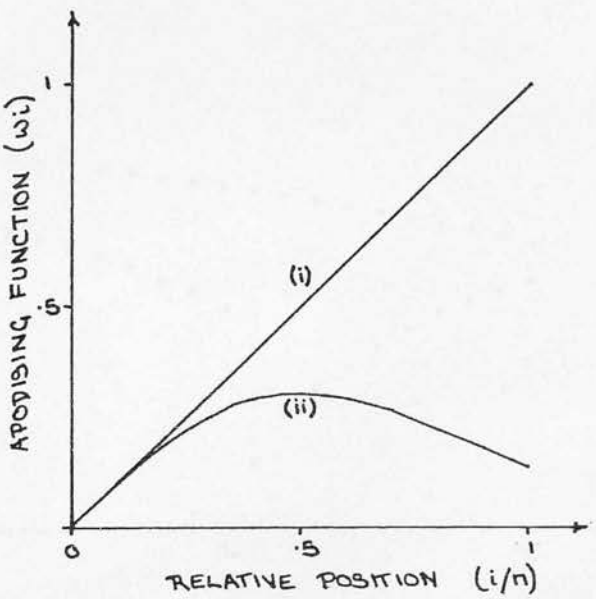

Figure 2.25: Effect of apodisation on array focal plane response (equal area rings; type 4).

(a) -15dB main lobe half width vs. δ .

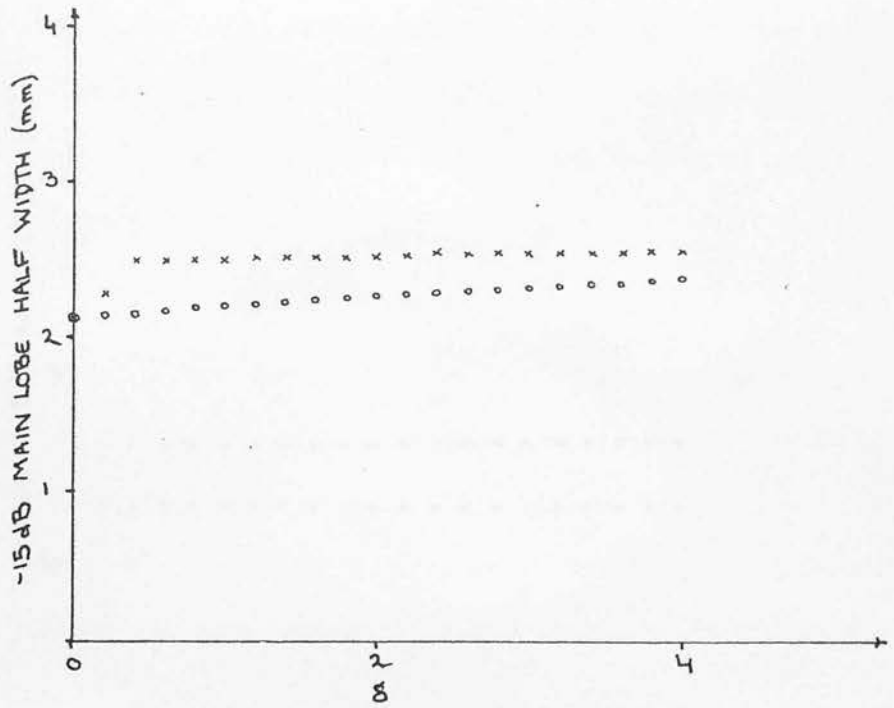

(b) 1st side lobe level vs. δ .

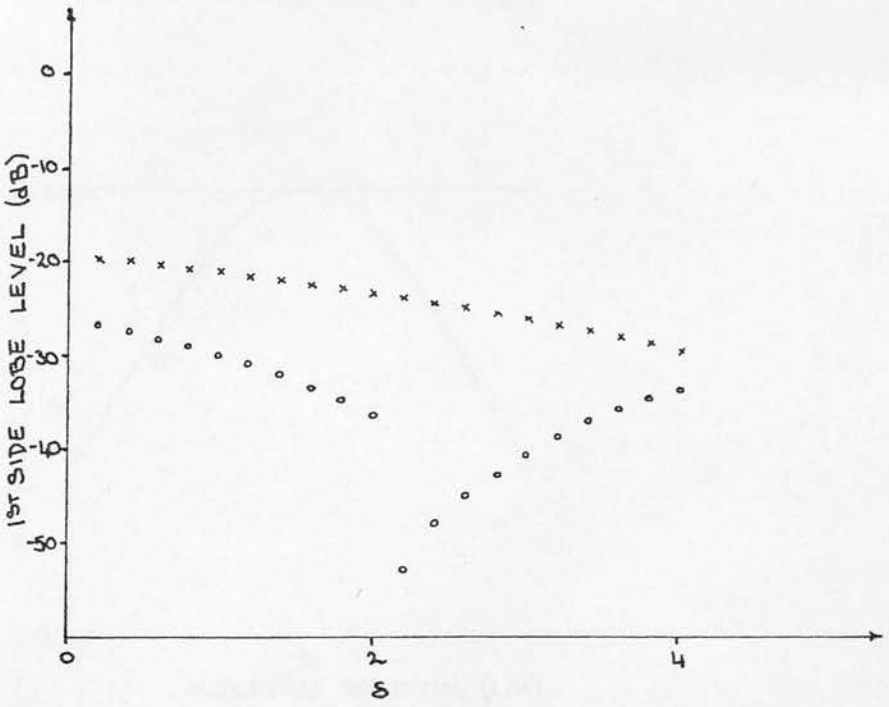

Figure 2.25: Effect of apodisation on array focal plane response (equal area rings; type 4).

(c) maximum side lobe level vs. δ .

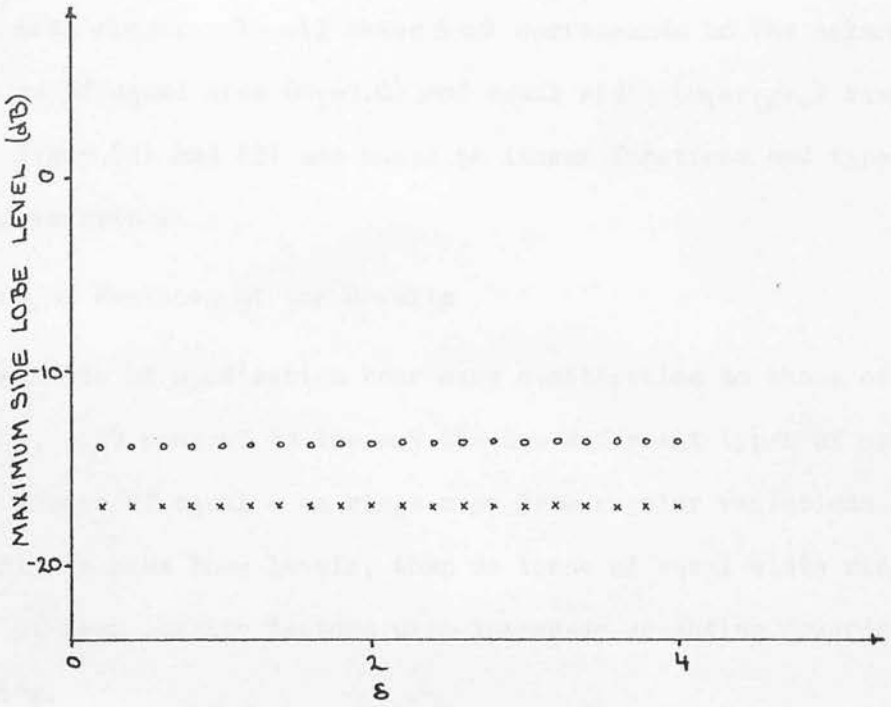

(d) apodisation (ω_i) vs. relative position (i/n) for extreme values of δ , (i) δ = 0.0, (ii) δ = 4.0.

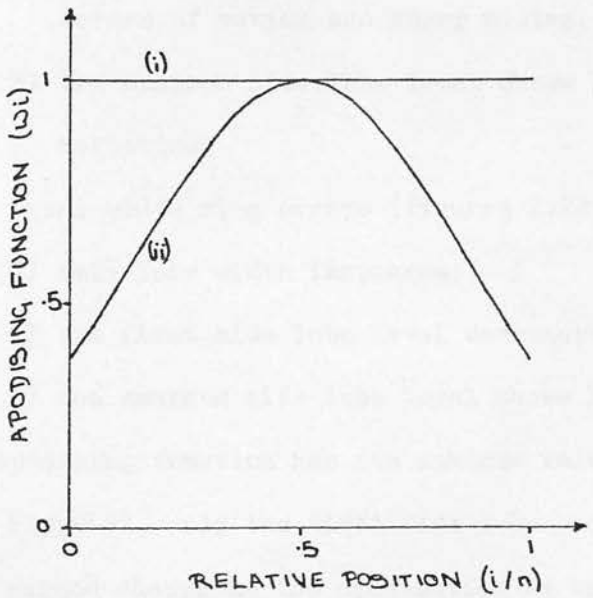

apodisation would become:

$$\omega_i = \frac{r_i}{r_n} \cdot \left(\delta \frac{r_i}{r_n} + 1 \right)$$

when applied to equal width rings. Type (4) has only been investigated for equal area rings. In all cases $\delta = 0$ corresponds to the natural apodisations of equal area ($\omega_i = 1.0$) and equal width ($\omega_i = r_i/r_n$) ring arrays. Types (1) and (2) are based on linear functions and types (3) and (4) on Gaussian.

2.7.3.1 Major Features of the Results

The effects of apodisation bear many similarities to those of ring arrangement, with respect to the way the two different types of array behave. Arrays of equal area rings show less regular variations, particularly in side lobe levels, than do those of equal width rings. Variation of beam quality factors with increased weighting towards the array centre.

(a) Equal area ring arrays (figures 2.21 and 2.23):

1) main lobe width increases;
2) the first side lobe level passes through a series of maxima and sharp minima;
3) the maximum side lobe level shows little variation.

(b) Equal width ring arrays (figures 2.22 and 2.24):

1) main lobe width increases;
2) the first side lobe level decreases monotonically;
3) the maximum side lobe level shows little variation.

When the apodising function has its maximum value at the mean radius of the array (type 4), only the first side lobe level of the 4 ring array shows any marked change as the apodisation is varied, (figure 2.25).

These features are very similar to the effects of varying the ring arrangement about the array's mean radius, see Section 2.7.2.1.

2.7.3.2 General Discussion

As has already been noted for variations in ring arrangement, where the major portion of the active area of the array is towards its centre, (i.e. rings arranged closer to the centre, or higher weighting of central rings), energy from this region is less well localised about the central axis and so the beam width increases. From investigations on the effects of number of rings (evenly spaced) it was observed that the maximum side lobe level occurs at the first off-axis point where side lobe contributions from each ring are most closely "in phase" as radial distance increases. Hence, if the contribution to the maximum side lobe is reduced from any given ring, the contribution to the main lobe will be reduced by a similar factor. Because contributions from each ring are added, the maximum side lobe level relative to the main lobe (i.e. in dB) changes only gradually.

The first side lobe is formed by a more complicated pattern of positive and negative contributions and may lie within the main lobe of inner ring contributions. Its more complex formation makes its variatio more difficult to predict and is reflected in the greater variations observed in its level. The pre-weighting effects of the "natural" apodisation of equal width rings has a similar effect on the response to further apodisation as it does to variations in ring arrangement, i.e. to reduce the effect of a given apodising function and particularly to make variations in first side lobe level more predictable.

2.7.3.3 Implications for Array Design

Lower side lobe levels with main lobe width improvement, or only slight degradation, are possible by apodising the array aperture. For

example, with type (1) apodisation applied to equal area ring arrays, marked minima in first side lobe level occur, with some degree of main lobe narrowing. Unfortunately, for equal width rings, decreasing side lobe levels are always associated with increasing main lobe width and a favourable compromise is less easy to find.

2.8 Summary

The ultrasonic field has been considered from a theoretical view point. The relationship between pulsed and continuous wave fields has been investigated using constructions found in the literature. A suite of programs to solve the equations defining the ultrasonic field for a given shape and excitation of radiator has been described. A detailed investigation of the effects of the radiator for annular arrays has been performed and the results of this are summarised below. Other practical considerations are involved in array design. These have not been considered here but appear in the next chapter on the design and construction of a prototype array. Many of the results on array design from this chapter were not available when the prototype was manufactured. It is, however, intended to test them in future arrays.

2.8.1 Summary of the Effects of Number of Rings, Ring Arrangement and Apodisation

(1) A reasonable approximation to a filled aperture is obtained using only 4 or 5 rings. Limiting values are approached by arrays of 10 rings.

(2) Any increase in the dominance of the outer region of the array relative to the centre, either by increasing the relative number of rings in that region or by increased weighting, will reduce the main lobe width. Improvement is

found only for a particular direction of change of apodisation or ring arrangement.

(3) For arrays of equal area rings the first side lobe passes through a series of maxima and minima. Values are found which offer an improvement over standard arrangements in both first side lobe level and main lobe width.

(4) For equal width ring arrays the first side lobe level changes almost monotonically in a direction opposite to the variation in main lobe width. An improvement in both parameters at once is not possible. However, a marked improvement in first side lobe level is noted in one case for only a slight degradation in main lobe width.

(5) Maximum side lobe level may generally be ignored unless very long pulses are used in the system.

2.8.2 Equal Width Versus Equal Area Rings

Although the above investigations have been conducted as if applied to equal width ring arrays and equal area ring arrays, in fact, the specific dimensions of the rings are unimportant, so long as they appear narrow, as the effects of their dimensions can be simulated electronically, to reproduce the desired geometrical effect. The decision on ring width may be left to be determined by other criteria, (Section 3.3.1.6).

2.8.3 Apodisation Versus Ring Arrangement

Improvement in the ultrasonic beam quality is possible by using either an apodising function or by an appropriate arrangement of rings within the aperture. Further improvement of the beam produced by a

useful ring arrangement, by apodisation of the aperture, would need further investigation. An ultrasonic transducer is an expensive item and once fabricated it cannot be easily modified. Any chosen pattern of rings is fixed for the life of the transducer. Apodisation, however, which is electronically implemented, is simple to alter and adjust. The gains which accrue from its use are at least equal to those possible by altering the ring pattern. The use of apodising functions to tailor the beam shape would, therefore, appear to be a better method. This also allows the maximum distance to be maintained between each ring and so minimise cross talk, (Section 3.3.1.7).

Chapter 3

THE DESIGN AND CONSTRUCTION OF ANNULAR ARRAYS

The design of a simple single crystal ultrasonic transducer involves relatively few decisions compared to that of an annular array.

3.1 Introduction

Ultrasonic transducers have gradually increased in complexity as the use of ultrasound has become more wide-spread. Plane single element transducers have developed through fixed focus transducers, into today's multi-element arrays. One dimensional arrays are now commonplace. These are connected to sophisticated electronic packages which effectively steer the ultrasound beam and provide swept focusing. (One dimensional arrays are linear or "phased" arrays, and annular arrays if the radial co-ordinate is considered as the one dimension.) Two dimensional arrays allowing beam steering and focusing in both lateral dimensions have been reported as experimental systems at an early stage of development.

The increased complexity of arrays implies that a greater number of parameters must be defined in their design than for single crystal transducers. A number of authors have published design procedures for annular arrays, Melton and Thurstone (1978) and Dietz et al. (1979). Other authors have considered the design of linear phased arrays which share some similar problems, (Vogel et al.(1979)). However, design procedure is central to array production and so a detailed discussion is given in Section 3.3.

3.2 Format of Chapter

The chapter is split into two sections, the first covering design procedure, and the second, manufacturing techniques. The section on design is further sub-divided. Firstly, the general design of annular

arrays is considered and certain design criteria are developed. These are then applied to the design of an array which fulfils the aims of the project laid out in Chapter 1. The chapter concludes with a specification for the array used to obtain the experimental results presented in Chapter 5.

3.3 Array Design

3.3.1 Design Procedure

The procedure for the design of an annular array is summarised by the flow diagram, figure 3.1. Although the procedure is shown as a steady progression from one stage to the next, in practice this is not always the case. Certain decisions may give rise to impractical or conflicting requirements at a later stage. The process must then be repeated a number of times with different initial values until an acceptable compromise is achieved.

Apodisation and signal processing have been included in the diagram. Although they are not part of the transducer itself, when performed electronically, they are closely associated with it. Similar theoretical techniques have been used to investigate their effects and have been discussed in Chapter 2.

3.3.1.1 Use

Before any other factor may be considered, the area of clinical application for the transducer must be clearly defined. Preferably this should be done in consultation with those who will eventually use the machine and after observation of current techniques.

3.3.1.2 Range

This is unambiguously defined once the area of clinical application has been decided upon. The only modifying factor is the possibility of

Figure 3.1: Annular array design, flow diagram.

DOTTED LINES INDICATE ONLY A WEAK INFLUENCE OF ONE DECISION ON THE NEXT.
* - PARAMETERS REQUIRED FOR ACTUAL ARRAY MANUFACTURE.

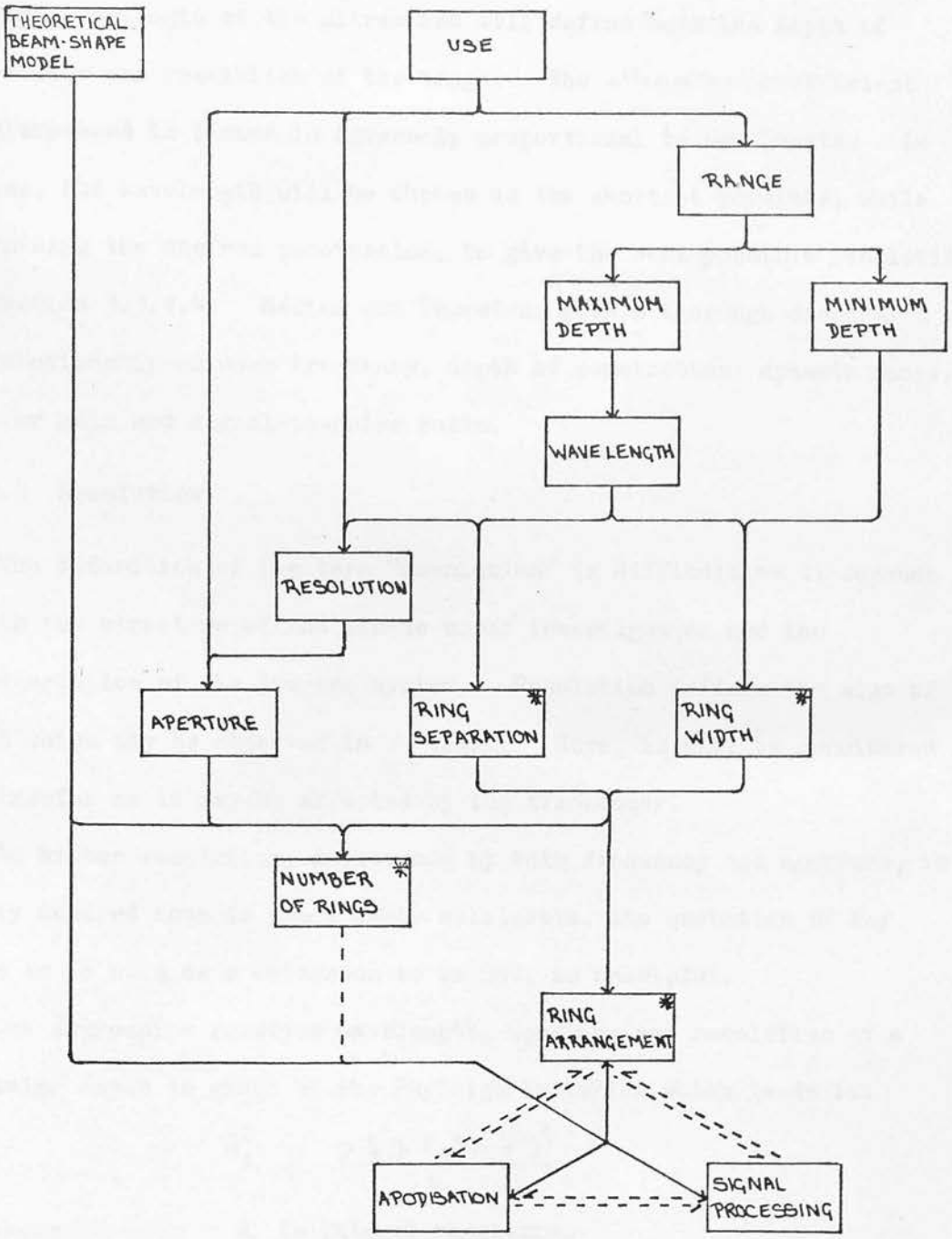

using a stand-off water bath. This may be considered where access to the site of interest is difficult possibly because of a large aperture array, or for other reasons discussed later in Section 3.3.1.6.

3.3.1.3 Wavelength

The wavelength of the ultrasound will define both the depth of penetration and resolution of the image. The attenuation coefficient for ultrasound in tissue is inversely proportional to wavelength. In general, the wavelength will be chosen as the shortest possible, while maintaining the desired penetration, to give the best possible resolution, see Section 3.3.1.4. Melton and Thurstone give a thorough discussion of the relationship between frequency, depth of penetration, dynamic range, receiver gain and signal-to-noise ratio.

3.3.1.4 Resolution

The definition of the term "resolution" is difficult as it depends on both the structure of the tissue under investigation and the characteristics of the imaging system. Resolution defines the size of detail which may be observed in an image. Here, it will be considered only insofar as it may be affected by the transducer.

As higher resolution, influenced by both frequency and aperture, is usually desired than is practicably attainable, the quotation of any figure to be used as a criterion to be met, is unhelpful.

One expression relating wavelength, aperture and resolution at a particular depth is given by the Rayleigh Criterion which leads to:

$$d_l = \frac{0.6\lambda (a^2 + z^2)^{\frac{1}{2}}}{a}$$

where d_l is lateral resolution
λ is wavelength
a is radius of the aperture
z_f is focal length

This expression applies to the CW focal plane response of a lens. In practice, λ is usually defined by the maximum depth of penetration z_2 (Section 3.3.1.3), and a, by the site of application (Section 3.3.1.1).

3.3.1.5 Aperture

Although aperture will be defined if a specific resolution is sought at a given wavelength, it has already been stated that practical considerations of size in relation to use, are more important.

3.3.1.6 Ring Width

When designing an annular array it is important that the ring widths fulfil a number of criteria if maximum sensitivity is to be obtained from the array over the complete range of interest. The path difference δ, (figure 3.2) between the inner and outer edges of the ring to an on-axis point z, is given by

$$\delta \simeq \frac{w r_i}{(r_i^2 + z^2)^{\frac{1}{2}}}$$

$$\simeq \frac{w r_i}{z} \qquad \text{for} \qquad z \gg r_i$$

If δ exceeds 0.5λ, the sensitivity of the array towards the point z, is reduced. In order to maintain an even sensitivity towards all on-axis points of interest, the width of the ring should be such that $\delta \leq 0.5\lambda$ for $z_1 > z > z_2$ (where z_1 is the minimum depth of interest). The point z_t, at which $\delta = 0.5\lambda$ is the near-field/far-field transition distance for the ring. It is, therefore, desirable to use only the far-field of any given ring.

The sensitivity of the ring towards an on-axis point $z \gg z_t$, is given approximately by:

$$\text{sensitivity} \propto \delta$$

$$\propto \frac{w r_i}{r_n}$$

Figure 3.2: Maximum contribution from i^{th} ring at z, only if $\delta \leq 0.5\lambda$.

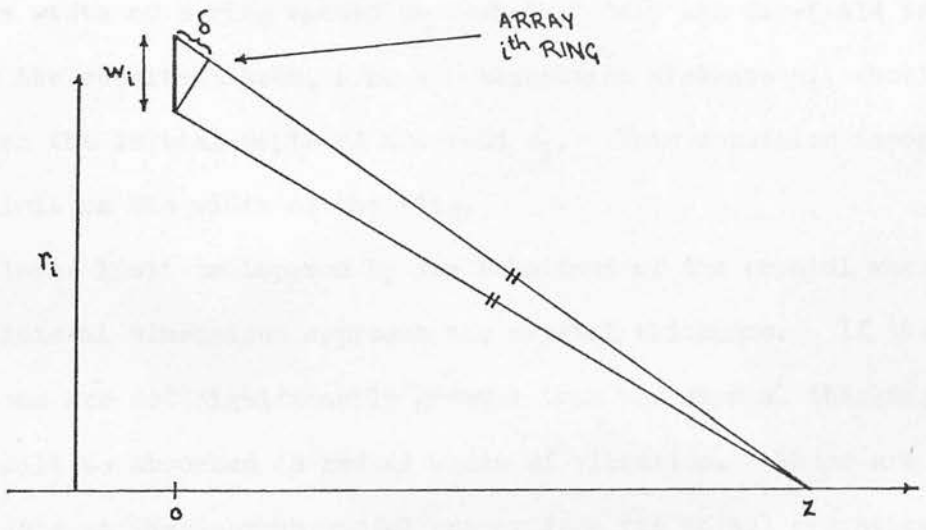

For large z, this function is approximately constant over diagnostic ranges and so the relative sensitivities of individual rings maintain a fixed relationship.

The transmitted pulse shape in the far-field suffers less "diffraction distortion" than in the near-field. Aligning pulses from separate rings in a swept focus is therefore easier in this region. The approximation used in defining the sweep function, that the transmitted pulse originates at the array's centre, see Section 4.2.4.1, is more reasonable.

The width of a ring should be such that only its far-field is used to form the resultant beam, i.e. its transition distance z_t, should be less than the initial depth of interest z_1. This condition imposes an upper limit on the width of the ring.

A lower limit is imposed by the behaviour of the crystal when any of its lateral dimensions approach the crystal thickness. If these dimensions are not significantly greater than the crystal thickness then energy will be absorbed in radial modes of vibration. These are undesirable as they absorb useful energy from the normal operating mode. They may also introduce unwanted frequency components into the transducer response. In this case, as these are usually of low frequency, they may be filtered out by the receiver electronics. An arbitrary lower limit is placed on the ring width of one wavelength, or twice the crystal thickness, as the crystal is usually operated as a half wave resonator. Dietz et al. (1979) have used a width-to-thickness ratio of 0.6, which is lower than this.

3.3.1.7 Ring Separation

A number of methods may be used to separate individual rings and isolate them acoustically and electrically.

(1) The array may be formed from individual crystal annuli separated by an acoustic and electric insulator which also holds them in place.

(2) It may be machined from a single disc by forming grooves between the annuli. The rings are then defined electrically and mechanically on only one side of the crystal.

(3) The rings may be defined only on the surface of the transducer by a suitable electrode pattern. Acoustic isolation between rings is provided by the crystal material itself.

The degree of isolation between rings varies over the three methods, as does the probability of exciting radial modes of vibration. Capacitive coupling between rings will be similar in all three cases. Acoustic isolation may vary considerably, being greatest in (1) and least in (3). Radial modes of vibration are least likely to occur where the mechanical extent of intact crystal is greatest, i.e. in (3).

All three methods of fabrication were attempted to produce arrays for use in this project. In both cases (1) and (2) where the integrity of the disc was broken the transmitted pulses from individual rings were observed to be unacceptably long. Using method (3) short pulses similar to those from commercial transducers could be obtained. Using techniques similar to those for producing printed circuit boards, accurate reproducible array patterns could be obtained (Section 3.4).

Where the fabrication technique leaves the array "disc" partially or wholly mechanically intact, i.e. (2) and (3), the separation of the rings becomes particularly important in defining the "cross talk" between them. Cross talk between channels will introduce an out of phase component into the signal from each, which will not be correctly

accounted for by the swept focusing electronics. This will reduce the focusing effect of the array. An arbitrary value of one wavelength is defined as a minimum ring separation for a wholly intact disc. This is similar to the minimum value for ring width. Values for cross talk between rings are given at the end of this chapter.

3.3.1.8 Number of Rings

The effects which number of rings has on the quality of focus which the array produces have been investigated theoretically in the previous chapter (Section 2.7.1). From these results a suitable number of rings may be chosen. The model used in this investigation considers rings to be infinitesimally narrow and so any number may be fitted within a given aperture. In practice rings are of a finite width and should have a finite separation (Sections 3.3.1.6 and 3.3.1.7). The number which may be placed within a given aperture is strictly limited. Within an aperture of radius a, the maximum number of contiguous equal area rings is given by:

$$n_{max} \leqslant \frac{a}{2w_{min}}$$

where w_{min} is the minimum ring width as defined in Section 3.3.1.6.

If the rings are instead, all defined to be of equal width w_{min}, then the maximum number of contiguous rings is increased to:

$$n'_{max} \leqslant \frac{a}{w_{min}}$$

If the rings are not contiguous but have a minimum separation w_{min}, as discussed in the previous section, then the minimum number of rings is reduced, in the latter case to approximately $0.5n'_{max}$, and in the former case to slightly greater than $0.5n_{max}$, the actual value being between n_{max} and $0.5n_{max}$. The results of the previous chapter may need to be modified in the light of these constraints where they suggest larger numbers of rings than may actually be accommodated.

3.3.1.9 Ring Arrangement and Apodisation

These have already been considered in the previous chapter. In a similar way to number of rings, ring arrangements may be affected by the finite width and separation of real rings.

3.3.2 Design of a Prototype Array

The aims of this project have been defined in Section 1.6. In order to investigate and evaluate annular array fabrication and swept focusing techniques an initial project on the design and evaluation of a contact B-scan swept focusing system was proposed. This would also allow confirmation of the theoretical model, enabling it to be applied with confidence in future designs. The eventual aim was the incorporation of an array into a mechanical real-time abdominal scanner.

The abdomen was chosen as the "target" site for investigation using the prototype system. This was for three reasons:

(1) eventual incorporation in an abdominal scanner;

(2) ease of accessibility, particularly for relatively large aperture arrays;

(3) local expertise and experience in general abdominal scanning.

Because of their relatively large diameter, annular arrays are often designed for use in conjunction with a water bath, (Kossoff (1975) and Melton and Thurstone). This also facilitates location of the transition distances of individual rings prior to the initial depth of interest. The intention that this array be a precursor of one fitted into a real-time head precluded this idea. In abdominal scanning the range of interest extends from approximately 10 to 200 mm under the skin's surface. Routine clinical practice suggests that 3.5 MHz is the highest frequency which will give this degree of penetration. This corresponds to a wavelength in tissue of about 0.44 mm.

To obtain a resolution of 0.5 mm midrange, i.e. at 100 mm depth, an aperture of about 62 mm would be required (Section 3.3.1.4). For a contact scanner this is clearly impracticable. The maximum transducer diameter useable in a contact transducer is about 30 mm. The prototype array was designed around a 30 mm diameter piezo-electric crystal. The overall diameter of the transducer is 36 mm and that of the active area is 24 mm. As this is a prototype array, effort was not put into obtaining the maximum active area for a given transducer diameter. The resolution, defined by the Rayleigh Criterion for a 24 mm diameter, 3.5 MHz radiator focused at various depths, is given in Table 3.1. Certain criteria which define maximum and minimum ring widths have been identified in Section 3.3.1.6. A 3.5 MHz, PZT-5A ceramic crystal has a thickness of about 0.5 mm when operating as a half-wave resonator. The minimum allowable ring width is therefore 1 mm. A ring of minimum width, located at the maximum radius of the aperture, i.e. 12 mm, has a transition distance z_t, of about 51 mm. Clearly this does not fulfil the condition that z_t be less than z_1, the initial depth of interest. It is not generally possible to fulfil this condition for a contact scanner and it is for this reason that a water bath is often used. In order to reduce fluctuations in sensitivity in the axial response of the array caused by having the transition distances of several rings within the range of interest, it was decided to stagger the z_t's of each ring to produce as smooth as possible a resultant response from their combination. Figure 3.3 shows the reception sensitivity responses of a series of evenly spaced annuli with a maximum radius of 12 mm excited with a short pulse of ultrasound. These results were obtained using the beam simulation programs introduced in Chapter 2. A number of such plots were considered and the optimum was that in which each ring has its minimum width, i.e. 1 mm. The combined reception

Table 3.1 Resolution (defined by the Rayleigh criterion) vs. depth, for a 3.5 MHz, 24 mm diam. radiator focused at each depth.

Depth (mm)	Resolution (mm)
20	0.5
50	1.1
100	2.2
150	3.3
200	4.4

Figure 3.3: Theoretical axial transmission or reception responses of individual rings, (a) ring 1, (b) ring 2, (c) ring 3, (d) ring 4.

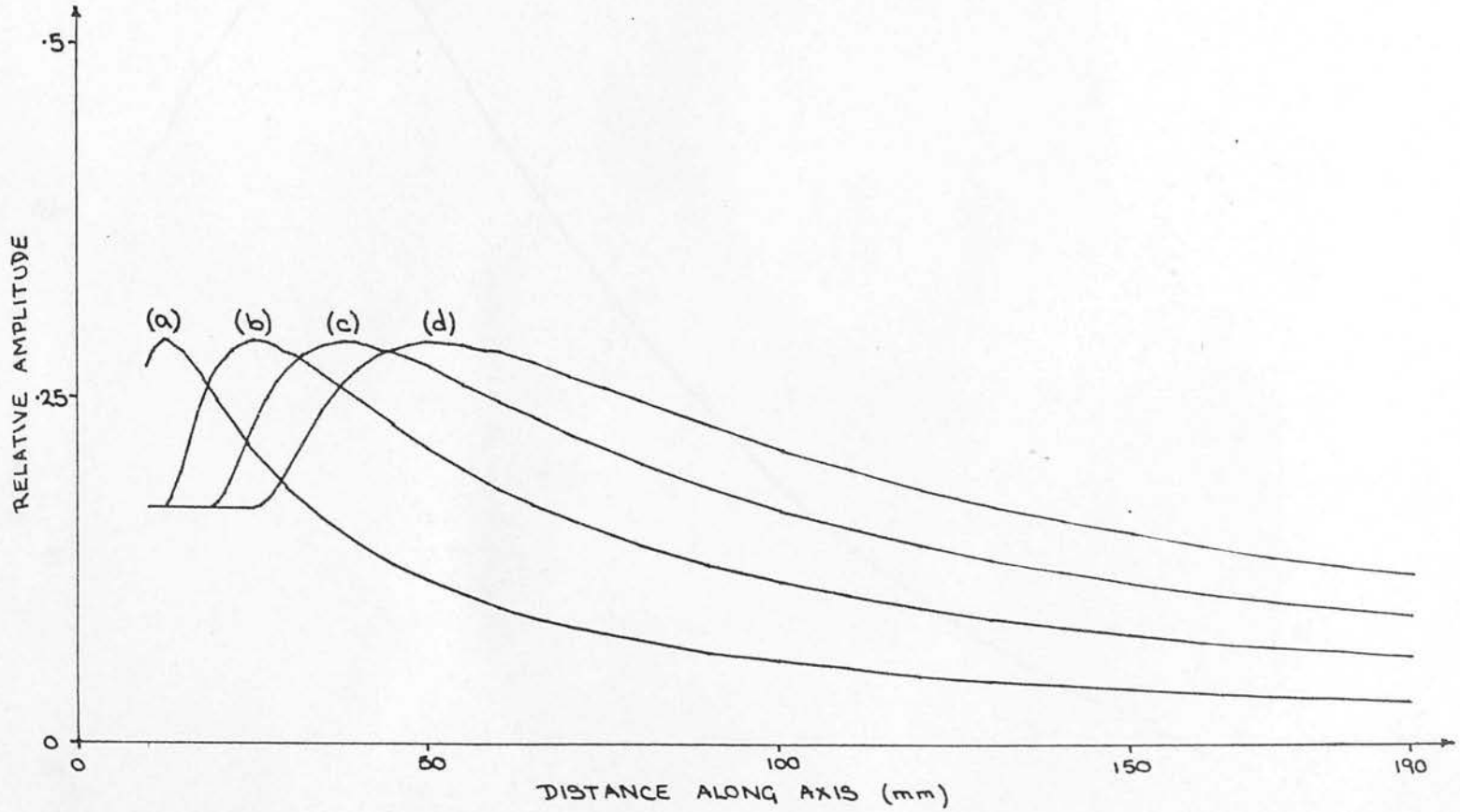

Figure 3.3 (e): Combined response assuming a swept focus.

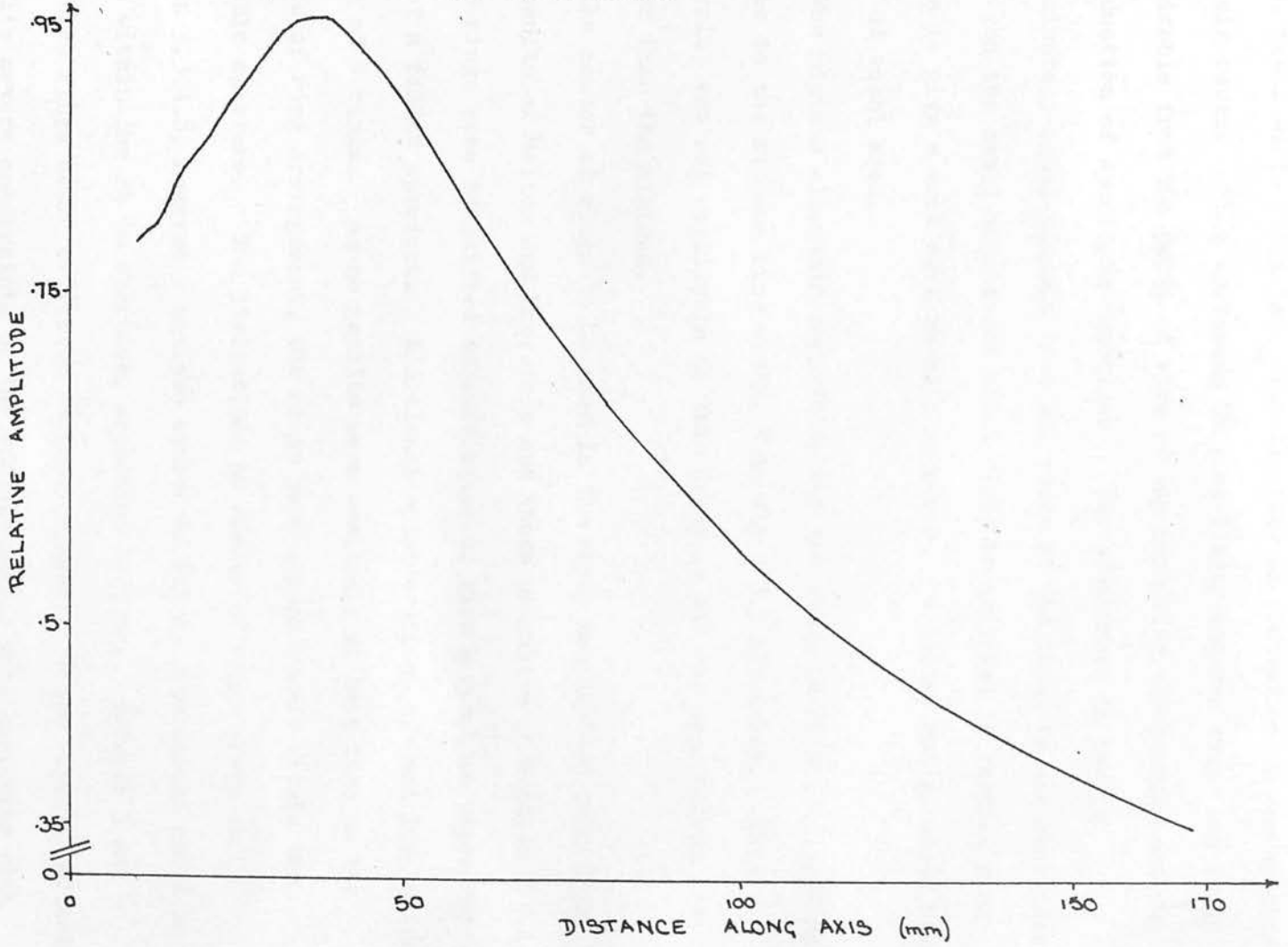

response of the rings assuming a swept focus is given in figure 3.3(e). The overall variation in sensitivity is $\pm$ 5 dB.

Sensitivity is proportional to area for $z \geqslant 2z_t$. In the far-field, equal width rings have sensitivities in proportion to one another as their radii. This variation of sensitivity between rings was found undesirable from the point of view of the receiving electronics and the introduction of apodising functions. The advantages to having approximately equal signals from all rings at the input to the receivers outweighs the small advantages which might be achieved by varying ring widths to give a more even on-axis response. A better design would have rings of equal area.

The minimum allowable separation for the rings (Section 3.3.1.7) is similar to the minimum ring width, 1 mm for a 3.5 MHz array. This constraint was not applicable to this array as all the separations are greater than the minimum.

The number of rings to be used in the array was decided upon from the results of Melton and Thurstone and those presented in Section 2.7.1. 4 or 5 rings were identified as sufficient to give a response approaching that of a filled aperture. Additional considerations of cost led to the choice of 4 rings. As no results were available at that time on the effects of ring arrangement, the rings were spaced evenly within the available aperture. The limitations on number of rings given in Section 3.3.1.8, suggest a maximum number of 6x1 mm wide annuli could be placed within the 24 mm aperture, separated by 1 mm. Between 3 and 6 equal area rings could be fitted suitably spaced. These figures indicate the quite severe constraints on the useable number when designing with relatively small array apertures.

3.4 Array Manufacture

The design and manufacture of simple single crystal transducers has been given by Bow (1979) based on backing and waveplating considerations published by Kossoff (1966) and Posakony (1975). This method, with slight modifications, has been used to produce annular array transducers with appropriate backing material and a quarter wave matching layer. Figure 3.4 shows the general construction of a prototype array.

The backing material is a mixture of Flexane 95 (Devcon Ltd), a two part room temperature vulcanising rubber compound, and tungsten powder, centrifuged down onto the back of the crystal. The quarter wave matching layer is a mixture of tungsten powder and Araldite MY753 potting compound (Ciba-Geigy Ltd.) machined and then lapped to the correct thickness. The crystal material is PZT-5A piezo-electric ceramic. Prototype arrays were formed from 30 mm diameter discs which had both sides silvered. Three methods of forming the actual array from the basic crystal were attempted. These have already been discussed in Section 3.3.1.7 and method (3) was the one used.

The crystal itself is left mechanically intact, the array being defined by etching away the electrode in the appropriate pattern on both sides. Small joining sections of the electrode are left between annuli on one side which forms the common or "ground" electrode. Fine insulated wires are soldered to the edges of the rings on the reverse side to carry the necessary signals. It is this side which eventually faces into the backing material.

The array is produced in a manner similar to the production of printed circuit boards. The crystal is first dipped into an ultra-violet sensitive etch resist lacquer, Kodak KPCR. When this is dry it is

Figure 3.4: Schematic of annular array transducer construction.

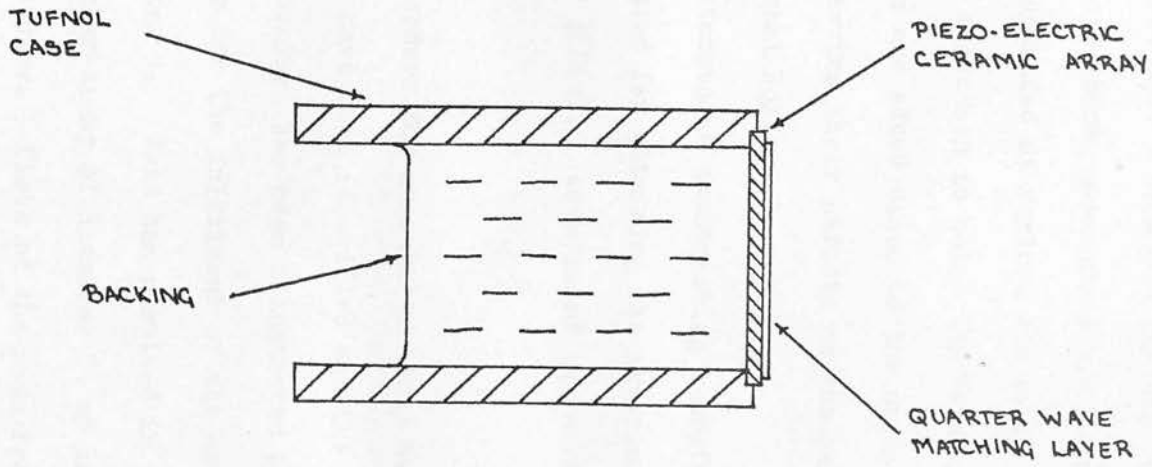

exposed via a suitable mask to ultra-violet radiation. Subsequent development in the appropriate developer and etching in ferric nitrate solution removes the silvering from the required regions. The mask was photo reduced for accuracy from a large scale drawing. Preparation, through coating, exposure, development and etching, is a process lasting about half a day. A further two to three days is required to add leads, back, wave plate and test the finished transducer. The process is illustrated at various stages in figure 3.5.

Series tuning inductors to match the impedance of individual rings to the transmitters are added close to the array. These were chosen empirically by observing their effects on the pulse-echo pulse shape and mounted on the crystal holder.

A number of attempts at constructing a useful prototype array were made. The array used for obtaining the experimental results given in Chapter 5 was array #2(c). Details of the array are given in Table 3.2.

3.5 Summary

The design procedure for an annular array has been discussed. Various constraints have been identified and the effects of these estimated. The procedure has been illustrated by considering the design of an array suitable for the fulfilment of the aims of this project referred to in Chapter 1. This has resulted in the manufacture of a 3.5 MHz, 4 ring annular array of diameter 24 mm intended for use as an abdominal contact scanner. Plots of the beam from this array and images produced using it are presented in Chapter 5.

Methods of fabricating arrays in the laboratory have been discussed and the most suitable is identified. This method has been used to successfully manufacture a number of arrays.

Figure 3.5: Annular array transducer construction:

(a) PZT disc and UV opaque mask,

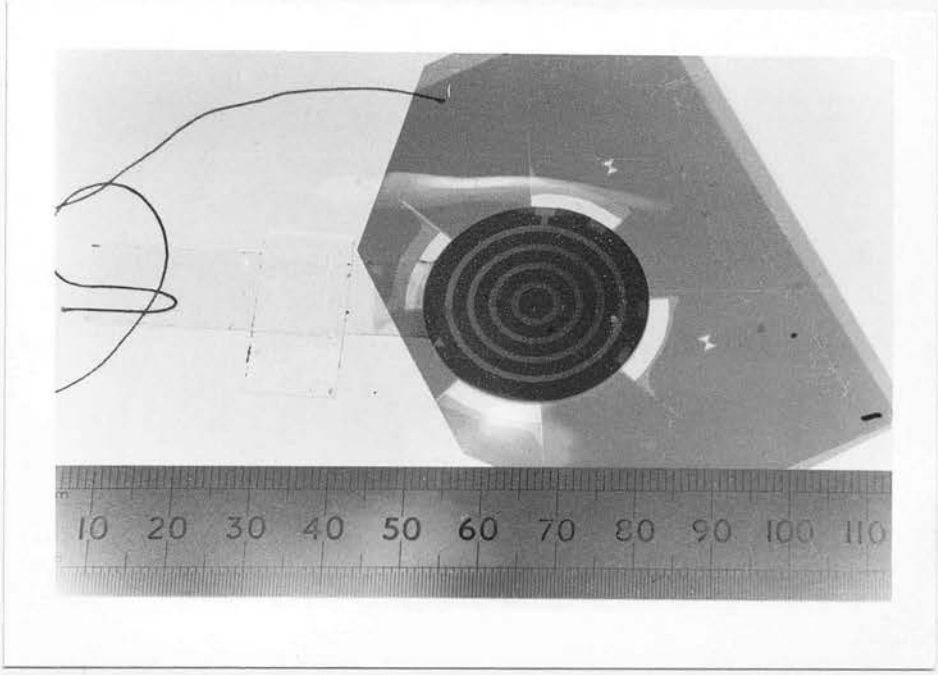

(b) Array showing electrical connections to individual annuli.

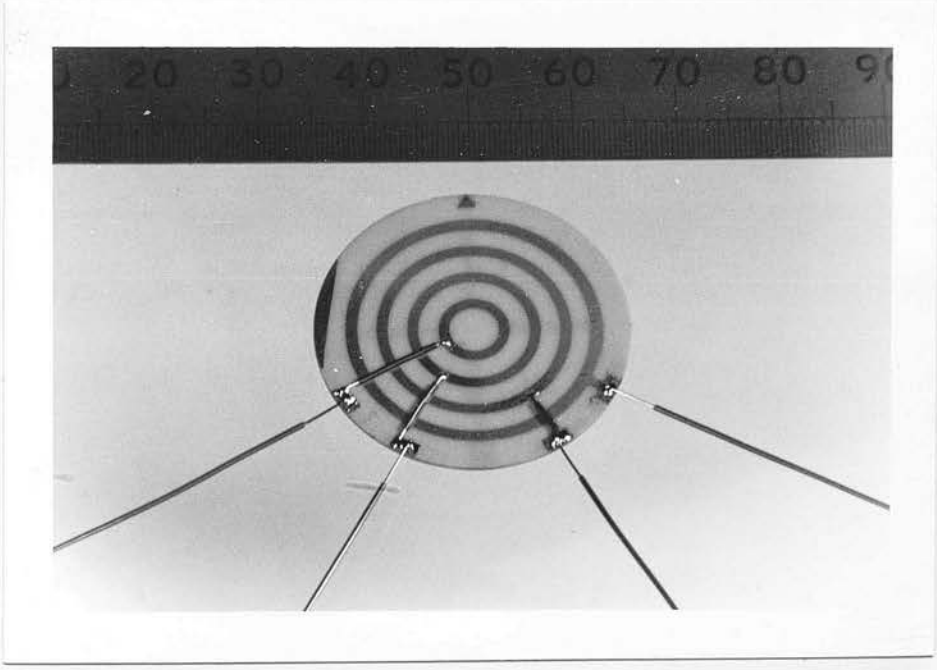

Figure 3.5: Annular array transducer construction:

(c) Array mounted in holder, prior to backing,

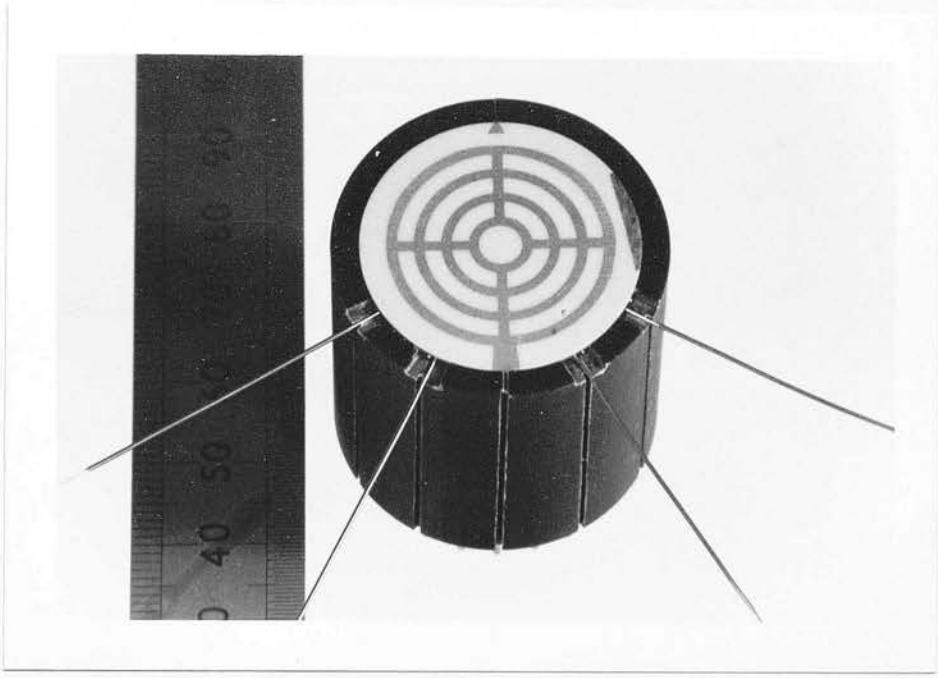

(d) Backed and waveplated (waveplate prior to lapping down).

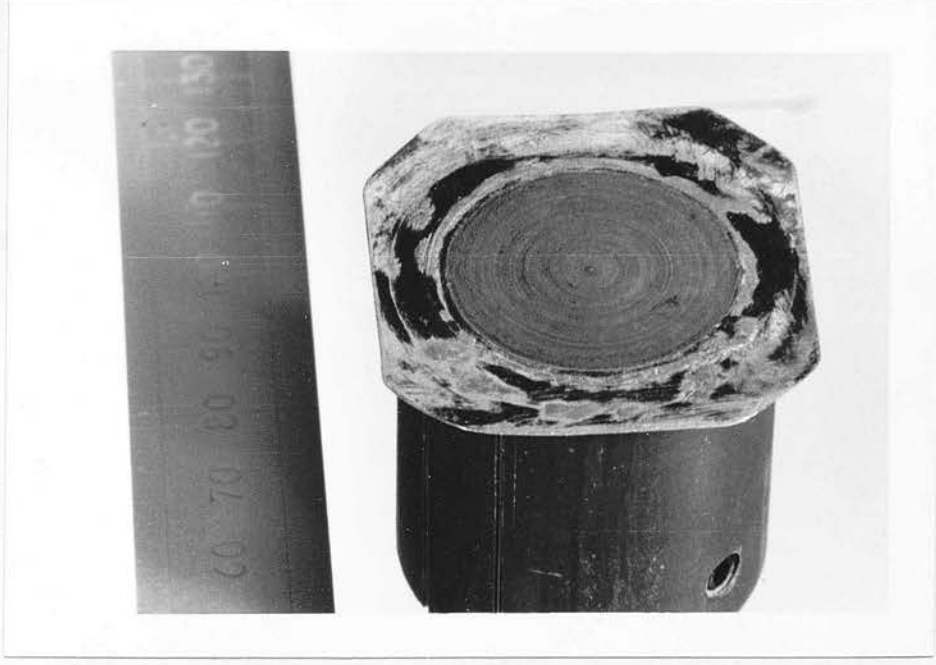

Table 3.2 Specification, annular array # 2c.

Nominal operating frequency: 3.5 MHz.

Approximate zero-crossing frequency of transmitted pulse: 2.5 MHz.

Dimensions:

	Radius (mm ± 0.025)		
Ring	Inner	Outer	Average
1	2.34	3.32	2.83
2	5.28	6.26	5.77
3	8.16	9.14	8.65
4	11.05	12.06	11.55

Tuning inductors (series):

Ring	Inductor (μH)
1	3.3
2	1.5
3	0.47
4	-

Crosstalk: (array driven continuous wave in air, with each annulus terminated in 47Ω).

Maximum cross talk between any two rings

at 3.5 MHz: -24dB

in frequency range 1.5 - 5.5 MHz: -16dB

Chapter 4

ELECTRONICS: DESIGN AND IMPLEMENTATION

The electronics of a dynamic focusing unit is centred on the provision of time variable echo delays.

4.1 Introduction

The design of an annular array is more complex than that of a single crystal transducer, likewise that of the electronic unit which generates and receives the signals for the array. The unit must be capable of all the standard functions of transmission and reception of ultrasonic pulses and these features must be replicated for each element of the array. Additionally, the unit must apply the correct dynamic delays to the signals received from each element, to achieve a dynamic focus. Processing of the signals from each ring before they are combined, is a further feature which may be incorporated into an array system.

4.1.1 General Features of a Dynamic Focusing System

The detailed configuration of a dynamically focused annular array system may vary considerably from one to the next. General features readily identifiable in them all are illustrated in figure 4.1.

The array is excited by one or more transmitters. Use of more than one transmitter facilitates achievement of a fixed focus on transmission. Echoes returning to the array are fed from each ring to the receiver electronics where they are amplified. They may then be processed separately either before or after the appropriate variable delay has been imparted. The effects of such processing as non-linear amplification have been discussed (Section 1.5.2). Subsequently the signals are combined. Combination usually takes the form of summation,

Figure 4.1: General features of a dynamic focusing system.

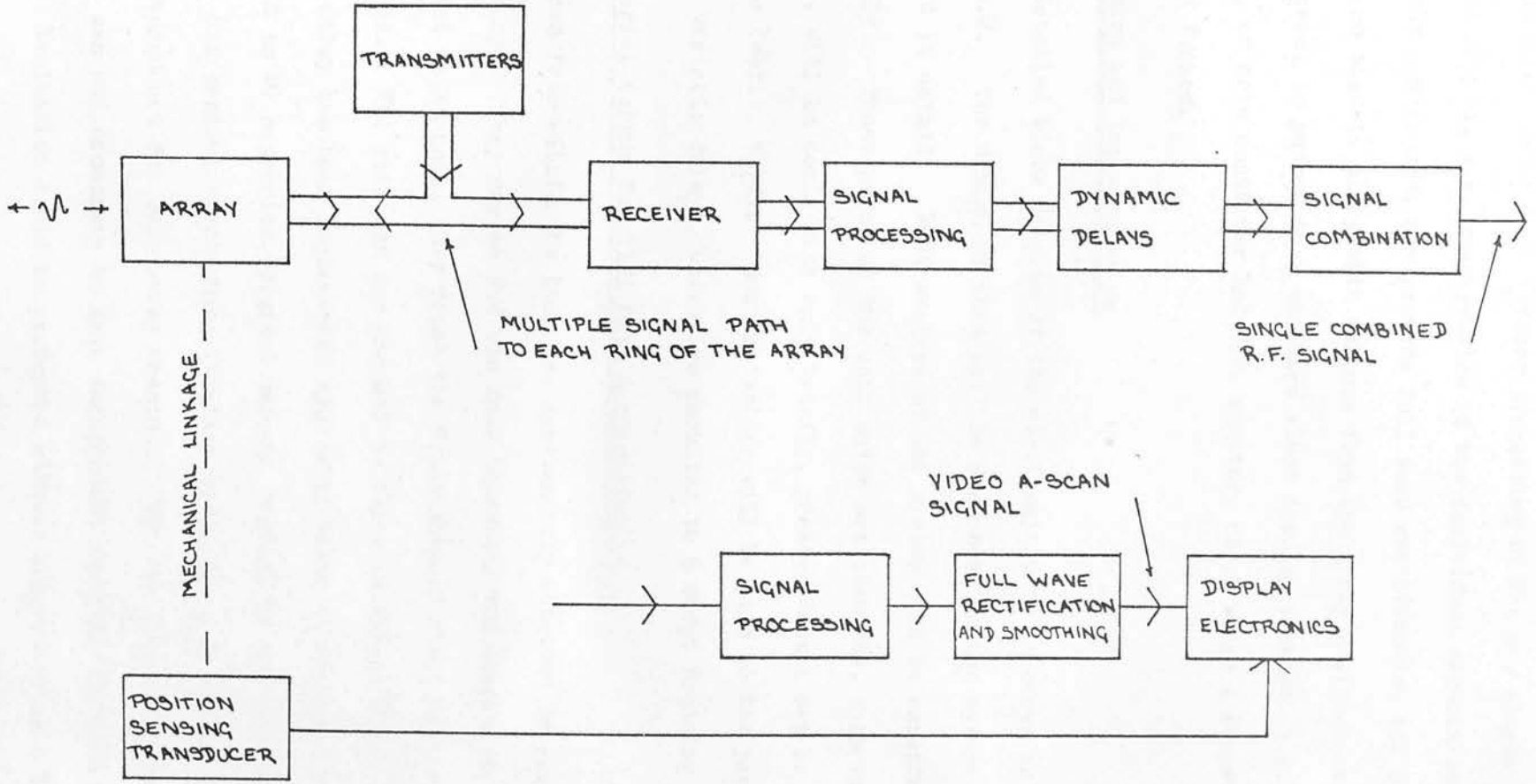

but multiplication or other form are equally feasible if they are electronically possible. Further processing of the now single composite signal, e.g. re-expansion if the individual signals were previously compressed, may precede full wave rectification and smoothing. This video signal, along with outputs from the array position-sensing transducers, is passed to a standard video display package, i.e. X-Y display, or scan converter and T.V. monitor, etc., where a B-scan image is formed.

4.2 Design and Implementation

A detailed block diagram of the electronic unit is shown in figure 4.2. The design of this will be discussed as the system is described in detail. Each section of the system will be considered separately. Those parts of the unit which are standard, such as the receiver, will be dealt with only briefly, greater detail may be found elsewhere (Wells, 1977). Most attention will be paid to the parts, e.g. the variable delays, which are peculiar to a swept focusing system.

4.2.1 Serial versus Parallel Data Acquisition

Echoes from within the body are continuously received by all rings of the array. They may be fed via four identical but completely independent paths until they reach the "combination" stage of the electronics. The path for one channel is shown in figure 4.3. The variable delay has been implemented digitally using an Analogue to Digital (A to D) converter, digital memory, Digital to Analogue (D to A) converter and control electronics (Section 4.2.3.2). A similar path must be reproduced for each array channel. For the proposed research system it was not necessary to have independent channels for each array element. Evaluation could be performed without compromise on a less extensive system.

Figure 4.2: Detail of annular array dynamic focusing system described in this work.

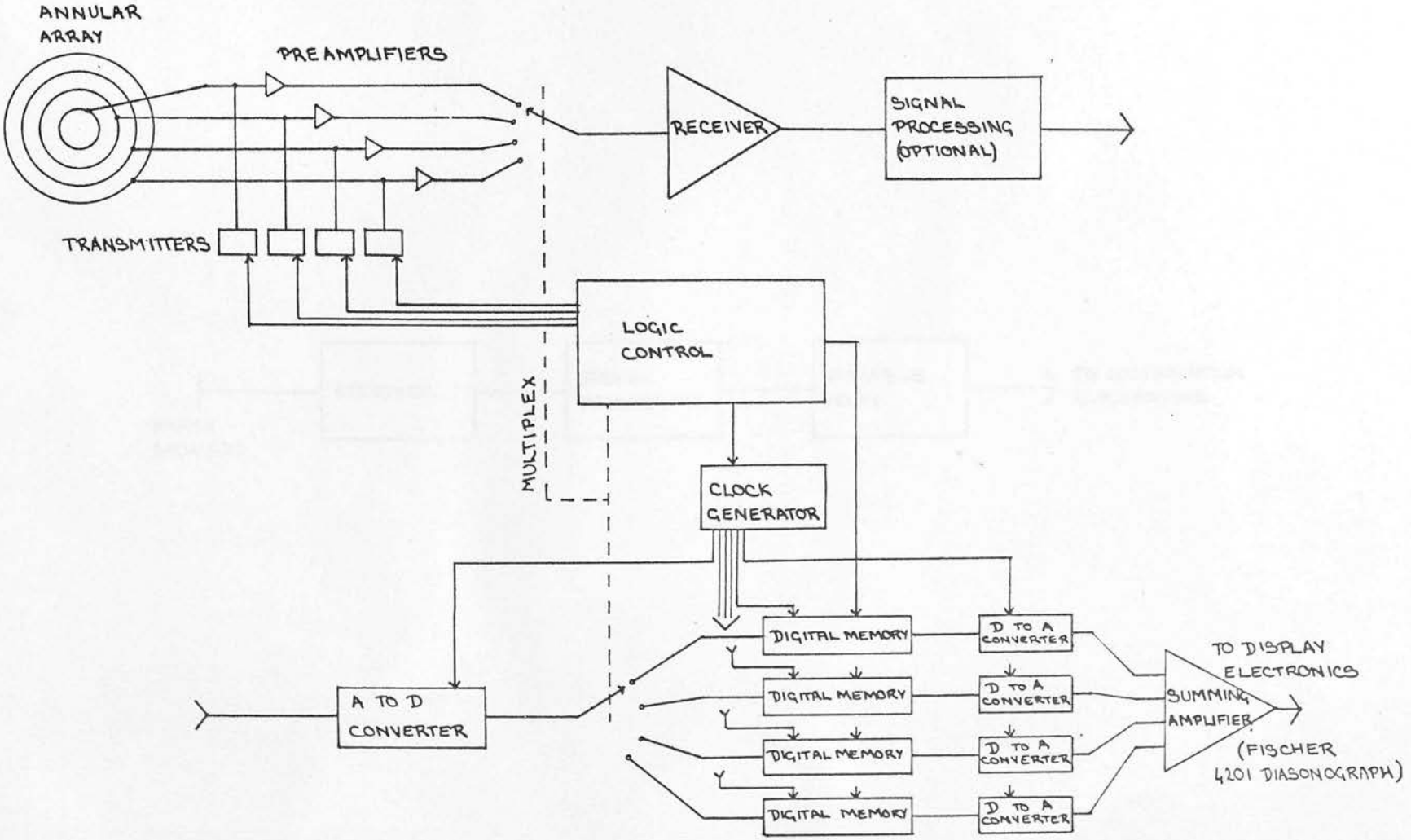

Figure 4.3: Signal path for an individual ring.

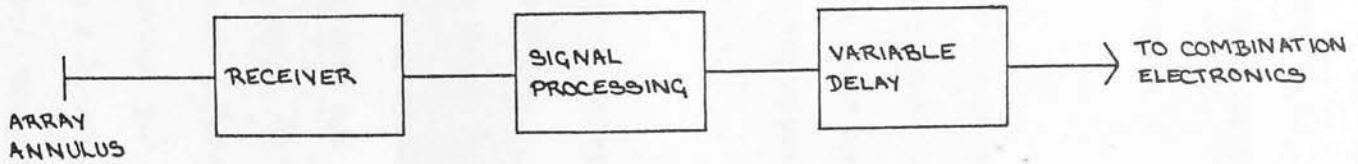

If echoes are only accepted on one ring at a time for each transmission pulse and then stored until a complete line of echoes has been received from each ring, much of the duplicate electronics may be done away with. A single channel is switched between rings on each new transmission pulse, see figure 4.2. "Serial data acquisition" or "collection", as this technique will be called, has advantages over parallel data collection.

Advantages:

(1) low cost;

(2) the same receiver and processing unit are used for each channel so that a series of parallel units do not have to be set up and matched;

(3) a novel focusing technique may be implemented, see Section 1.6.2.1.

Disadvantages:

(1) the maximum possible pulse repetition frequency (p.r.f.) is reduced;

(2) there is greater sensitivity to tissue movement.

Consider an abdominal scanning system with a maximum depth of penetration of 190 mm. To transmit and receive one line of information for one ring takes about 247 μsec. To do this for four rings and then to read out and display the stored information takes about 247 x 5 μsec = 1.235 msec. This implies a maximum p.r.f. of about 800 Hz. For interfacing with a unit such as a Diasonograph where the p.r.f. is normally 600 Hz, this is perfectly adequate. For inclusion in a mechanical real-time scanner where the p.r.f. is normally about 3,000 Hz, it would not be sufficient.

Tissue may move between generating a line of echoes to be received and stored on one channel and generating a line for the next. Consider

the time between an echo being generated for ring 1 and the same echo being generated for ring 4. The time elapsed is 3 x 247 μsec = 741 μsec. In this time the tissue must remain stable compared with the wavelength of the ultrasonic pulse. Let a reasonable stability be 0.1 wavelengths. At 3.5 MHz in tissue, this is 0.044 mm. (If two equi-amplitude sinusoids are parted by 0.1 wavelengths their combined amplitude falls by 5%, a separation of 0.2 wavelengths produces a 19% fall.) Hence, the tissue must not move with a speed in excess of $(0.044 \times 10^{-3})/(741 \times 10^{-6}) = 60$ mm sec^{-1}. Movement of the abdomen due to respiration occurs at a rate of approximately 15 cycles per minute. If the maximum displacement is 40 mm then the tissue speed is of the order of 10 mm sec^{-1}, below that which would seriously degrade the focus.

The disadvantages become more acute for larger numbers of rings. They restrict the use of serial data collection to:

(1) static B-scan imaging in regions where tissue movement is slow;

(2) "frame-grab" mode on real-time scanners.

They do not restrict the attainment of the original aims of this project, in that the array system may be fully investigated by beam plotting and imaging static phantoms. When the array is to be incorporated into a real-time scanner the electronic unit may readily be modified to a fully parallel system.

4.2.2 Components of the Electronic Unit

The various sections of the swept focusing electronics are listed below and also illustrated in the form of a block diagram in figure 4.2.

(1) Transmitters and attenuator banks.

(2) Receiver "front-end" protection and preamplifiers.

(3) Multiplexer.

(4) Amplifier with Time Gain Compensation (T.G.C.).

(5) Signal processing block.

(6) Low pass filter.

(7) Analogue to digital converter.

(8) Digital memories.

(9) Digital to analogue converters.

(10) Fixed input clock.

(11) Swept output clocks.

(12) Signal combination.

(13) Full wave rectification and smoothing.

(14) Display and position sensing electronics (Fischer 4201 Diasonograph).

(15) Digital control circuitry.

The electronic unit was designed initially for interface to a Fischer 4201 Diasonograph, static B-scanner. The B-scan unit provides a pulse to control the timing of the swept focusing unit, from which an A-scan video line is fed into the Diasonograph digital scan converter.

Items (1), (2), (4), (13) and (14) are standard circuits of which examples may be found in many instruments and texts on ultrasonics and so they will be dealt with only briefly. Those parts which are peculiar to a swept focusing system and which differentiate it from the standard system will be dealt with in more depth, particularly items (6) - (11) which form the delays.

Item (15), the control logic, contains a 50 MHz crystal controlled and temperature stabilised master oscillator from which delays and other timing signals are derived with an uncertainty of $\pm$ 10 nsec. This corresponds to $\pm$ 0.035 of a period at 3.5 MHz. Signals derived from the control logic may be referred to in association with the parts of the unit to which they apply. Its detailed operation will not be discussed as it is standard logic circuitry.

4.2.2.1 Transmitters and Attenuator Banks

A separate transmitter is connected to each ring of the array. Their firing times are delayed relative to one another. In this way a fixed focus can be achieved on transmission. The type of focus, e.g. point focus or line focus, and the depth at which the focus occurs are defined by the magnitudes of the relative delays.

Each transmitter fires on reception of a TTL pulse from the control logic. There is a variation in transmitter output pulse height of $\pm 3\%$, from pulse to pulse, due to the short recovery time allowed between pulses, 250 μsec. Each transmitter is capable of providing at least 320 volts across any ring of the array, with a pulse width of 1 μsec. The output from each transmitter is fed via a switchable π attenuator network giving 0, 10, 20, 30 and 0, 2, 4, 6, 8 dB attenuation steps. Apodisation may be achieved on transmission by introducing different attenuations into each transmitter line or by adjusting the transmitter supply voltages.

4.2.2.2 Receiver "Front-End" Protection and Preamplifiers

The preamplifiers are at all times connected across their respective rings. In order to protect these sensitive first stages from the high excitation voltages produced by the transmitters, some form of "front-end" protection must be included. This is a standard circuit with two back to back diodes as its basis. Impedance matching is also incorporated, to correctly couple the transducer impedance to that of the preamplifier input stage. Following the protection circuit is a three stage FET preamplifier for each ring. These have a 70dB maximum gain, a band width of 10 MHz and a dynamic range of 50 dB.

4.2.2.3 Multiplex Unit

Immediately following the initial protection and first preamplifier

stage is an r.f. multiplex unit which switches the outputs one ring at a time to the receiver, until a complete line of information has been stored in the unit's memory, from each ring. Multiplexing in this way necessitates the use of only one receiver, signal processing block and stages in the variable delays prior to the memories.

4.2.2.4 Main Receiver

The main receiver is a standard three stage FET wide band r.f. amplifier with T.G.C. facility. It has a gain of 48 dB, with a band width of 1.5 - 10 MHz and dynamic range of 60 dB. The time gain controls available are near gain, delay and slope. The output is capable of driving a 50 Ω load.

4.2.2.5 Signal Processing

This may take any electronically feasible form. The most common types of processing involve dynamic range compression. It is envisaged that logarithmic compression would be used at this point, the advantages of which have been discussed in Section 1.5.2. No form of processing was used in obtaining the results presented in Chapter 5.

4.2.2.6 Signal Combination

An inverting summing amplifier is used to sum the r.f. signals from each channel. This allows an apodising function to be implemented on reception by suitable weighting of the amplifier inputs. Any other form of signal combination electronically feasible, could be incorporated as an alternative.

4.2.2.7 Full Wave Rectification and Smoothing

The single r.f. signal from the summing amplifier is full wave rectified and smoothed. This signal feeds a 50 Ω line driver which

provides the A-scan video signal to be fed into the scan converter of the Diasonograph. The driver output begins to saturate at ~1V and clips at ~1.8V, to prevent damage to the Diasonograph input. The noise level at this output is ~10mV.

4.2.3 Dynamic Delays

Dynamic delay of the signals from each region of the array lies at the heart of the swept focusing system. As echoes are returned from increasing depth the delay imparted to each channel must be altered so as to maintain the signals in phase at the delays' outputs.

4.2.3.1 Variable Delay Lines

Three major means of imparting the appropriate delays are identified in the literature:

(1) analogue lumped-constant tapped delay lines;

(2) Charged Coupled Device (CCD) analogue serial delay lines;

(3) digital delays (using random access memory or shift registers).

Variable delays using analogue lumped-constant tapped delay lines involve the switching of signals from each ring onto the appropriate delay line tap. The tap is chosen to give the requisite delay for that ring, for that point in the receive cycle. The coherent summation of the signals from each ring appears at the end of the delay line. McKieghen and Buchin (1977) list some of their disadvantages as "bulky, expensive and introduce insertion losses and phase distortion", particularly when used for long delays. A further disadvantage is that the minimum delay increment is limited by the distance between taps. To obtain very fine increments requires many taps.

CCD analogue serial delay lines operate by passing a charge "packet" proportional to the voltage at the device input, along its surface from under one "capacitor" to the next. The device samples the input waveform and stores it, up to the maximum number of "bits" it possesses. By reading the data out at a different clock rate from that at which it was written in or at a varying clock rate, fixed or variable delays may be obtained.

CCD's are sampling devices. An ultrasonic pulse has a bandwidth similar to its centre frequency. To avoid aliasing, a sampling rate of at least twice the highest frequency component, equivalent to 3 times the centre frequency, is necessary. Rates of 4 - 5 times the centre frequency are desirable in practice. A nominally 3.5 MHz pulse should be sampled at 17.5 MHz and a 5 MHz pulse at 25 MHz. Sampling rates for devices available at the start of this project were limited to the low megahertz range, necessitating multiplexing two or more devices together to effectively increase the sampling rate.

CCD's exhibit a limited signal-to-noise ratio. McKieghan and Buchin quote 30 dB at a 4 MHz clock rate for the Reticon SAM-64 device. A dynamic range of 26 dB at a clock rate of 20 MHz was exhibited by a Fairchild CCD 321A device on evaluation. The maximum analogue bandwidth available from this device was 4 MHz.

Leakage of charge from under each "capacitor" in a CCD limits the maximum time that a signal may be held. The maximum delay is limited by this.

Use of CCD's as variable delays in beam steering and swept focusing applications is evident in the literature. It is also evident that such devices have been custom made at institutions where CCD's are being actively researched, see Eaton et al. (1980) and Melen et al. (1977), at

Stanford University. The devices available commercially are limited in number and performance and there seems little commercial interest in producing and marketing new devices.

Digital delays, like CCD's, rely on sampling and temporary storage of the r.f. signal. A to D converters working at the necessary clock rates are expensive. The dynamic range of the signal is limited by the maximum number of bits to which the converter will digitise. It may not be possible to obtain sufficiently large memories operating at this speed, necessitating the multiplexing together of a number of lower speed memories. High speed wideband D to A converters are required to produce the conversion back to an analogue signal.

As with CCD's, delays are imparted either by holding the data in memory and then reading out at a fixed clock rate, fixed delay, or a variable clock rate, fixed plus variable delay. Quasi-continuous variation of the delay is possible. Unlike CCD's digital memories can hold data indefinitely without degradation. Degradation occurs only at the A to D and possibly D to A stages and is independent of the length of delay. McKeighen and Buchin, when comparing various types of variable delays, concluded that digital techniques offer the optimum solution. Corl et al. used digital techniques in their non-destructive evaluation system. A vast quantity of digital circuitry already exists and the market is still rapidly expanding. The cost of devices continues to fall.

The choice of delays was made on the following considerations:

(1) versatility and flexibility;

(2) quality of signal reproduction at the output;

(3) cost;

(4) availability.

Analogue tapped delay lines probably offered the cheapest solution but are less versatile and may introduce insertion losses and phase distortion

for long delays. They are commonly used by commercial manufacturers but were not considered appropriate for the proposed research system. CCD's offered a promising solution but were found technically difficult to use and had not the required specification. Their availability was uncertain. Digital methods offered versatility and flexibility, a high quality of reproduction and ready availability. The use of serial data collection enabled cost to be kept to an acceptable level.

4.2.3.2 A Variable Digital Delay Line

Figure 4.4 is a block diagram of the variable delay electronics for one ring. The data input to the variable delay block is an r.f. ultrasonic signal with a nominal centre frequency of 3.5 MHz and bandwidth of approximately 1.5 - 5.5 MHz. The circuitry has been designed to handle pulses of centre frequency up to 5 MHz. In order to sample the incoming r.f. signals adequately a sample rate of five times the centre frequency, three times the highest frequency component, was chosen, i.e. 17.5 MHz. In order to prevent aliasing of higher frequency components back into the signal band a low pass filter was included before the A to D converter. This is a Matthey 7th order eliptic function low pass filter type FLM550P with an upper cutoff frequency of 5.5 MHz. The A to D converter is a single 64 pin integrated circuit, TRW type TDC 10075, 8 bit, fully parallel (flash) monolithic A to D converter. Its maximum digitisation rate is typically 25 MHz and it has an analogue bandwidth extending to 7 MHz. Its 8 bit capacity implies a maximum dynamic range of 48 dB.

The sample clock is provided by a fixed frequency oscillator similar to those used to provide the swept clocks. After digitisation, successive data samples are read into successive memory locations in a 4k x 8 bit Random Access Memory (RAM). In order to obtain the required speed of operation using relatively inexpensive, readily available devices,

Figure 4.4: An analogue variable delay line using digital techniques.

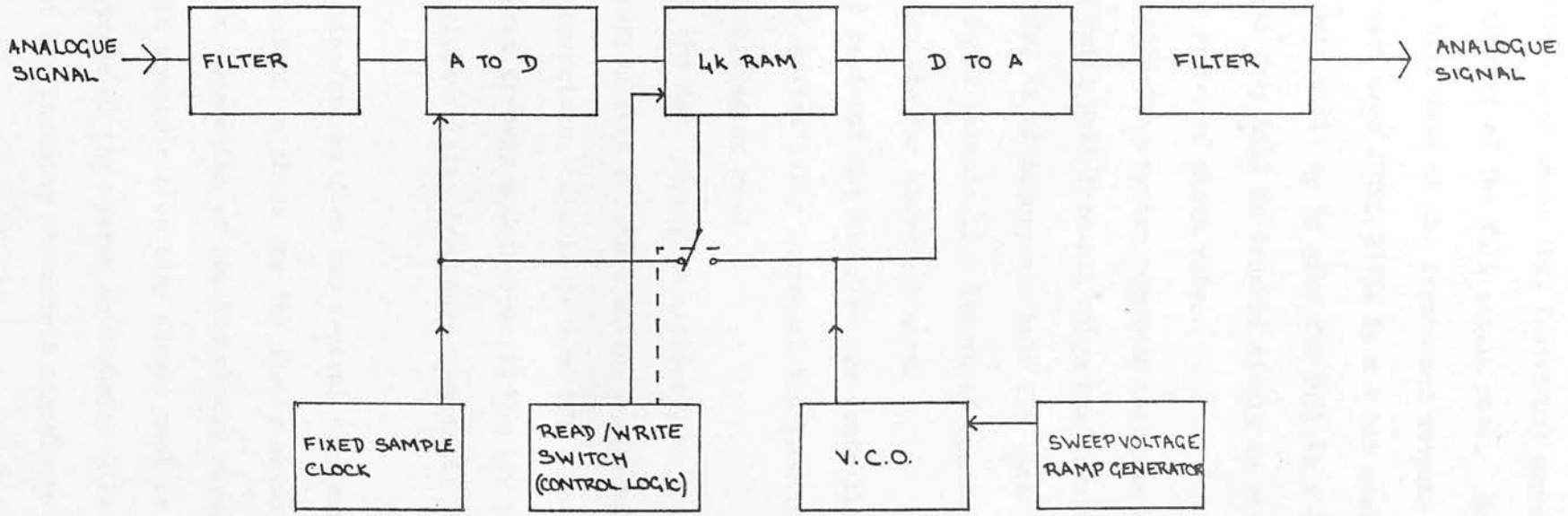

4 separate 1k x 8 bit RAM's were multiplexed together. Switching between RAM's in this manner means that individual memory chips are driven at only one quarter of the full sample rate. High speed data latches are used to hold data at the inputs and outputs of the 1k blocks. The memory devices used were INTEL 2115A 1k x 1 bit static N-Channel MOS RAM's. These were built up to give the full 4k x 8 bit memories. In further discussion they will be treated simply as single 4k x 8 bit RAM's capable of the required clock rate.

A serial data collection system requires that the echo data from each ring be stored until data from all rings has been collected. At a clock rate of 17.5 MHz, 4k of memory can hold 234 μsec of information. This corresponds to an ultrasonic line length of approximately 180 mm which was thought adequate for abdominal work.

On write-in and read-out the memories are controlled by the fixed or swept clocks which sequentially increment the location addresses at which data is to be written or read.

From the memory the data passes to a video D to A converter. The devices used were encapsulated screened units, Analogic type MP8318, 8 bit video D to A converters, capable of a 40 MHz clock-in rate. The D to A output is passed through a Cathodean 10 MHz low pass filter to remove any residual clock-related frequency components from the output r.f. wave form.

Variable delay line/stores form the central components of a swept focusing system. Central to these are the clocks which control the rate of data transfer. Consideration of how the clocks should be implemented and controlled and the specification they should meet is of great importance to the success of the system as a whole. It is desirable to control the phases of the incoming ultrasonic signals to within 0.1 of a

period, i.e. about 29 nsec, and achieve a variation in delay between channels of between 0 and 3 μsec. Before going into detail of how this control is achieved the actual functions of frequency versus time and some idea of the precision required will be considered.

4.2.4 Variable Delay Control Functions

4.2.4.1 Dynamic Receive Focus Control Function

An ultrasonic B-scan is made up of a series of successive lines, each of which represents the echoes received from structures within the body located along the axis of the transducer when pointed in a given direction. Consider a single reflector on the axis of the transducer, figure 4.5. The go-return path for a wave originating at the transducer centre is different for different points on the transducer face. The path length for a point B, near the transducer edge is greater than that for the point A, near its centre. This path difference also varies with the depth z_R, of the reflector. Because of the difference in path lengths, echoes returning to the transducer may arrive there out of phase, thereby reducing the transducer's response to the reflector. To maximise the response of the transducer to on axis reflectors, a lens may be introduced into the path of the beam. Because the velocity of ultrasound in the lens is chosen to be different from that of the medium as a whole, the lens is able to compensate for the different path lengths by delaying signals returning to A relative to those returning to B, but only for a specific depth of reflector. Use of an annular array and variable electronic delays enables echoes returning to various parts of the array to be correctly delayed relative to one another for all depths of reflector. The response of the transducer is enhanced towards on-axis reflectors over an extended range limited by the performance of the electronic delays and aperture of the transducer.

Figure 4.5: Differing path lengths from a field point to points on the transducer face.

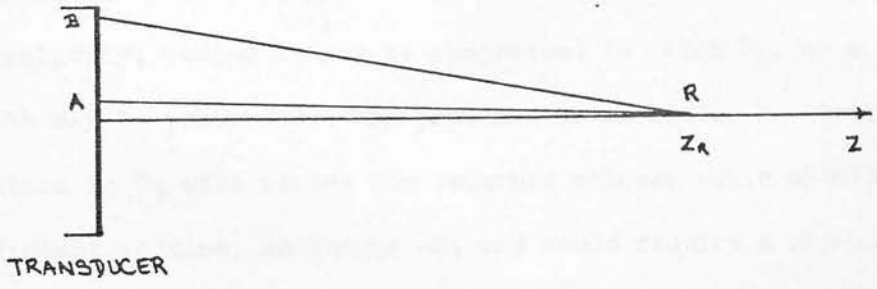

Consider a three ring annular array being used to visualise a series of equally spaced on-axis reflectors, figure 4.6. The pulse from the transducer is assumed to originate at its centre. Echoes are received at the three annuli and fed into three electronically variable delays. The echoes received at the array centre remain equidistant. Those received at a radius r, start arriving later and are no longer spaced equidistantly. Equi-phase signals may be obtained at the delay outputs by queueing the echoes along until the first echo is aligned in each memory and then reading the memories out together, repeatedly trimming the relative delays of each channel by altering their clock-out rates so as to keep the echoes synchronised. Effectively, vector D_3 is stretched, like a rubber band, until it is aligned with D_1. Alternatively, vector D_1 may be compressed to match D_3, or a combination of both may be performed. In practice it is better to stretch D_3. Any variation in D_1 will render the returned echoes, which should be equidistant in time, no longer so, and would require a non-linear time base to be implemented by the display electronics to maintain registration. Stretching D_3 entails sweeping the output clock from a lower to a higher frequency. Compressing D_1 requires the opposite. In order to adequately sample the ultrasonic pulses, high sampling rates are necessary. It then becomes increasingly difficult to run the electronics at even higher frequencies to achieve a high to low frequency sweep to compress a line. (It would be possible to scale all the read-out frequencies down, however this increases the time required to perform the operation, which is undesirable.)

Consider data stored in two adjacent memory locations written-in at a frequency f_oHz. The time interval between the data bits is $1/f_o$ sec. If the memory is then read-out at a clock frequency of f_1Hz. the time

Figure 4.6: Time relationship of echoes received at the central and outer annuli from equidistant reflectors (note: first echoes have been aligned).

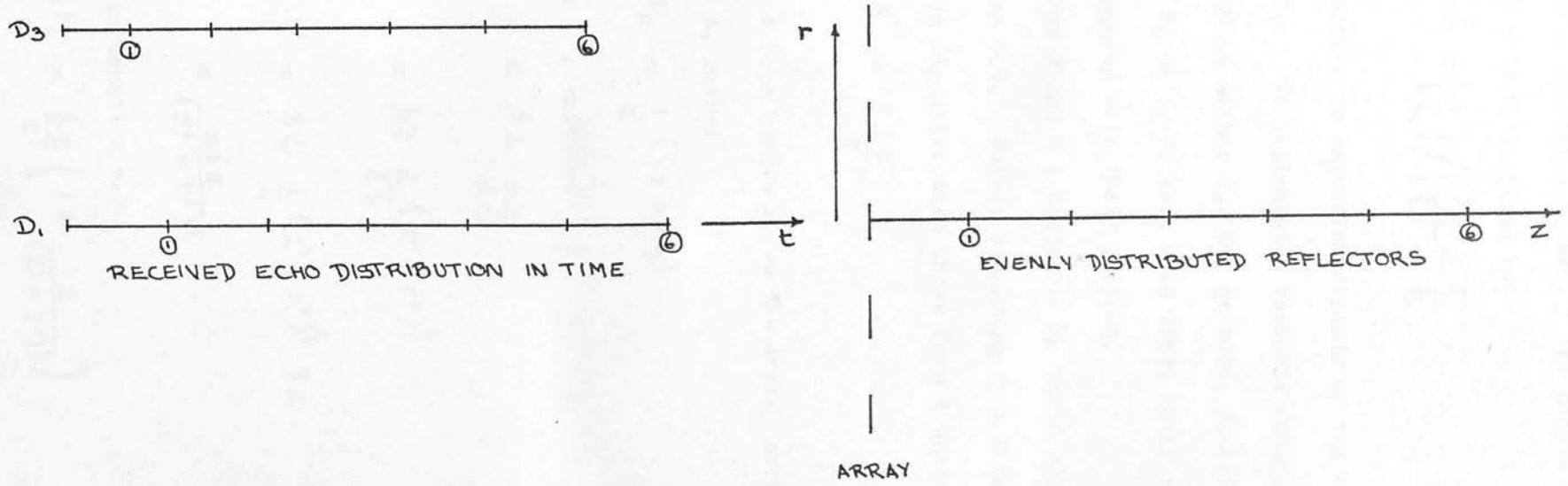

interval between the bits becomes $1/f_1$ sec. The compression/expansion ratio of the data ε, is given by:

$$\varepsilon = \left(\frac{1}{f_0}\right) \Big/ \left(\frac{1}{f_1}\right) = \frac{f_1}{f_0} \qquad ---4.1$$

Whether it is a compression or expansion depends on the relative magnitudes of f_0 and f_1. To implement a variable delay, ε is made a function of time by making either f_0, f_1, or both, functions of time. It is assumed that if f_0 or f_1 do vary with time, their rates of variation are slow compared with their periods.

Consider reflectors A and B a distance δz apart along the transducer axis, figure 4.7. Echoes returning from B to the centre of the array arrive a time δt_c later than those from A where:

$$\delta t_c = 2\frac{\delta z}{c} \qquad ---4.2$$

Echoes returning from B to a radius r, on the array, arrive a time δt_r later than those from A, where:

$$\delta t_r = \frac{1}{c}(\delta z + \delta y) \qquad ---4.3$$

If δy and δz are small quantities:

$$\delta y = \delta z \frac{dy}{dz}$$

$$= \delta z \frac{d}{dz}(z^2 + r^2)^{\frac{1}{2}}$$

$$= \delta z \frac{1}{2}(z^2 + r^2)^{\frac{1}{2}} 2z$$

$$= \frac{z\delta z}{(z^2 + r^2)^{\frac{1}{2}}}$$

Substituting for δy in equation 4.3:

$$\delta t_r = \frac{\delta z}{c}\left(1 + \frac{z}{(z^2 + r^2)^{\frac{1}{2}}}\right) \qquad ---4.4$$

Figure 4.7: Sweep function derivation Section 4.2.4.1.

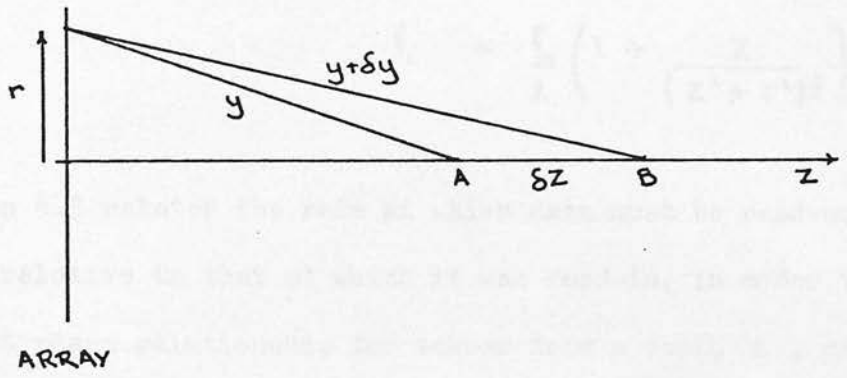

In order to achieve a focus at all depths z, δt_r must be made equal to δt_c for all z, by applying a variable compression/expansion function to one or other. That is:

$$\delta t_c(z) = \varepsilon(z)\, \delta t_r$$

Substituting for ε from equation 4.1 gives:

$$\delta t_c = \frac{f_1}{f_0} \delta t_r$$

Substituting for δt_c and δt_r from equations 4.2 and 4.3:

$$\frac{\delta z}{c}\left(1 + \frac{z}{(z^2 + r^2)^{\frac{1}{2}}}\right) = \frac{f_1}{f_0} 2 \frac{\delta z}{c}$$

$$\therefore \qquad f_1 = \frac{f_0}{2}\left(1 + \frac{z}{(z^2 + r^2)^{\frac{1}{2}}}\right) \qquad ---4.5$$

Equation 4.5 relates the rate at which data must be read-out of a delay memory relative to that at which it was read-in, in order to maintain a constant phase relationship for echoes from a depth z, returning to a radius r, on the array.

To convert f_1 to a function of time, note that along the axis:

$$t = 2\frac{z}{c}$$

Hence:

$$f_1(t) = \frac{f_0(t)}{2}\left[1 + \left(1 + \frac{4r^2}{c^2 t^2}\right)^{-\frac{1}{2}}\right] \qquad ---4.6$$

Note that if f_1 is to be swept from time zero, its initial value is $0.5\, f_0$. This is a large range over which to sweep frequency and entails high initial rates of change. However, actual imaging usually takes place from an initial depth of about 10 mm. If the initial delay is compensated for by queueing data up in the memories, so that echoes

arriving from 10 mm depth are aligned for each channel before sweeping, the sweep range is reduced to about 0.1 f_o.

4.2.4.2 Synthetic Aperture Control Function

An initial assumption in the above derivation was that the transmitted pulse originates at the array centre. The resulting sweep function produces a swept or zone focus effect on reception. In the system that has been built, using serial data acquisition, it is possible to produce an effective swept focus on transmission as well. This is implemented by transmitting and receiving on only one ring at a time. For any given ring the transmission pulse now originates at a radius r. Following a similar derivation to that outlined above, the sweep function required to produce a swept response on both transmission and reception is:

$$f_1(t) = f_o(t)\left(1 + \frac{4r^2}{c^2t^2}\right)^{-\frac{1}{2}} \qquad ---4.7$$

The use of this function in conjunction with an annular array is one of the novel features of this system. Its relationship to other focusing techniques described in the literature has been discussed in Section 1.6.2.1. The improvements in beam shape which accrue are investigated in Section 5.6. The functions defined by equations 4.6 and 4.7 are illustrated in Figure 4.8.

4.2.4.3 Representative Ring Radius

In the above derivation the radius r, appears. In an actual array, rings have a finite radius. If imaging is to be performed only in the far-fields of all the rings, choice of a representative radius for each ring is simple. There, the pulse from each ring is virtually identical in shape and simply scaled in magnitude depending on the ring area.

Figure 4.8: Clock frequency vs. time.

(a) for a dynamic focus on reception only (equation 4.6).

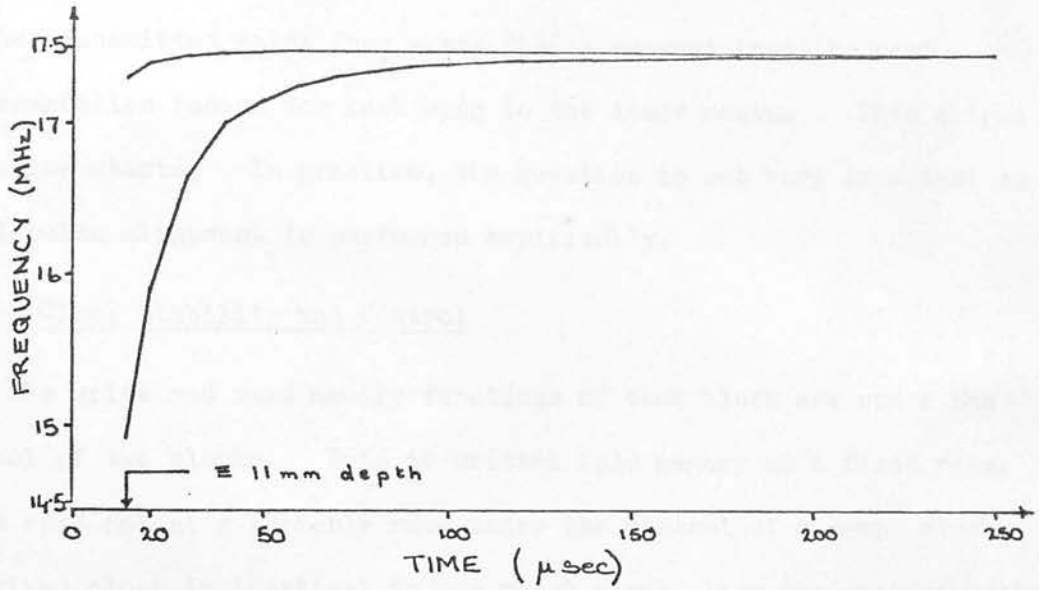

(b) for synthetic aperture focusing (equation 4.7).

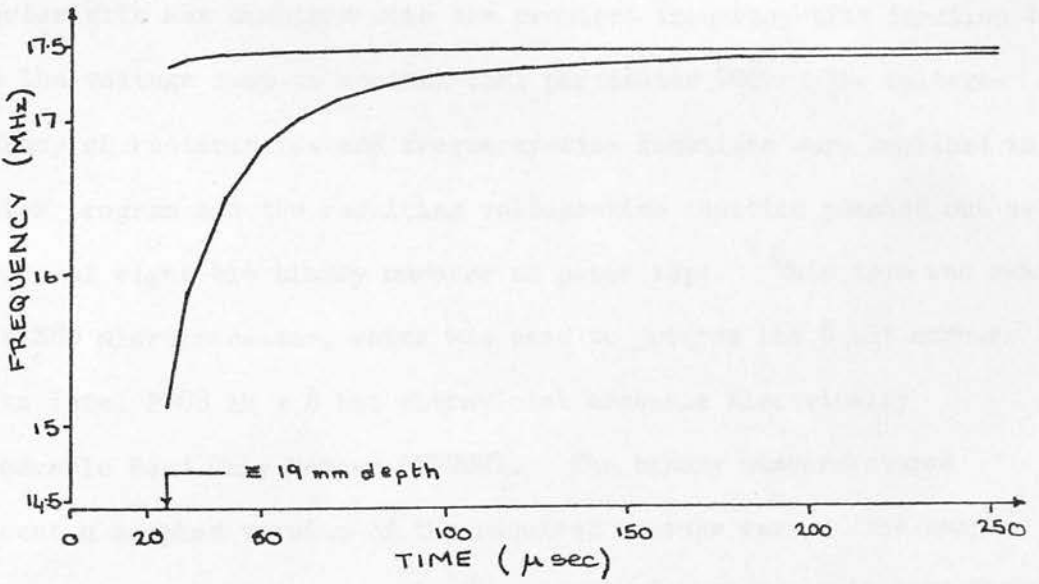

Any consistent radius may be used to correctly align the pulses, e.g. inner radius of each ring, average radius, r.m.s. radius, etc. If, however, it is intended to perform contact B-scanning, it is impossible to design an array in which only the far-fields of the rings are used (Section 3.3.2). Pulse shape in the near-field is more complex and changes with depth. The results of computer simulations of the transmitted pulse from array #2(c) suggest that the best representative radius for each ring is the inner radius. This aligns the pulse starts. In practice, the question is not very important as final pulse alignment is performed empirically.

4.2.5 Clock Stability and Control

The write and read memory functions of each block are under the control of two clocks. Data is written into memory at a fixed rate. It is read out at a variable rate under the control of a swept clock. The fixed clock is identical to the swept clock, less the voltage control circuitry. Figure 4.9 is a block diagram of the memory control system.

The voltage-frequency characteristics of the Voltage Control Oscillators (VCO) were plotted under static conditions. The appropriate characteristic was combined with the required frequency-time function to yield the voltage ramp to control that particular VCO. The voltage-frequency characteristics and frequency-time functions were combined in a computer program and the resulting voltage-time function punched out as a sequence of eight bit binary numbers on paper tape. This tape was read into a Z80 microprocessor, which was used to program the 8 bit numbers into an Intel 2708 1k x 8 bit ultraviolet erasable Electrically Programmable Read Only Memory (EPROM). The binary numbers stored represent a sampled version of the required voltage ramp. The sample interval chosen was 1 μsec. As the length of each sweep is less than 234 μsec, more than one sweep may be stored in each PROM. Changing to

Figure 4.9: Memory control logic.

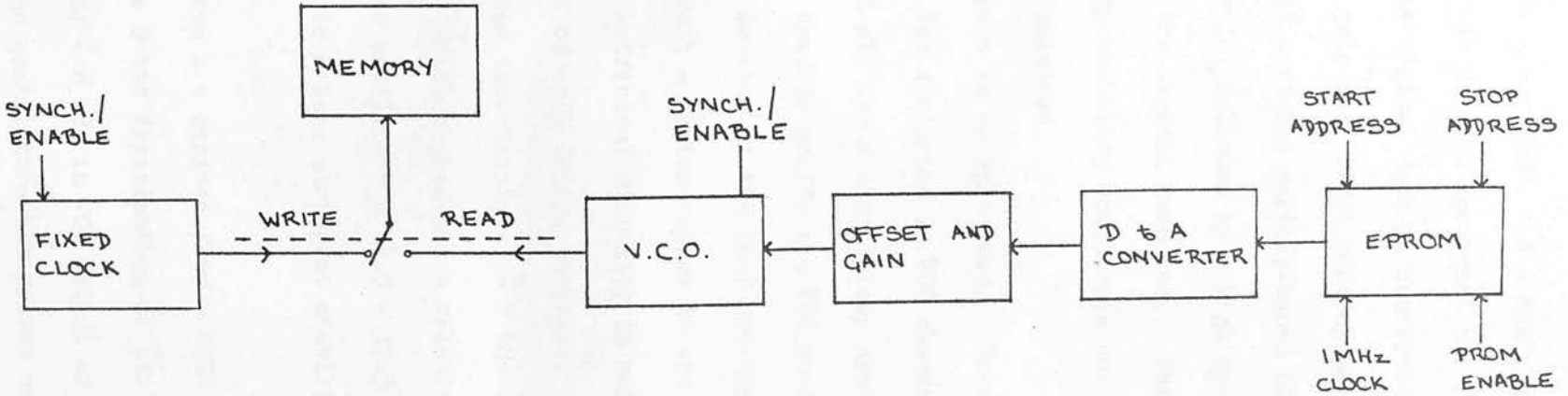

a different sweep is simply a matter of changing start and stop addresses, or plugging in a new PROM. A 1 MHz clock derived from the 50 MHz master oscillator is used to increment the PROM address at which data is being read. The digital data is converted to analogue, smoothed and passed via gain and offset control amplifiers to a VCO.

Each VCO consists of a stable varicap-tuned LC tuned circuit, with a linearised characteristic, followed by a high speed comparator to provide a TTL output to the digital memories. The VCO's are built with close tolerance high stability components and fully encapsulated in rubber and electrically shielded.

The EPROM to VCO chain is an open loop. There is no feed back to compensate for drift or for variation in VCO characteristics under swept conditions. Bernadi et al. use a closed loop system in which an error signal is generated and used to modify the VCO control voltage to ensure accurate performance. Because of the cost and time involved it was decided not to develop such a system unless it was proven necessary.

The clocks require sufficient stability to maintain the ultrasonic echo train at the output of each delay, co-phasal to with $\pm$ 0.1 periods. This implies an oscillator uncertainty of $\pm$ 2 kHz over the period of each sweep (about 300 μsec.), which represents a relative variation of $\pm$ 1 part in 8 thousand in the oscillator's 14.5 - 17.5 MHz frequency range. McKeighen and Buchin quote a less stringent stability requirement of 1 part per 1000.

The VCO control ramps are derived from a PROM look-up table via D to A converters. The 8 bit digitisation of the voltage control ramp implies an uncertainty of $\pm$ 6 kHz in VCO output or $\pm$ 1 part in 3000.

The stability of the oscillators themselves over a 1 hour period was measured at three fixed frequencies, see Table 4.1. Errors due to

Table 4.1: Voltage-controlled oscillator stability vs. frequency.

Frequency (MHz)	Stability (kHz)	Relative Stability
15.00	± 1.50	± 1 part in 10,000
16.25	± 2.45	± 1 part in 5,000
17.50	± 7.60	± 1 part in 2,000

variations in control ramp do not appear in these measurements. Other observations made from day to day at a fixed frequency of 17.5 MHz imply a VCO stability of better than $\pm$ 1 part in 4000.

Dynamic performance of the VCO's was estimated by observation of actual echo trains. Final setting up of the VCO frequency versus time characteristic was performed empirically. Echoes returning to the array from an on axis spherical reflector in a water tank, were observed on each channel, see Section 5.3. The VCO voltage ramp gain and offset adjustments were used to obtain the best possible echo alignment over a complete line. Phase errors were typically $\pm$ 0.07 periods, and had a worst case extreme of about $\pm$ 0.2 periods (equivalent to $\pm$ 1 part in 5600 and $\pm$ 1 part in 4000, respectively).

The long term, unattended behaviour of the swept delays has not been fully investigated as they were always carefully adjusted before each trial session. It is felt that some form of feed-back control is probably desirable. Some reduction in the demands made on the VCO's would be possible by combining fixed geometrical focusing with swept focusing. A number of authors have described annular arrays formed from concave bowls for use as part of a swept focus system (e.g. Arditi et al.). This reduces the maximum relative delay between rings and the rate at which the VCO frequency must be changed.

4.2.6 Interfacing

The unit has been designed for ease of interface to a standard B-scanner. The transducer mount may be adapted to fit the arm of the particular scanner in use. A p.r.f. pulse from the B-scanner is fed into the swept focusing unit and initiates reading out of a video A-scan line which is fed into the B-scanner's scan converter in place of its own receiver output.

The maximum rate at which the swept focusing unit can produce A-scan lines is 800 Hz, see Section 4.2.1. If the B-scanner attempts to drive the unit above this frequency it will only produce lines on alternate p.r.f. pulses.

To obtain the images presented in Chapter 5 the swept focusing system was used with a Fischer Diasonograph 4201 Static B-Scanner with digital scan converter.

4.3 Summary

An electronic unit has been described which accepts signals from a 4 ring annular array, compensates for the phase variations with depth of the signal from each ring and produces a video A-scan output suitable for input to the scan converter of a standard static B-scanner. Signals are input serially from each ring of the array in turn. This method reduces overall cost without curtailing its versatility as an evaluation system. Associated disadvantages disqualify it from use in real-time imaging where parallel data collection would be necessary. Digital delays have been identified as the most suitable for use as dynamic delay elements and to meet the storage requirements of serial data acquisition.

Control functions have been derived for the rephasing of the echo signals. A synthetic aperture function which accounts for the off-axis origin of transmitted pulses when the rings are fired individually, has been described. Using this novel feature, a dynamic focus response may be obtained on transmission as well as reception.

The necessary VCO stability to maintain the echoes co-phasal throughout the depth of the scan was considered. A stability close to this is possible with the open loop control system used.

Interface of the unit to a static B-scanner was described.

Chapter 5

EVALUATION OF THE DYNAMIC FOCUSING SYSTEM

Dynamic focusing presents a means of overcoming the compromise inherent to the design of fixed focus probes.

5.1 Introduction

The aims of this project have been laid out in Section 1.6. Annular array design has been investigated theoretically in Chapters 2 and 3. The manufacture of an array and associated electronics has been described in Chapters 3 and 4. The feasibility and focusing capabilities of the prototype system are assessed experimentally in the present chapter, which also compares theoretical and experimental results to confirm the reasonable use of theoretical predictions in future designs. Assessment of the array's focusing capabilities is performed from iso-echo contour maps and images of phantom targets.

5.2 Format of Chapter

The swept focusing system has been designed as a flexible unit, so that the conditions under which it is being operated are clear, the control settings and setting up procedure are discussed in detail (Section 5.3). A number of different focusing modes have been investigated and these are outlined in Section 5.4. Section 5.5 compares computer beam simulations and experimental beam plots. This is followed by the main body of the chapter where the focusing capabilities of the system are assessed.

5.3 Control Settings

The control settings and setting up procedure prior to obtaining beam plots are given below. Details of the array used are given in

(1) Apodisation: a weighting factor proportional to ring radius was used on both transmission and reception. For each channel the excitation voltage and the gain of the final summing amplifier were appropriately adjusted.

(2) Time gain compensation: the T.G.C. facilities of the main receiver amplifier were switched out, so that the receiver gain was constant with time.

(3) Attenuators: transmitter attenuation was set at -30 dB. The receiver attenuator was adjusted so that the maximum on-axis A-scan echo amplitude from the target was approximately 1 volt. Transmitter and receiver attenuator settings were noted so that the relative sensitivities of the different focusing modes could be calculated.

(4) Transmit focus: the excitation delays for each channel relative to channel 4, were calculated for the desired focal position and then digitally programmed into the electronics.

(5) Receive focus: the position of the receive focus is dependent on a set of initial delays and the clock sweep function programmed into the swept function control ROM's. Final setting up of the receive focus was performed empirically after approximate setting of the initial delays and programming of the ROM's with the appropriate function. A steel ball moveable along the transducer axis, was used as a target.

The initial delays were adjusted while observing echoes from it at the near point (30 mm), until they were aligned in each channel. The ball was moved to the far point (170 mm), and the echoes again observed. A fixed multiplying factor (gain) and off-set control are available for minor adjustment of the sweep functions. The gain control was used to align echoes from the far point. Alignment was checked at other points along the axis. A fixed receive focus was set up in a similar manner to the transmit focus but using the initial delays, the sweep function being disabled.

With one exception, see Section 5.4, the receive swept focus was always adjusted with the array unfocused on transmission. In calculating the receive sweep function an assumption is made that the transmitted pulse originates at the centre of the transducer (Section 4.2.4.1). This is a reasonable assumption for points in the far-field. It becomes increasingly unrealistic as the near-field is entered. The pulse shape in the near-field is complicated and relatively long as contributions from each ring barely overlap. Even empirical adjustments become difficult. In general, alignment was performed for the initial cycles of the respective echoes. Observing the sums of various echo pairs and adjusting for a maximum was also found useful. In this respect the synthetic aperture focus is particularly advantageous. Only a single pulse from one ring is present in the transmission field on each transmit-receive cycle. The respective near-field echoes are therefore much simpler and more easily aligned. The sweep function takes into account the off-axis

origin of the transmitted pulses (Section 4.2.4.2).

For obtaining phantom images, the control settings were as for beam plotting with the exception of the attenuation and T.G.C. controls. These were adjusted as would normally occur in imaging, to obtain the optimum image.

5.4 Focusing Modes

Storage and variable delay of the received signals from each ring of an array presents a flexible choice of focusing modes. The transmission focus may be varied by relative delay of the excitation to each ring. Point foci at predefined depths produced by spherical wavefronts, or a line focus produced by a conical wavefront, are possibilities. A large number of combinations of transmit and receive focus exist. Those chosen for investigation are listed in Table 5.1. Provision of the swept foci are discussed in Section 4.2.3. Mode (4) differs slightly from the others in that adjustment of the receive swept focus was performed with the array focused on transmission.

Comparison of the prototype array with a commercial transducer is possible by driving it from one channel of the swept focusing unit. Unfortunately, probes (9) and (10) were not available at the time the beam plots were performed, as they would have provided a fairer comparison for the 24 mm aperture array. The 13 mm diameter probe is one used regularly for abdominal work in a busy diagnostic radiology department. Its imaging performance is considered good, better than that of some 19 mm probes. Because of its limited size it does not have as strong a focusing action as the larger array, particularly at depth, i.e. 100 - 200 mm.

Table 5.1: Focusing modes.

Index	Transmit focus	Receive focus
1	Unfocused	Unfocused
2	Unfocused	Swept focus
3	Point focus (90 mm)	Swept focus
4	Point focus (90 mm)	Swept focus*
5	Point focus (130 mm)	Swept focus
6	Point focus (90 mm)	Point focus (90 mm)
7	Swept focus (Synthetic aperture focus)	Swept focus
8	Fischer[1], 13 mm diam., 3.5 MHz, Medium Internal Focus (MIF) probe	
9	Diagnostic Sonar[2], 19 mm diam., 3.5 MHz, Long Internal Focus (LIF) probe	
10	Fischer, 19 mm diam., 3.5 MHz, LIF probe.	

Notes:

* See text

(1) Fischer Ultrasound, Bankhead Crossway South, Edinburgh, Scotland.

(2) Diagnostic Sonar Ltd., Livingstone, Scotland.

5.5 Comparison of Theoretical and Experimental Results

Both pulsed and continuous wave field simulations are based on solution of the same equation describing the acoustic field (equation 2.1, Section 2.4). Experimental confirmation of theoretical predictions for the pulsed wave field is available in the literature, see Section 2.4.1.2. Further confirmation for the pulsed field of an annular array is presented here.

The computer program described in Section 2.6.2 simulates the pulsed transmission or reception field of an annular array. Derivation of the transducer's pulse-echo response from this simulation is not strictly possible in general. Multiplying together transmission and reception responses to obtain the pulse-echo response has limited applicability, see Section 2.4.1.3. However, as only pulse-echo plots of the experimental field are available, this method has been used to provide comparable theoretical plots.

5.5.1 Discussion

Theoretical and experimental axial plots and cross-sectional plots at depths of 30, 50, 90 and 130 mm for the unfocused, and unfocused transmission-swept focus reception array are presented in figures 5.1 - 5.4. The axial plots are normalised to their individual axial maxima. The theoretical cross-sectional plots are normalised to the on-axis value of the corresponding experimental plots.

A similar shape for the unfocused-unfocused and unfocused-swept focus axial responses is predicted theoretically and confirmed experimentally. The experimental plots are, however, more peaked in the region of the maximum than is theoretically predicted.

Agreement between theoretical and experimental cross-sectional

Figure 5.1: Unfocused pulse-echo axial response, (a) experimental, (b) theoretical.

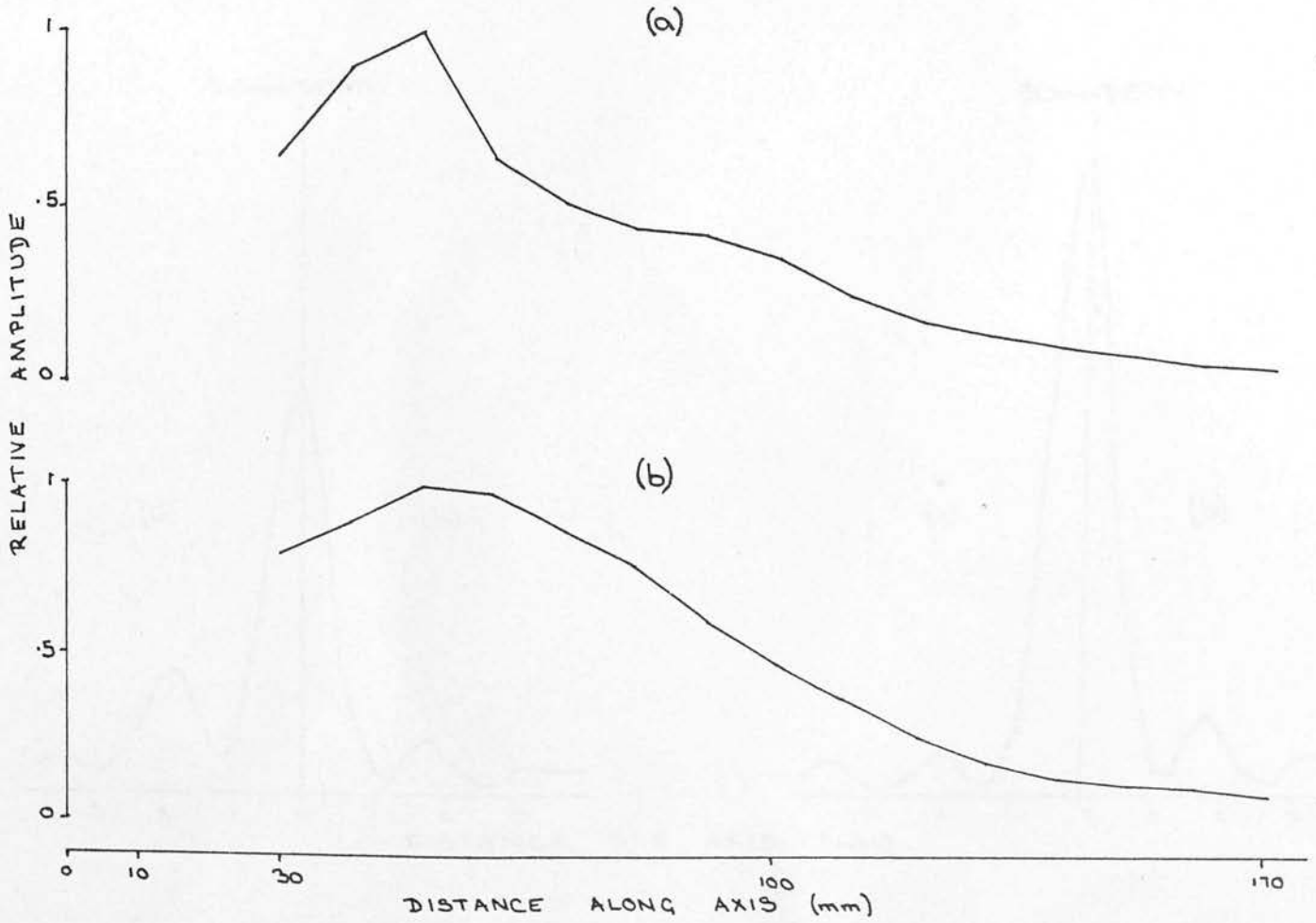

Figure 5.2: Unfocused pulse-echo cross-sectional response, (a) experimental, (b) theoretical.

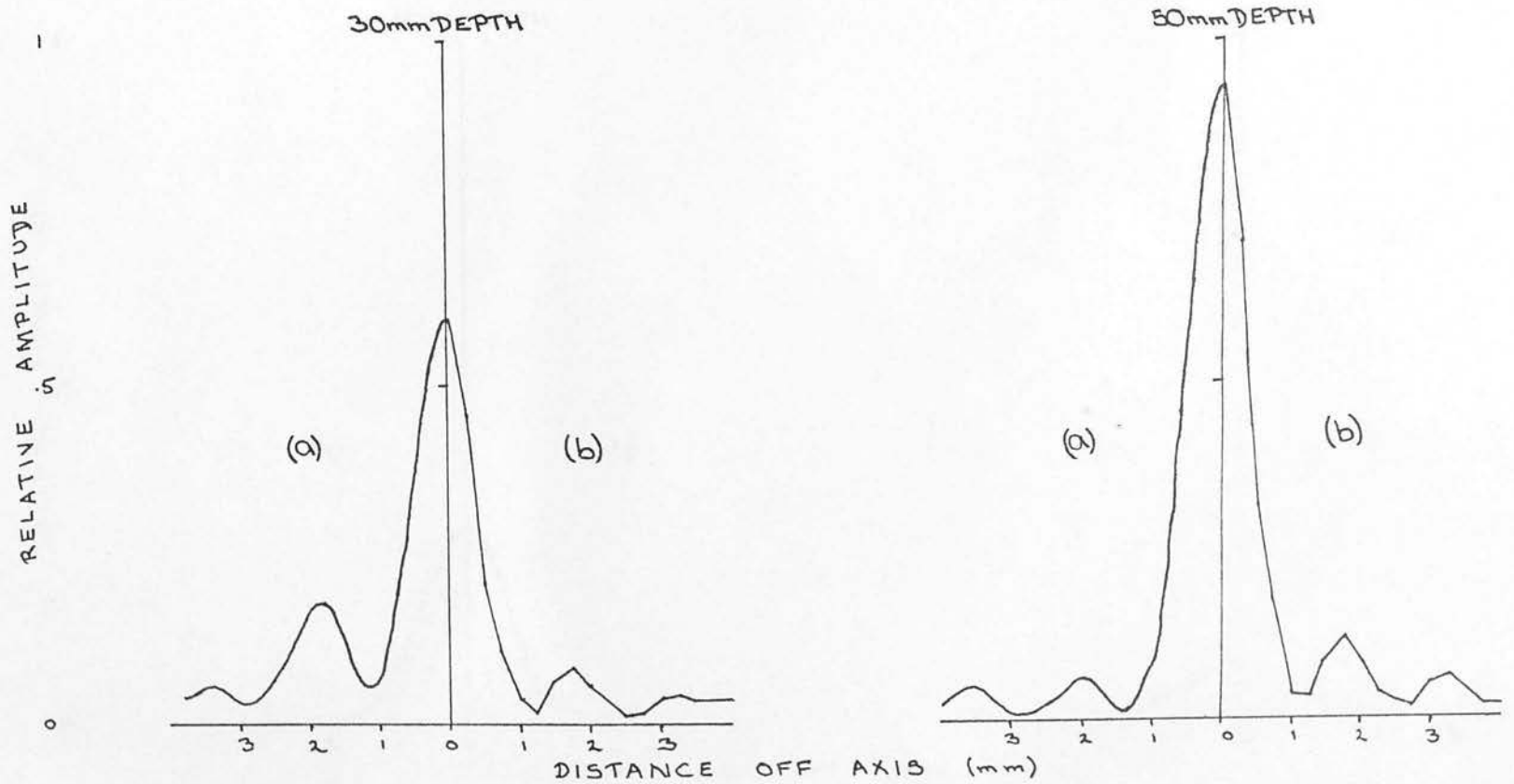

Figure 5.2: Unfocused pulse-echo cross-sectional response, (a) experimental, (b) theoretical.

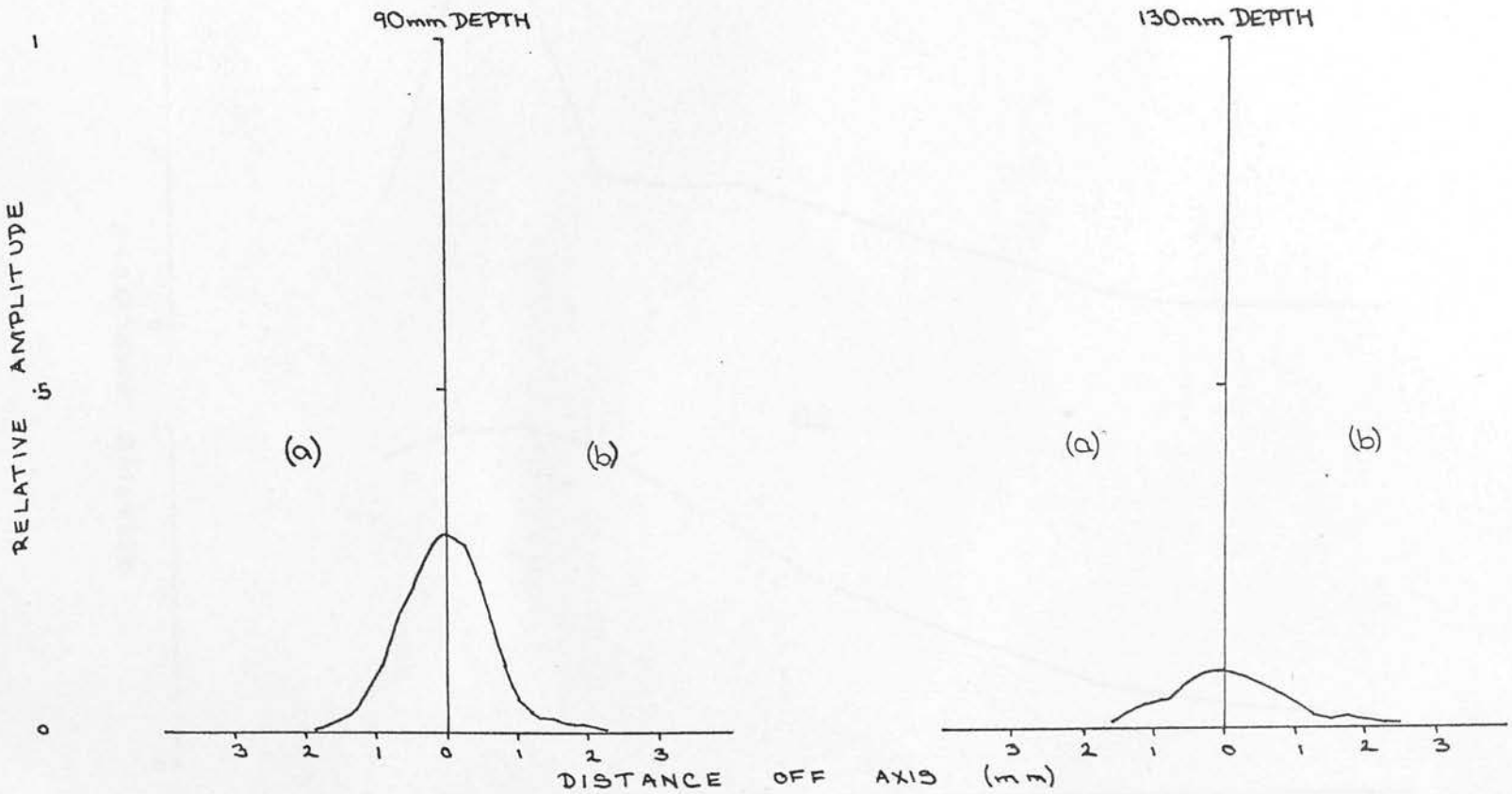

Figure 5.3: Unfocused-swept focus pulse-echo axial response, (a) experimental, (b) theoretical.

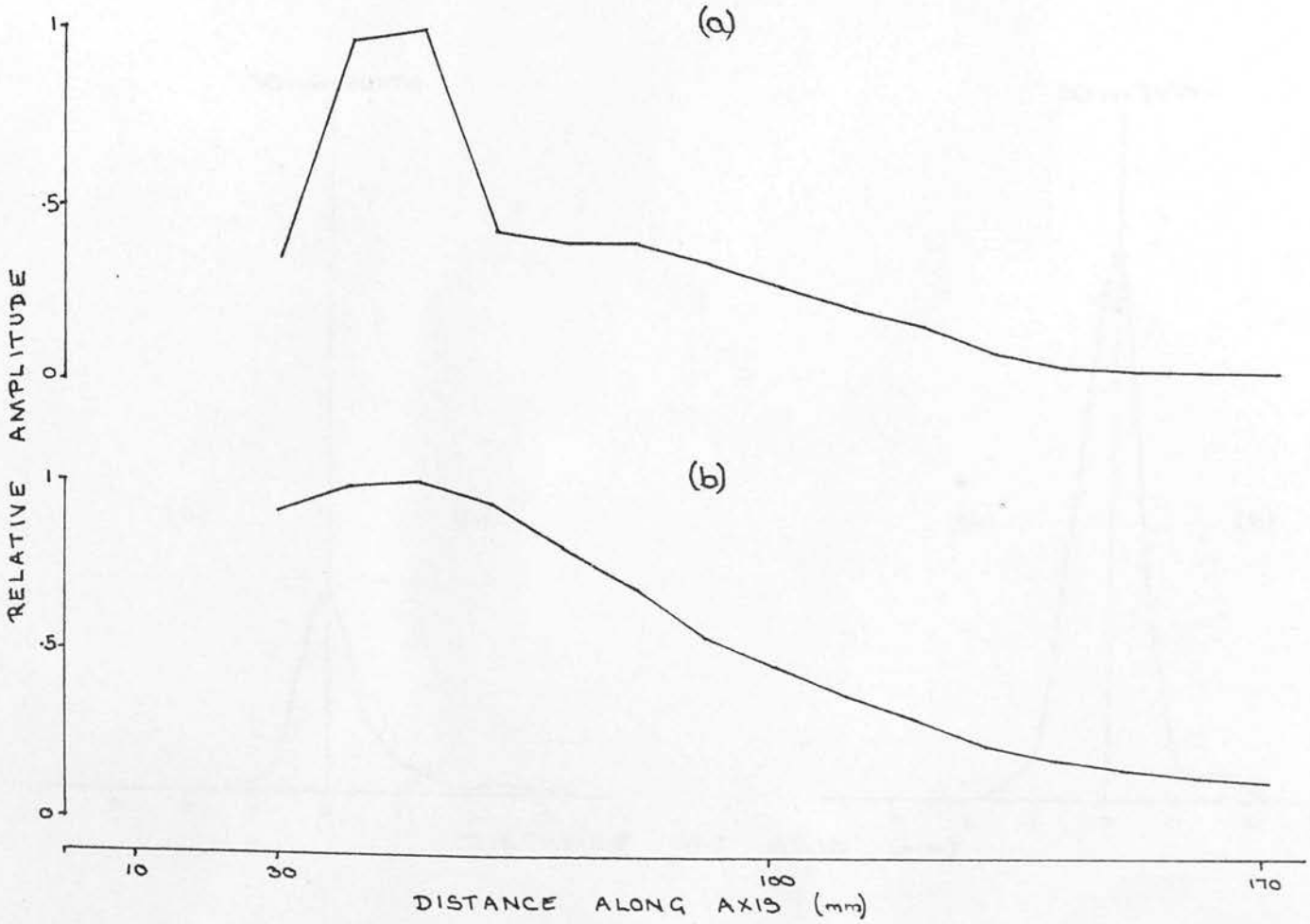

Figure 5.4: Unfocused-swept focus pulse-echo cross-sectional response, (a) experimental, (b) theoretical.

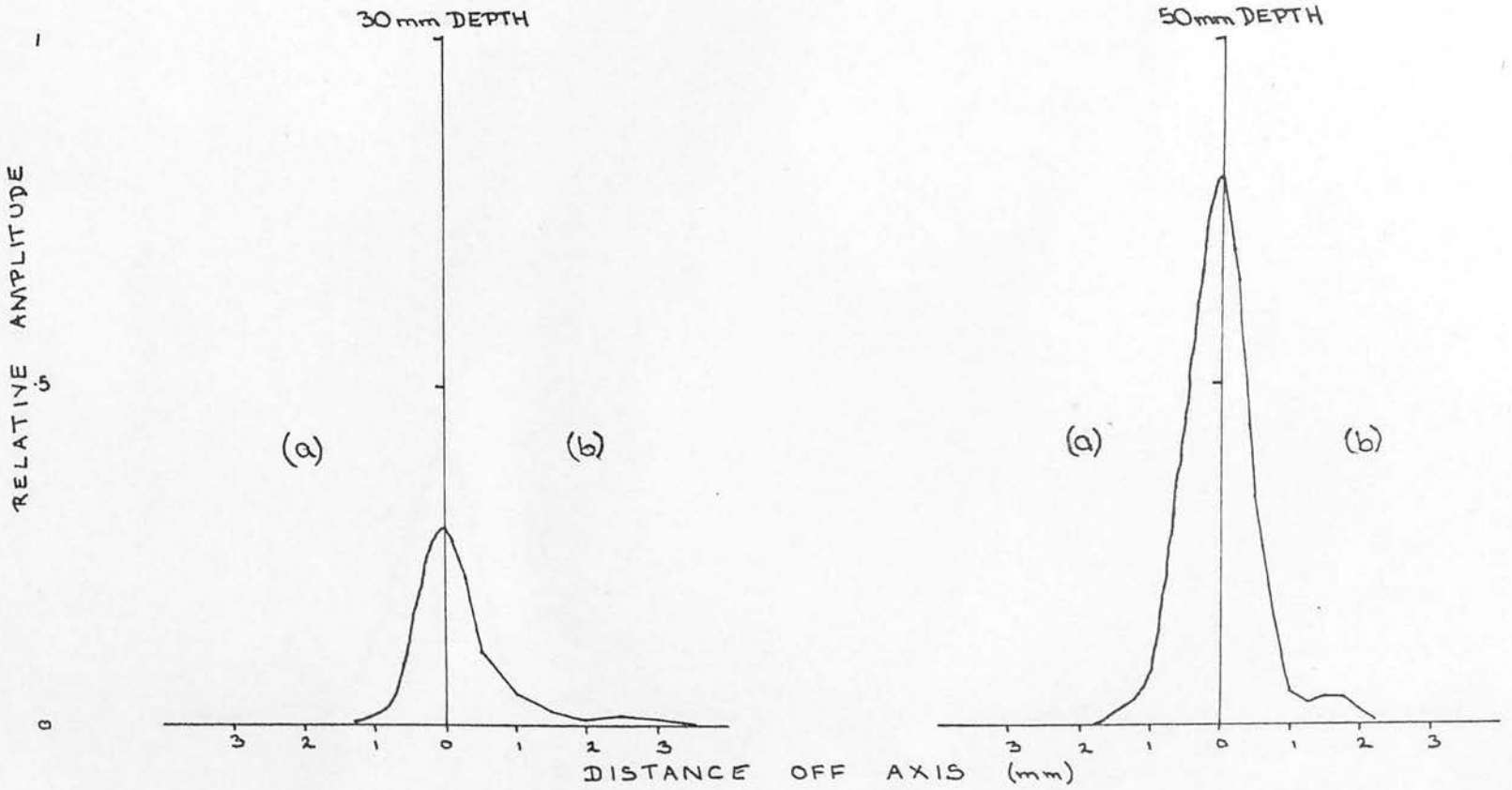

Figure 5.4: Unfocused-swept focus pulse-echo cross-sectional response, (a) experimental, (b) theoretical.

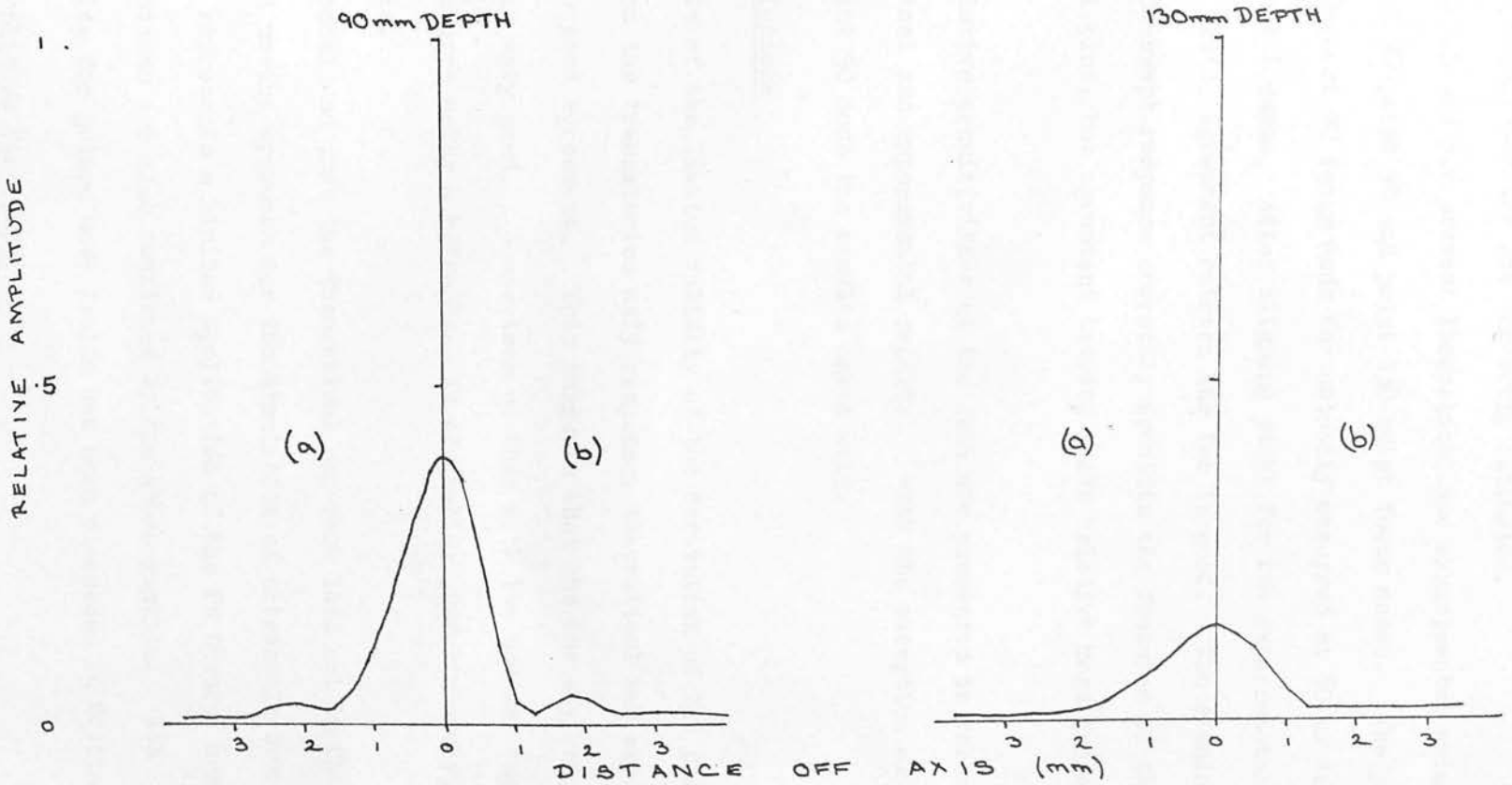

plots is quite good. Positioning of side lobes is correctly predicted although the magnitudes are not correctly estimated.

Figures 5.5 and 5.6 present theoretical and experimental axial plots for the point 90-point 90 and point 130-swept focus modes. The peak of the point 90-point 90 focus mode has actually occurred at 80 mm depth in the experimental case. After aligning peaks for the experimental and theoretical plots, agreement between the two is good. The simulation of the point 130-swept response correctly predicts the features of the experimental plot, but agreement between their relative magnitudes is poor.

The relative sensitivities at the foci are presented in Table 5.2 for theoretical and experimental results. With the exception of the point 90-point 90 mode the results agree well.

5.5.2 Conclusions

In spite of the limited validity of the derivation of the pulse-echo response from the transmission only response, theoretical and experimental results show good agreement. This suggests that the one way response simulation is very good. Comparison of this with the one way experimental response measured using a hydrophone is desirable; unfortunately, none was available.

It is concluded that the theoretical approach laid out in Chapter 2 represents a useful approach for the simulation of ultrasonic beams. The CW solution represents a limited application of the PW theory, hence its basic assumptions are also confirmed by the above results. Its interpretation for pulsed wave fields has been discussed in Section 2.5.2.

5.6 Echo Amplitude Distributions

5.6.1 Plotting technique

The transducer was mounted in a water tank. A small spherical

Figure 5.5: Point 90-point 90 focus pulse-echo axial response, (a) experimental, (b) theoretical, (note: theoretical response shifted so that peaks are aligned).

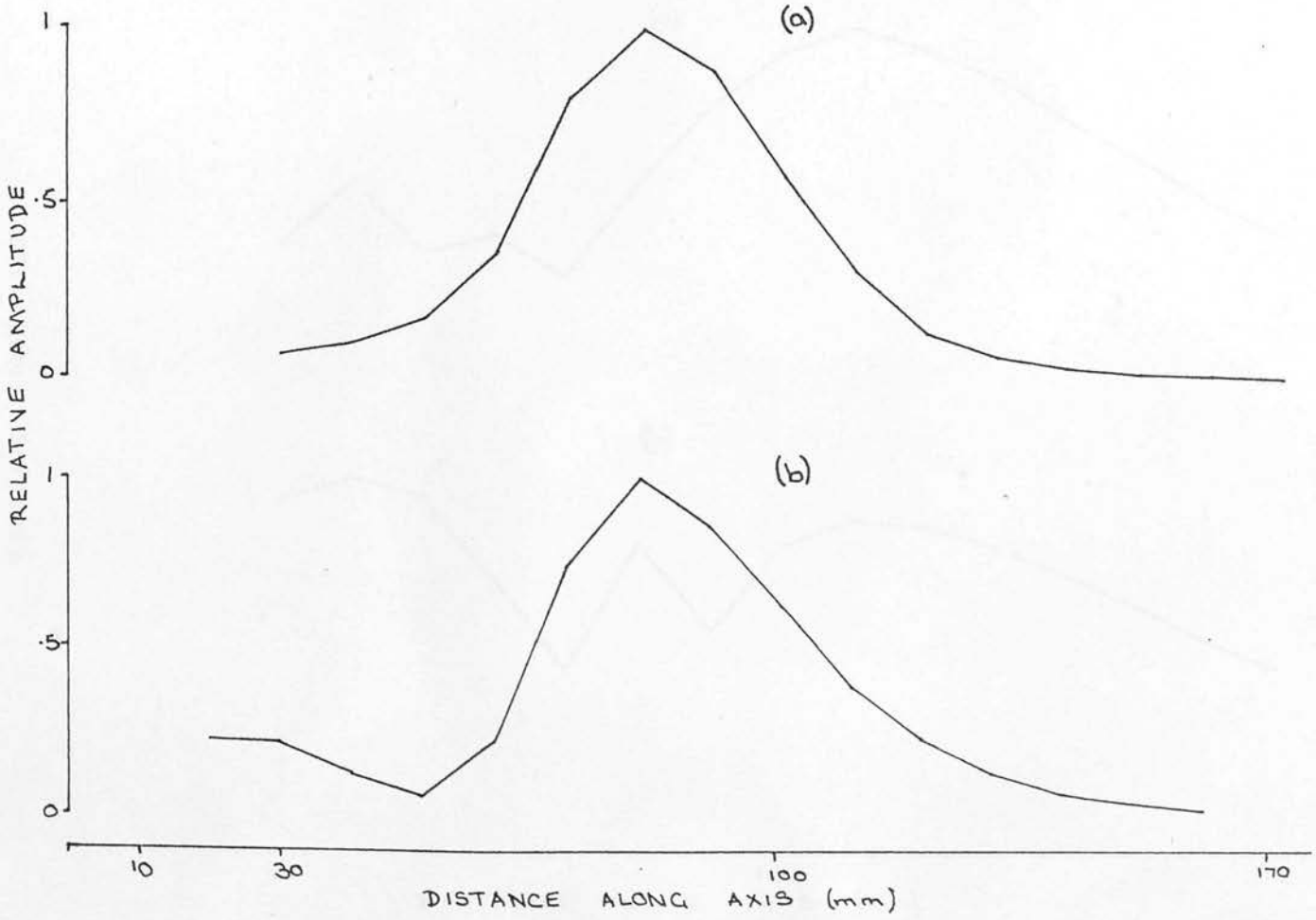

Figure 5.6: Point 130-swept focus pulse-echo axial response
(a) experimental, (b) theoretical.

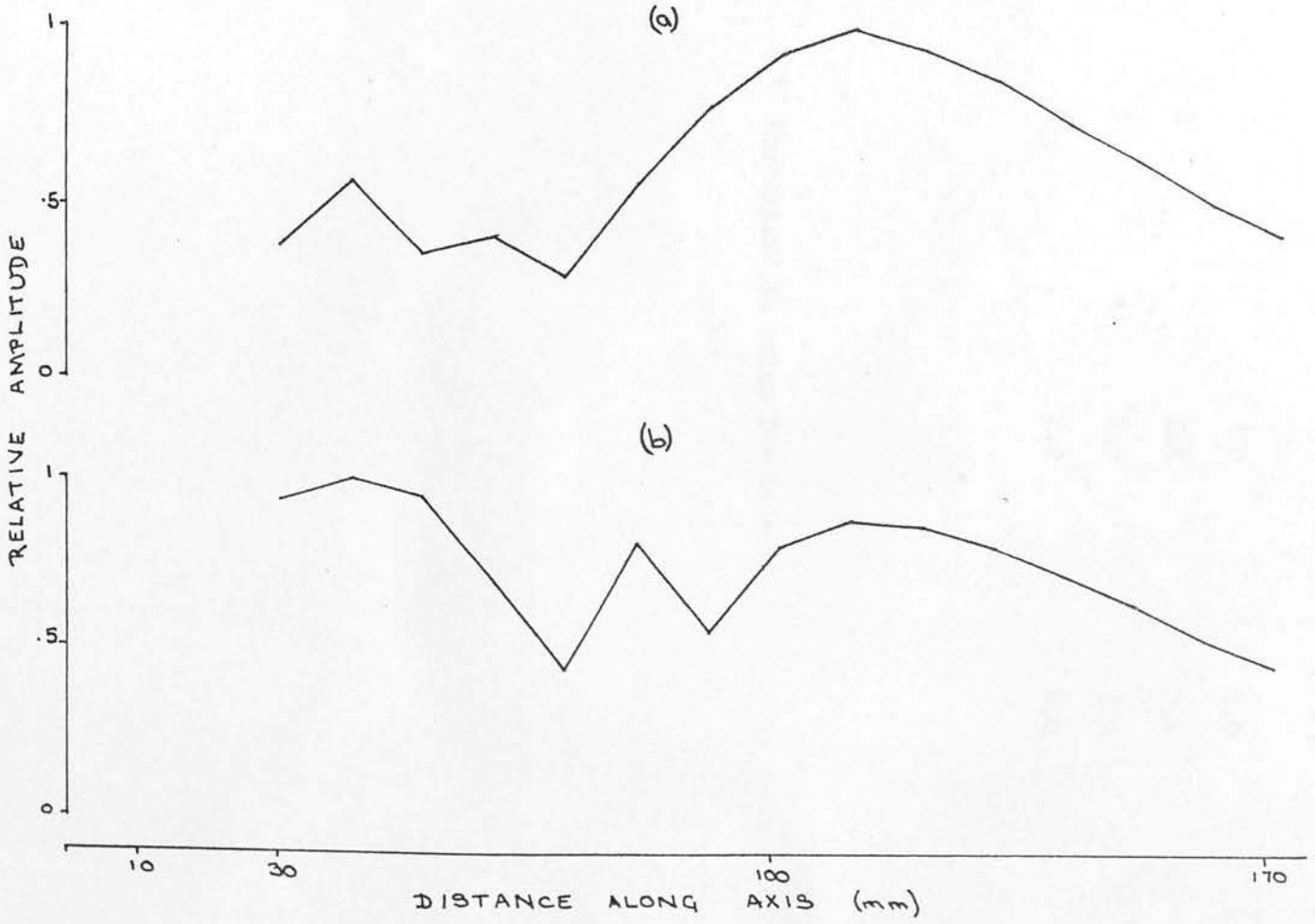

Table 5.2: Experimental and theoretical relative sensitivities.

Mode	Experiment*	Theory*
1	1.0	1.0
2	2.4	2.6
5	2.3	2.3
6	2.2	4.0

Notes:

* Normalised to value for Mode 1.

steel ball mounted on a rigid wire was automatically scanned along a line through the transducer axis, in a plane perpendicular to it. A positional signal was fed to an X-Y oscilloscope's X-plates and the A-scan video signal from the swept focusing unit to the Y-plates. Records of the beam cross-sections were made on 35 mm film.

Scans were performed at 10 mm axial intervals from 30mm to 170 mm. The oscilloscope spot size limited the display dynamic range to 20 dB. To increase this, plots were repeated at alternate depths with the Y-input sensitivity increased by 20 dB. The signal could then be observed down to the level of about -40 dB. "Ringing" of the transmitter pulse prevented useful results being obtained closer to the array than 30 mm.

The ball target size may be chosen freely within wide limits. The resulting beam profile is unaffected by variations in ball diameter of between 1.6 and 100 λ (Hospital Physicists Association publication 1978). The ball used had a 4 mm diameter, i.e. 9 λ.

Measurements made from enlargements of the 35 mm negatives have been used to produce the required iso-echo contour and axial echo amplitude plots. These are presented in figures 5.7 - 5.14, in the order they appear in Table 5.1.

5.6.2 General Features

A quantitative summary of the major features of the plots is given in Table 5.3. A detailed discussion of them is presented in the following sections. Column 1 lists the depths of occurrence of the on-axis maxima. These do not necessarily coincide with the nominal focal points because of the interaction between the focusing action of the ring's geometries, unfocused maximum at 50 mm, and that of the pulse delays.

Figure 5.7: Tx. Unfocused: Rx. Unfocused: Axial response and iso-echo amplitude contours of annular array #2c.

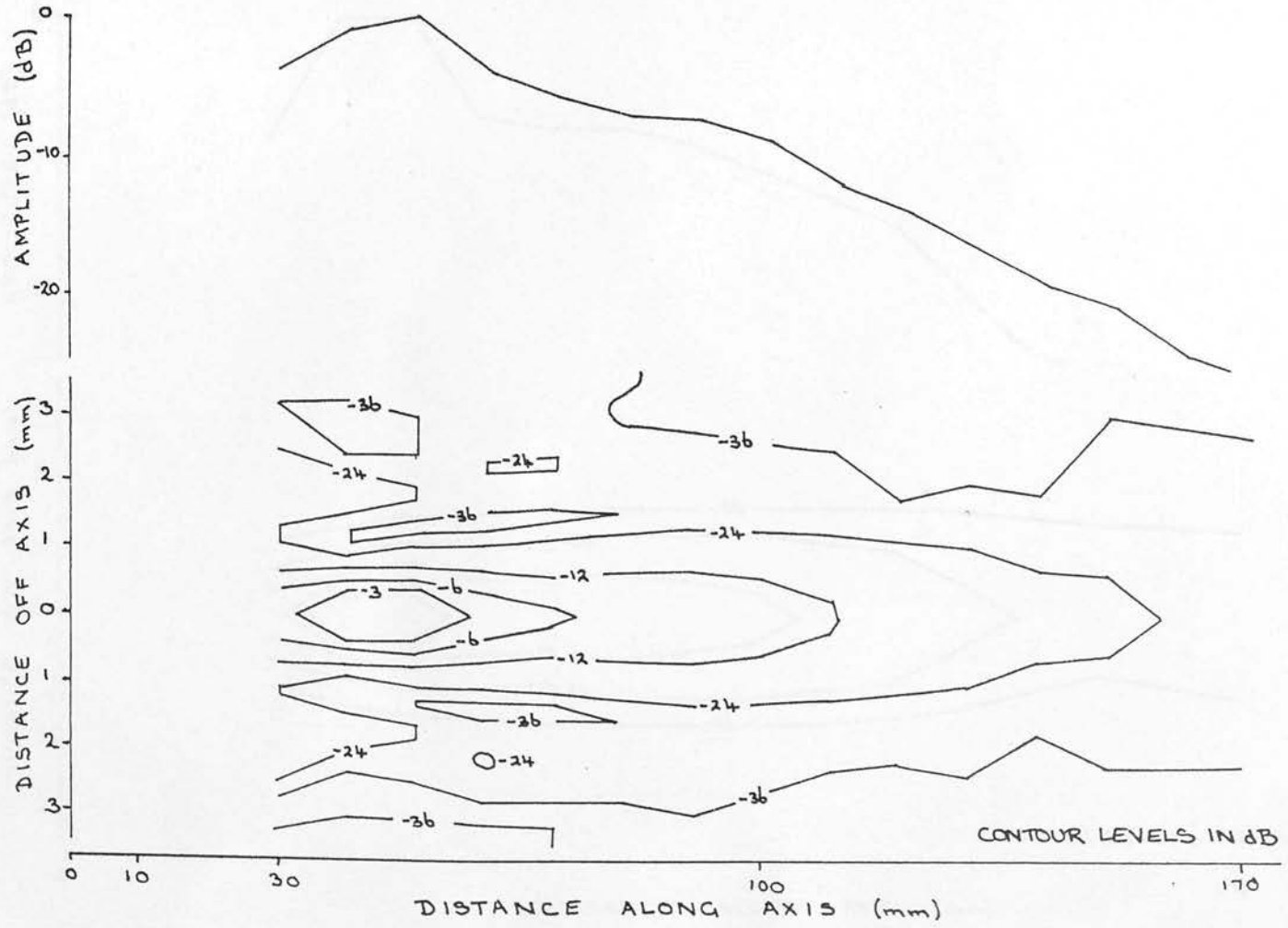

Figure 5.8: Tx. Unfocused: Rx. Swept focus: Axial response and iso-echo amplitude contours of annular array #2c.

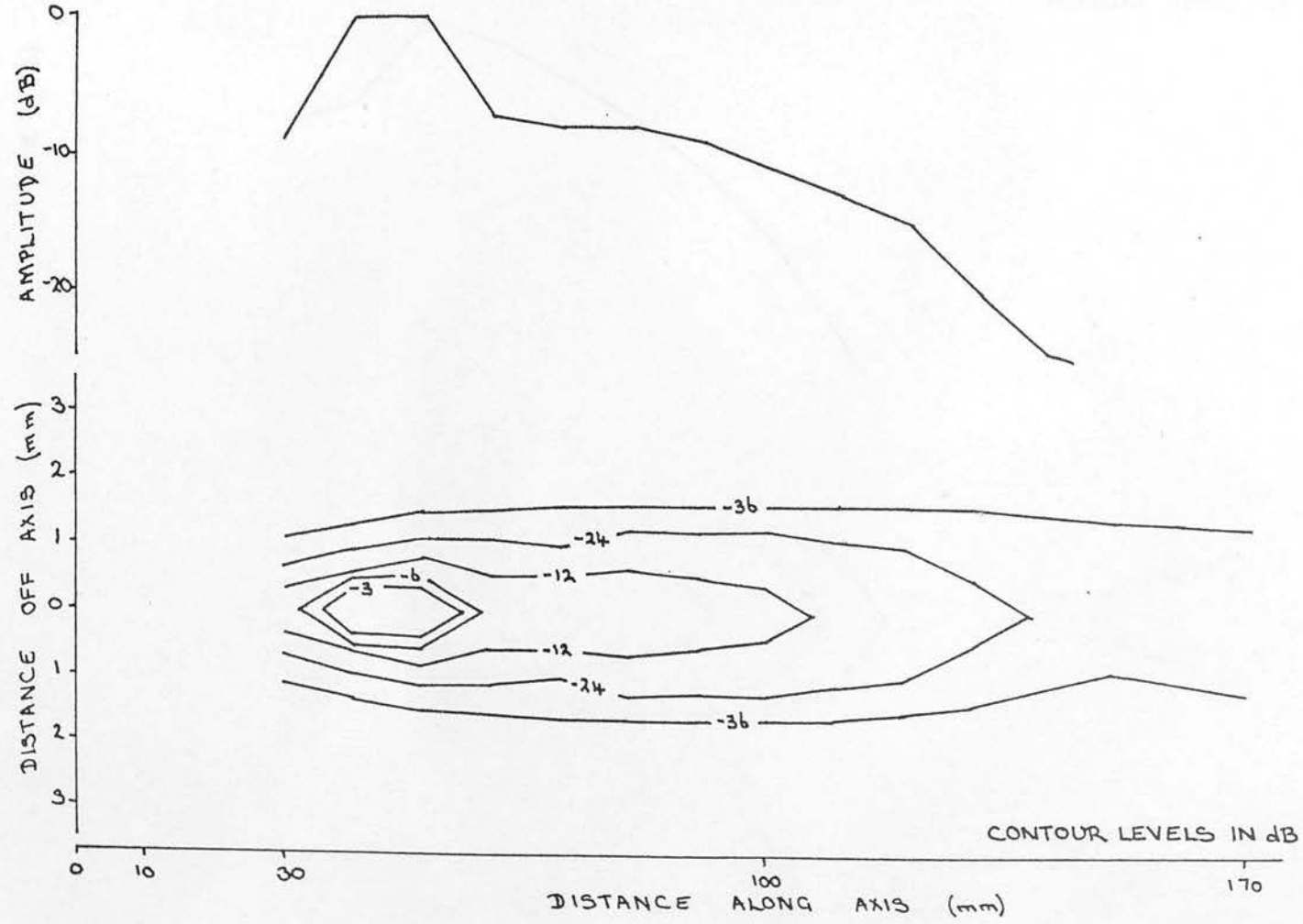

Figure 5.9: Tx. Point focus (90mm): Rx. Swept focus: Axial response and iso-echo amplitude contours of annular array #2c.

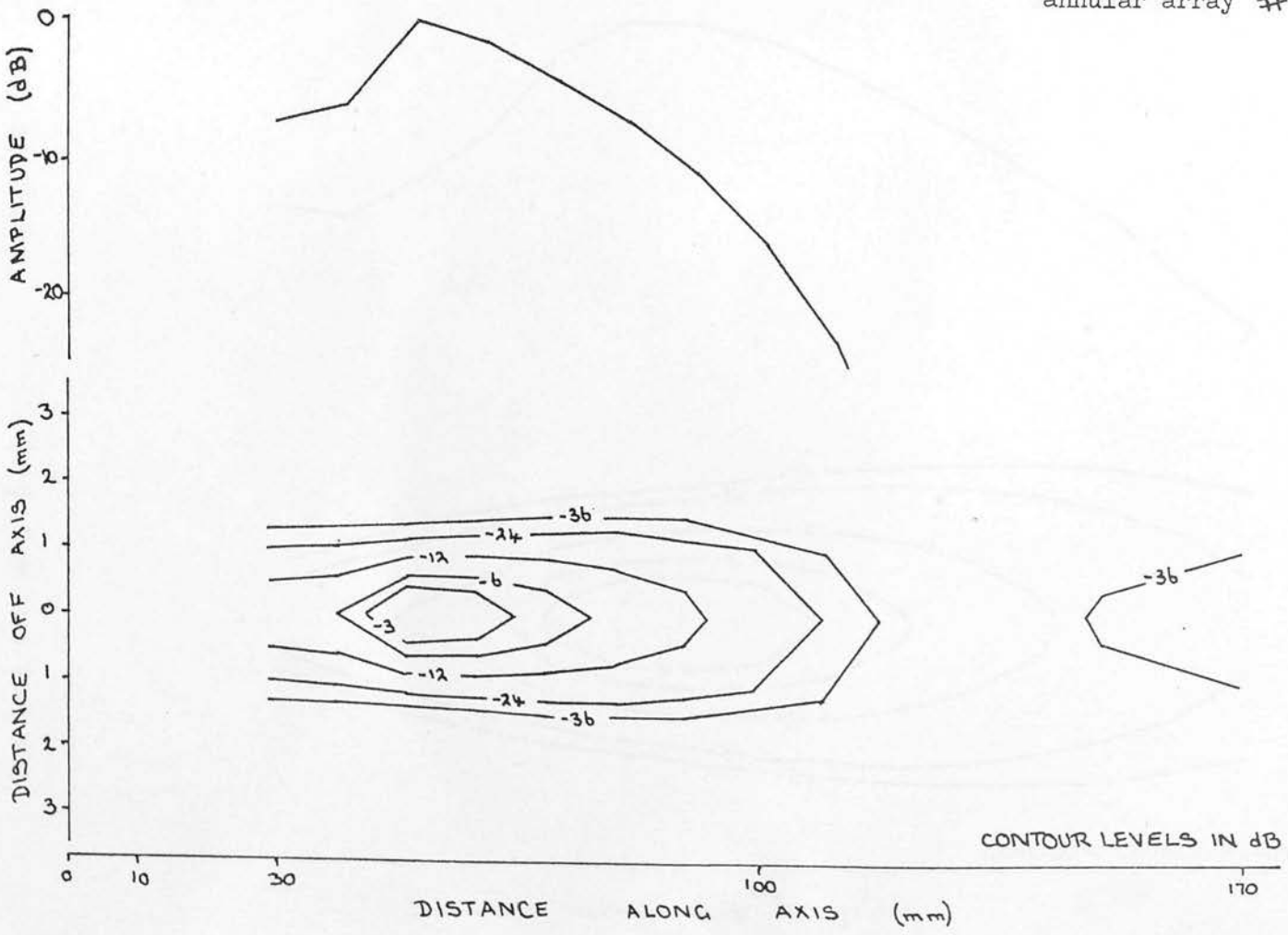

Figure 5.10: Tx.Point focus (90mm): Rx.Swept* focus: Axial response and iso-echo amplitude contours of annular array #2c.

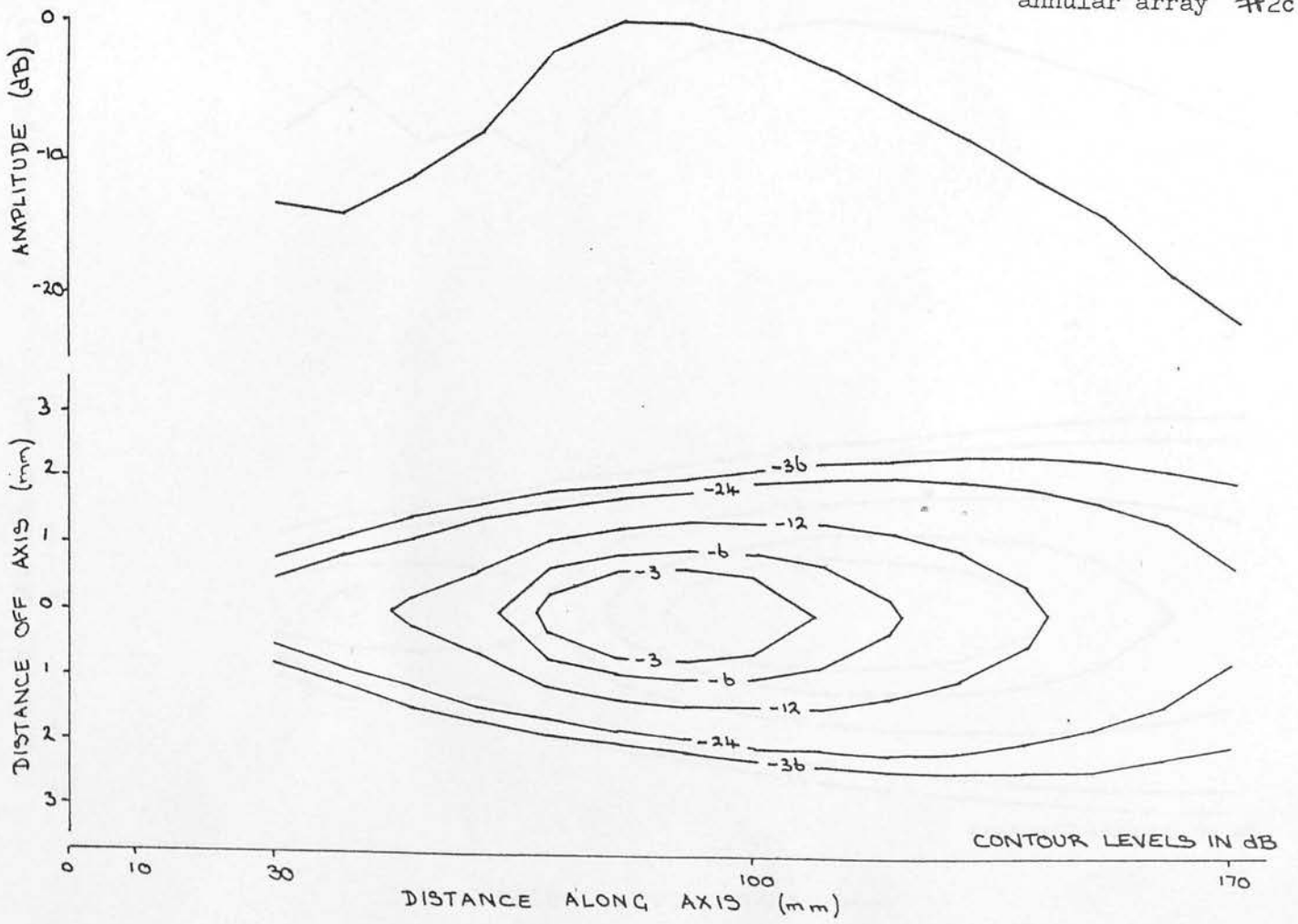

Figure 5.11: Tx. Point focus (130mm) ; Rx.Swept focus: Axial response and iso-echo amplitude contours of annular array #2c.

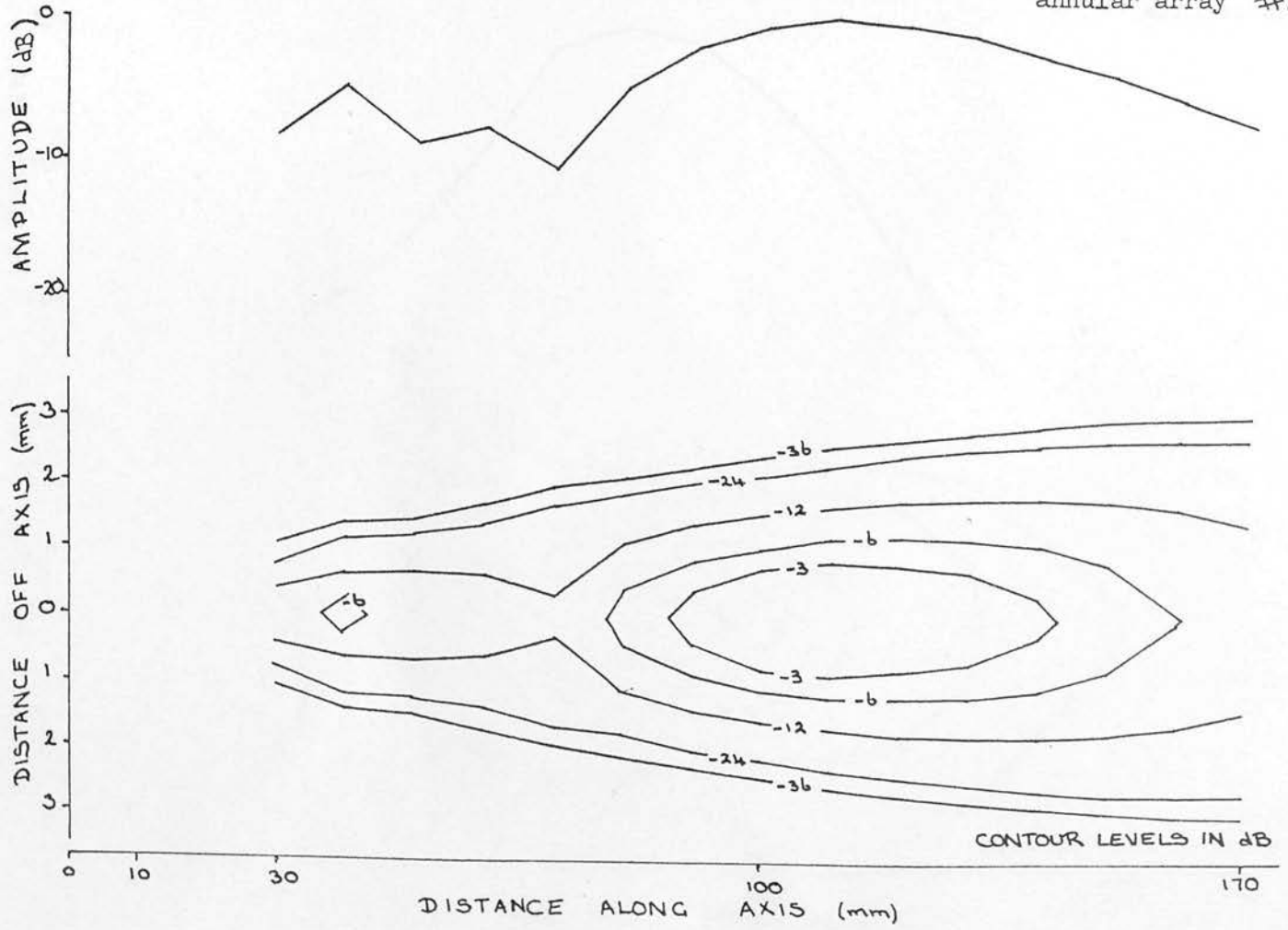

Figure 5.12: Tx. Point focus (90mm): Rx.Point focus (90mm): Axial response and iso-echo amplitude contours of annular array #2c.

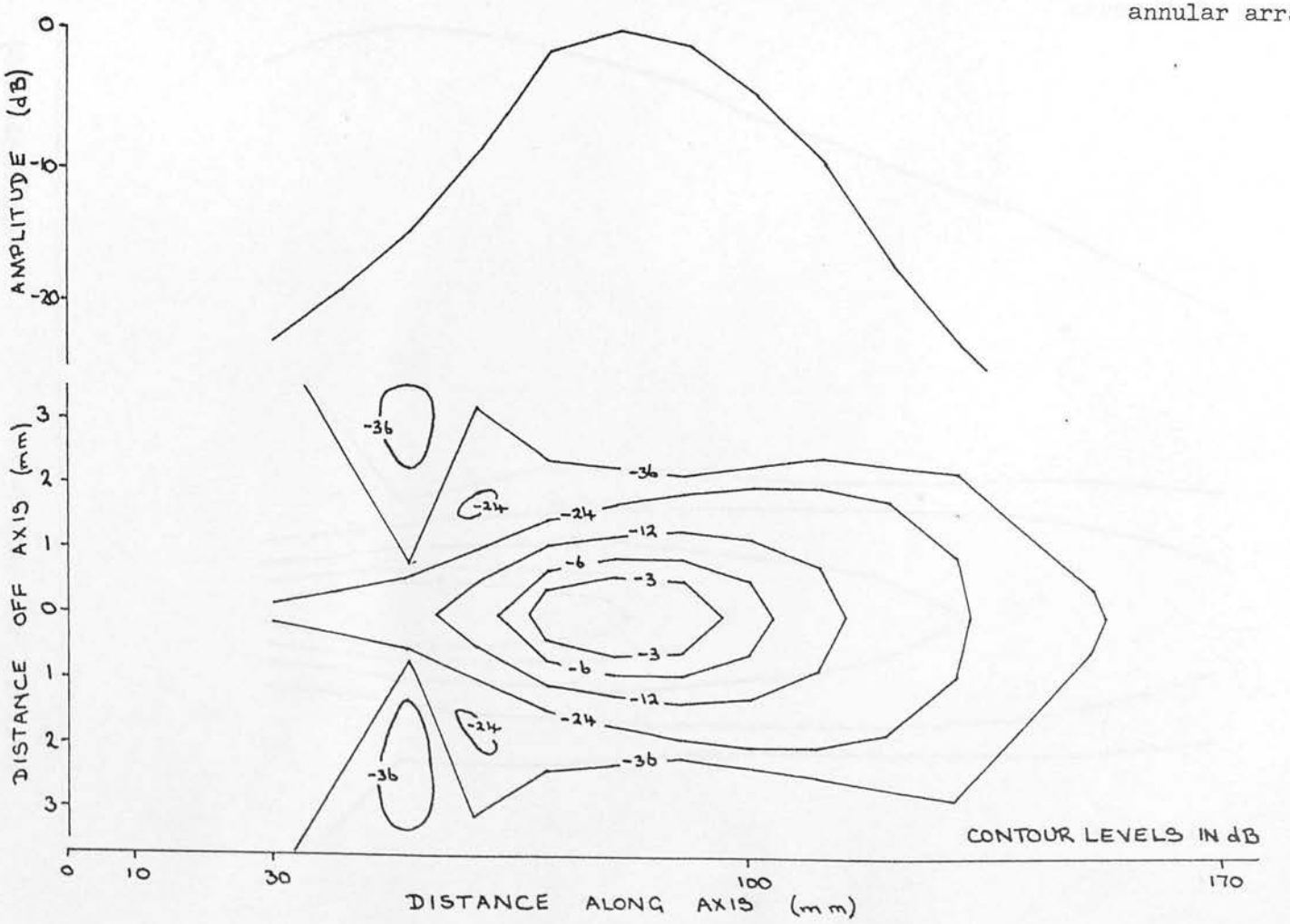

Figure 5.13: Tx. Swept focus: Rx.Swept focus: Axial response and iso-echo amplitude contours of annular array #2c.

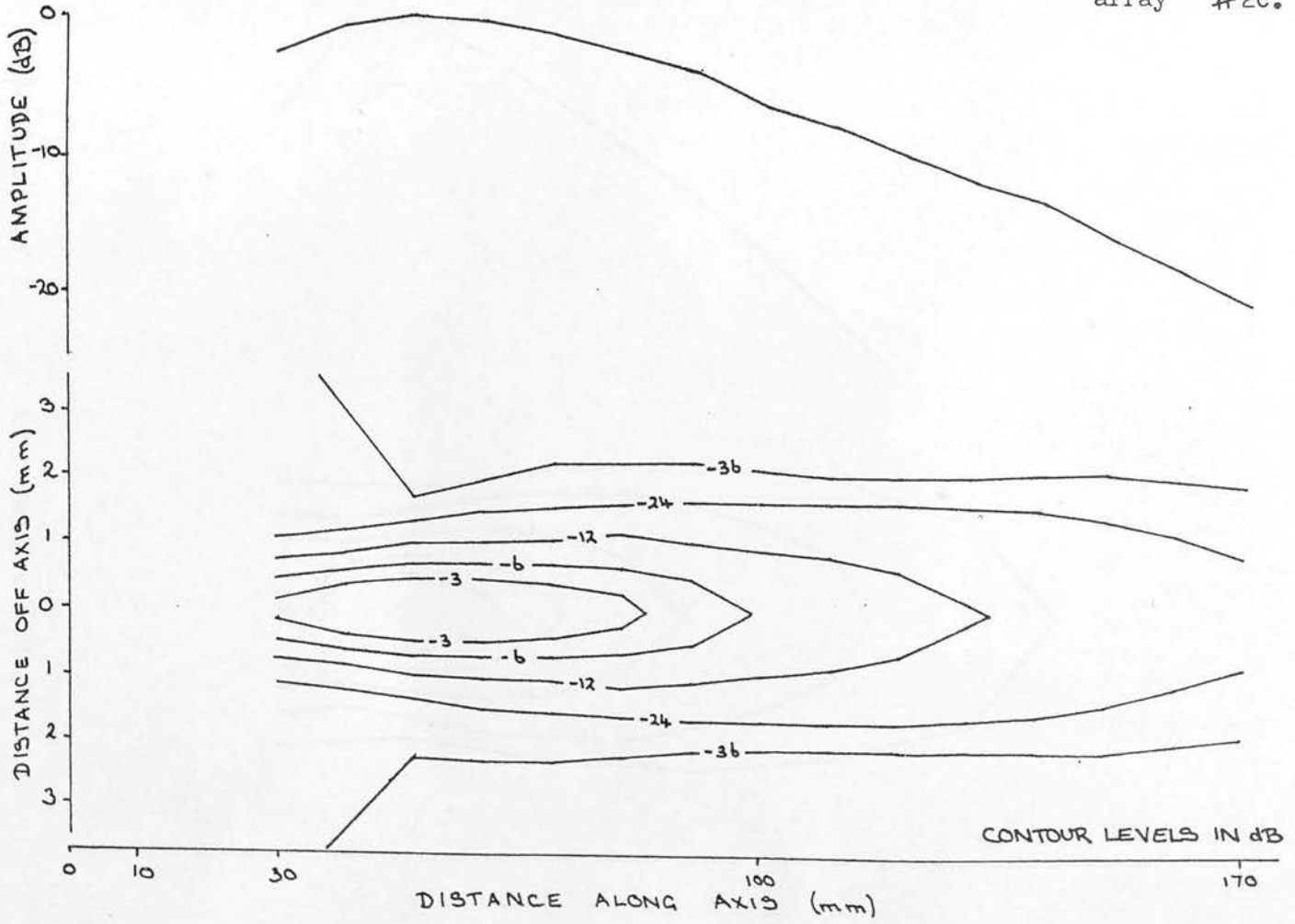

Figure 5.14: Axial response and iso-echo amplitude contours of a Fischer, 13mm diam. MIF probe.

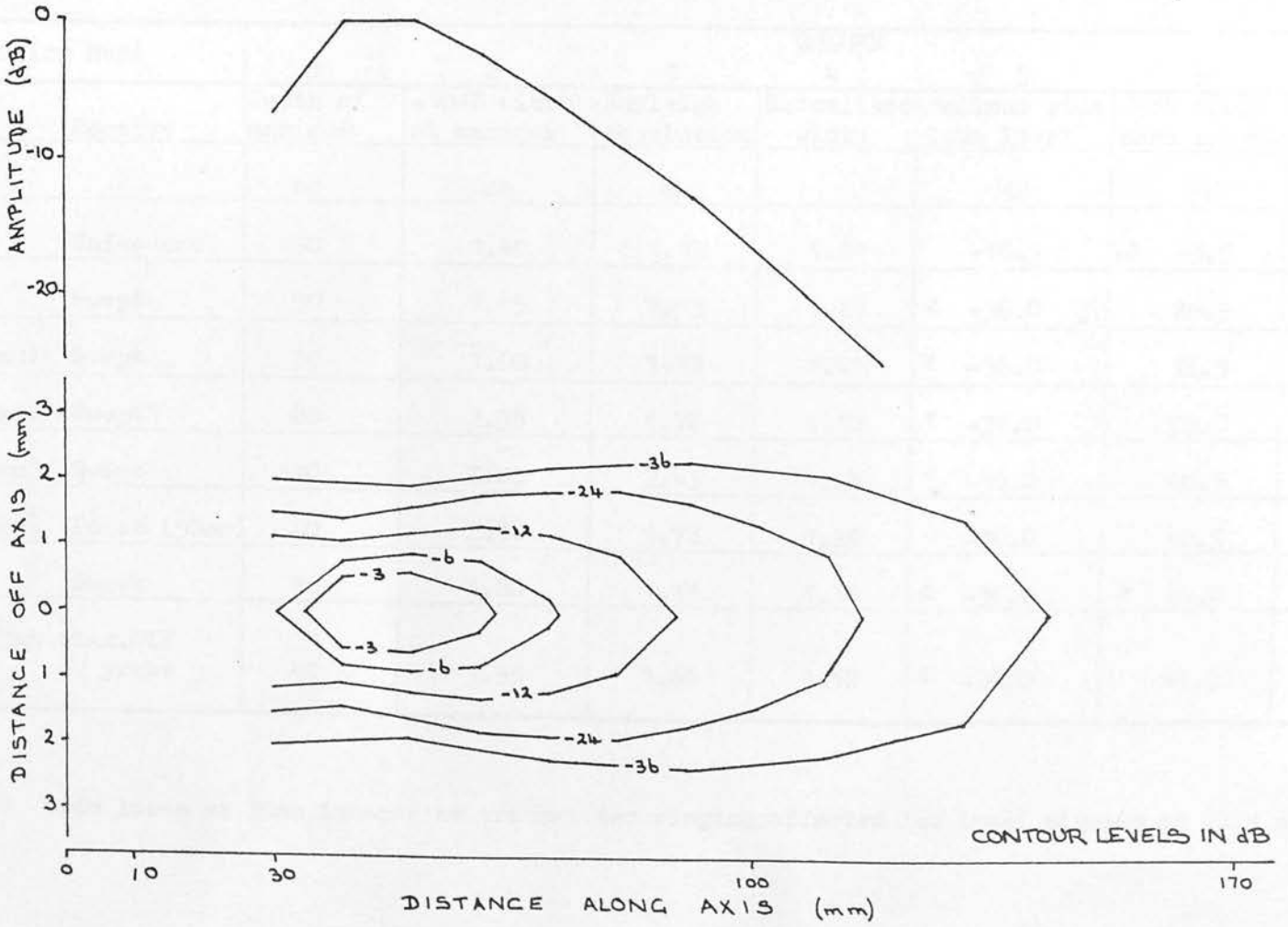

Table 5.3: Summary of iso-echo amplitude contour map features.

Focusing Mode		COLUMN 1	2	3	4	5	6	7
Transmit	Receive	Depth of maximum	-10dB width at maximum	Rayleigh resolution	Normalised width	Maximum side lobe level[1]	-6dB focal zone length	Relative sensitivity
		mm	mm	mm		dB	mm	
Unfocused	Unfocused	50	1.40	1.13	1.24	-18.5	> 43.5	0.22
Unfocused	Swept	50	1.45	1.13	1.28	< -36.0	26.5	0.51
Point (90mm)	Swept	50	1.60	1.13	1.41	< -36.0	36.5	0.76
Point (90mm)	Swept*	80	2.35	1.78	1.32	< -36.0	59.0	0.64
Point(130mm)	Swept	110	3.00	2.43	1.23	< -36.0	90.5	0.51
Point (90mm)	Point (90mm)	80	2.30	1.78	1.29	-30.0	40.5	0.49
Swept	Swept	50	1.80	1.13	1.59	< -36.0	> 69.0	1.00
Fischer 13mm diam.MIF probe		40	1.95	1.65	1.18	< -36.0	41.0	0.95

Notes:

(1) Side lobes at 30mm ignored as transmitter ringing affected low level signals at this depth.

It is apparent from the beam width measurements that the width of the focused beam is greater than that of the unfocused, even when the focus occurs at the same depth as the unfocused maximum (compare modes 1, 2 and 7, Table 5.3). The path lengths from the array's inner and outer regions are different and uncompensated for in the unfocused array (figure 5.15). For array #2c the outer area has a greater sensitivity than the inner because it is larger. The contribution associated with it is greater. The conditioning applied to the returned signal defines the beam shape by the maximum amplitude observed with time at a given point and so the main lobe is defined mainly by the shape of the outer ring response, which is relatively narrow. Energy from the centre of the array becomes associated either with the side lobes or regions before or after the main pulse. On focusing, the energy from all parts of the array is constructively associated together at the focus. This enhances sensitivity. Energy previously in the side lobes is now associated with the main lobe and so side lobe levels drop. However, energy from towards the centre of the array is less well localised about the axis than is that from the outer regions and so the beam becomes slightly broader as well.

Implementation of a dynamic receive focus improves the overall shape of the beam, reduces side lobe levels and increases sensitivity, see figures 5.7 and 5.8 and Table 5.3. It does not extend the "focal" region compared to the unfocused mode. Judicious selection of transmit and receive foci can significantly extend the focal region (point 130-swept and swept-swept modes, Table 5.3).

5.6.3 Discussion

5.6.3.1 Beam Width (Table 5.3, Columns 2-4)

The -10 dB beam full widths at the axial maxima are presented in

Figure 5.15: Uncompensated path lengths in the unfocused beam (Section 5.6.2).

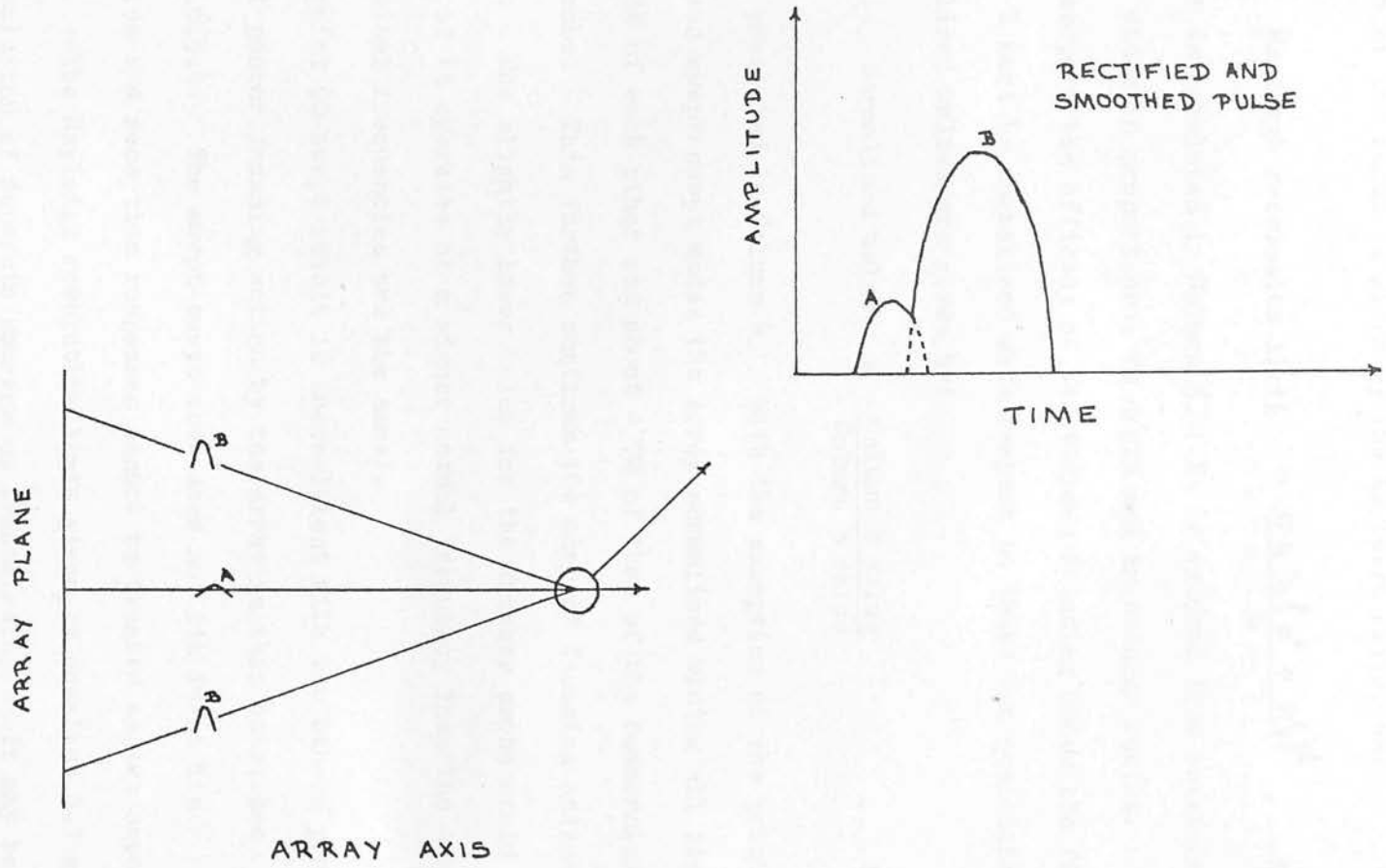

Table 5.3, Column 2. It is assumed that the axial maximum is the point at which the beam is "most" focused. A measure of the expected beam width at the focus is given by the Rayleigh criterion:

$$\text{Rayleigh resolution limit} = \frac{0.6\,\lambda\,(a^2 + z_f^2)^{\frac{1}{2}}}{a} \quad \text{---} \; 5.1$$

This limit is tabulated in Column 3. It is evident from equation 5.1 that beam width is proportional to depth and transducer radius. In order to compare the efficacy of the various focusing modes the figures in Column 2 must be normalised with respect to these two quantities. The normalised values are given by:

$$\text{Normalised value} = \frac{\text{Column 2 value}}{\text{Column 3 value}} \quad \text{---} \; 5.2$$

These are presented in Column 4. With the exception of the point 90-swept and swept-swept modes the array normalised widths all lie within $\pm$ 3% of each other and about + 7% of that of the commercial Fischer probe. This further confirms the correct focusing action of the array. The slightly lower value for the Fischer probe would be explained if it operates at a higher actual frequency than the array (their nominal frequencies are the same).

The point 90-swept result is inconsistent with the others probably because of poorer focusing action by the array in this case, see Section 5.6.3.4. The swept-swept mode does not fit in as its transmission and reception responses cannot be treated as two separate processes. The Rayleigh resolution limit given by equation 5.1 applies to the resolution of separate sources on transmission. It may be usefully applied as a normalisation factor in a pulse-echo system where the transmission and reception processes for the complete source occur separately. For the synthetic aperture focusing mode, pulse-echo

responses occur separately for each ring and are then combined to form the overall pulse-echo response. This cannot be split into a separate transmission process for the whole array, followed by a reception process, and so normalisation based on equation 5.1 is not applicable.

Under imaging conditions, time gain compensation is applied to the received signal. This compensates for attenuation of the signal with depth and for variations in on-axis sensitivity. Its effect on beam width is to increase it at points away from the maximum, particularly at depth. A relatively deep axial maximum may then be advantageous. Time gain compensated plots are discussed in Section 5.6.3.5.

5.6.3.2 Side Lobe Levels (Table 5.3, Column 5)

The maximum side lobe levels relative to the on-axis field maxima are quoted in Column 5. Side lobes present at 30 mm depth have not been included as "ringing" of the transmitter pulse affected these figures. The side lobe levels are reduced by focusing, in most cases to below -36 dB, i.e. the minimum differentiable level. Side lobes present below this level are evident in some of the images presented later where signal compression before display increases the observed dynamic range.

5.6.3.3 Sensitivity (Table 5.3, Column 7)

Column 7 presents the amplitude sensitivities of the various focusing modes relative to the most sensitive. Transmitted pulse amplitude in the far-field is proportional to the excitation voltage V_E, and transducer area A. The reception sensitivity of the transducer towards a similar point is proportional to area. These quantities are used to normalise the maximum echo amplitude e_{max}, obtained using each focusing mode. In all modes except the swept-swept mode this leads to:

$$\text{sensitivity} \propto \frac{e_{max}}{\sum_i (A_i V_{E_i}) \sum_j (A_j)} \qquad \text{---5.3}$$

where A_m is the area of the m th ring

V_{E_m} is the excitation voltage applied to it.

For the commercial transducer i = j = 1. Because the transmission-reception process occurs separately for each ring in turn for the swept-swept mode the denominator in equation 5.3 reduces to $\sum_i (A_i^2 V_{E_i})$, for this case.

The sensitivities fall into a reasonably predictable order. The swept-swept focus appears as the most sensitive, closely followed by the commercial probe. After these the other focused modes appear in order of depth of axial maximum. Those modes exhibiting an unfocused process appear lowest. Only the point 90-point 90 appears away from its expected position alongside the point 90-swept* mode, see also Section 5.5.1. The reason is unknown. When performing actual imaging, the swept-swept focus appears less sensitive than, for example, the point 130-swept mode. It requires a higher transmitter output to attain a similar image brightness. This is because less of the transducer's area is used on transmission. In terms of transmitted energy, it is more sensitive as illustrated by the figures in Table 5.3.

5.6.3.4 Extent of Focal Zone (Table 5.3, Column 6)

Column 6 presents the focal zone lengths measured between -6 dB points. The axial responses of unfocused-unfocused and unfocused-swept modes are very similar. That of the latter being more peaked. This similarity is predicted theoretically (Section 5.5.1). By choosing "complementary" transmit and receive foci a greatly extended focal zone can be achieved, for example with the point 130-swept mode, see figure

5.11. An extended focal region is also evident for the swept-swept and the point 90-swept* foci.

The differences between the point 90-swept and point 90-swept* modes illustrate a deficiency in the swept receive function algorithm used with a contact transducer. The sweep function is derived assuming a simple transmitted pulse originating at the array centre. Break down of this assumption can lead to features such as those shown in figure 5.9, where an on-axis minimum occurs between 130 and 140 mm. The degree to which this occurs is greater, the closer the transmitted wave is focused to the array, if the receive sweep function is set up with the transmitted wave unfocused. With the transmitted wave focused at depth there are no adverse effects, see figure 5.11 for the 130 mm transmit focus. Setting up of the receive swept focus with a focused transmitted wave also obviates the problem, see figure 5.10 for the point 90-swept* mode. The synthetic aperture algorithm does not suffer from this drawback as a more realistic assumption is made about the transmitted pulse's origin.

5.6.3.5 Time Gain Compensated Distributions (Table 5.4)

Iso-echo amplitude contour maps assuming a flat axial response have been drawn for unfocused-unfocused, point 90-swept*, point 130-swept and swept-swept modes, see figures 5.16 - 5.19. These represent the transducer response in a non-attenuating medium, with an ideal time gain compensation function applied. Only main lobe contours are illustrated, side lobe contours have been omitted. The iso-echo amplitude contour lines form approximately linear functions of depth. Angles of divergence may be calculated for specific contours. These, and the -3 dB beam width at 50 mm depth, are presented in Table 5.4.

Figure 5.16: Tx.Unfocused: Rx.Unfocused: Iso-echo contours, simulated time gain compensated array response.

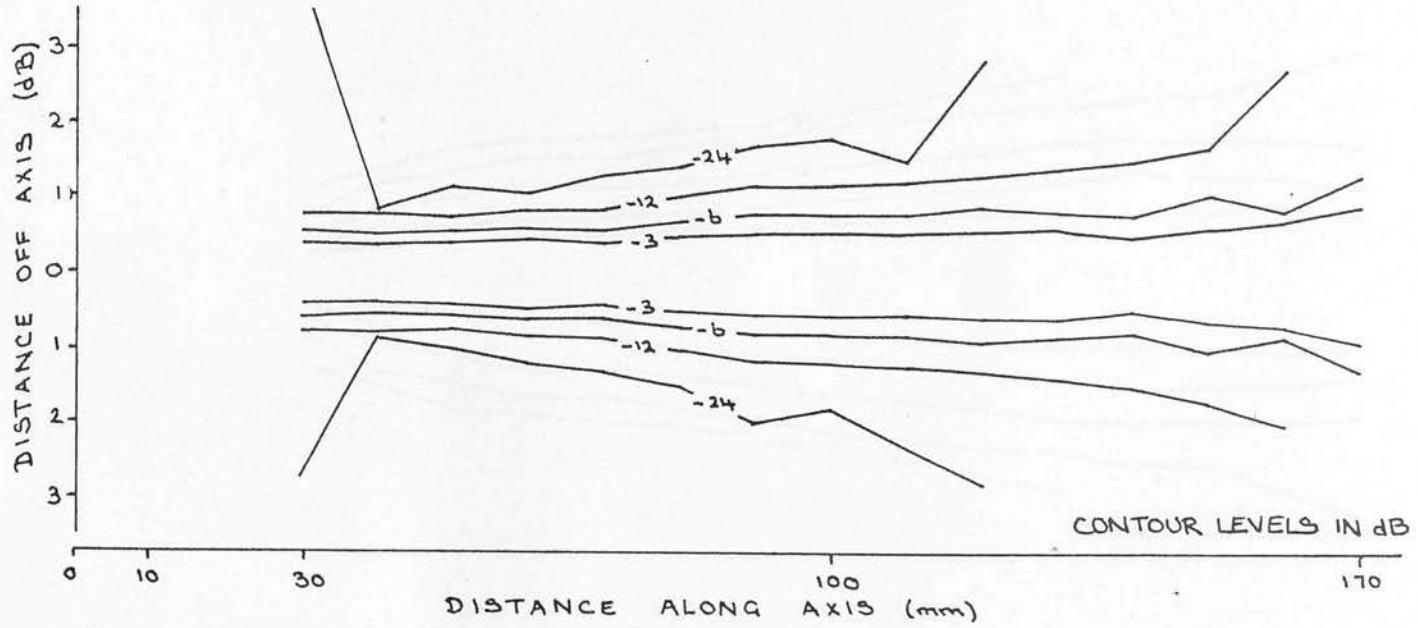

Figure 5.17: Tx.Point focus (90mm): Rx.Swept*focus: Iso-echo amplitude contours, simulated time gain compensated array response.

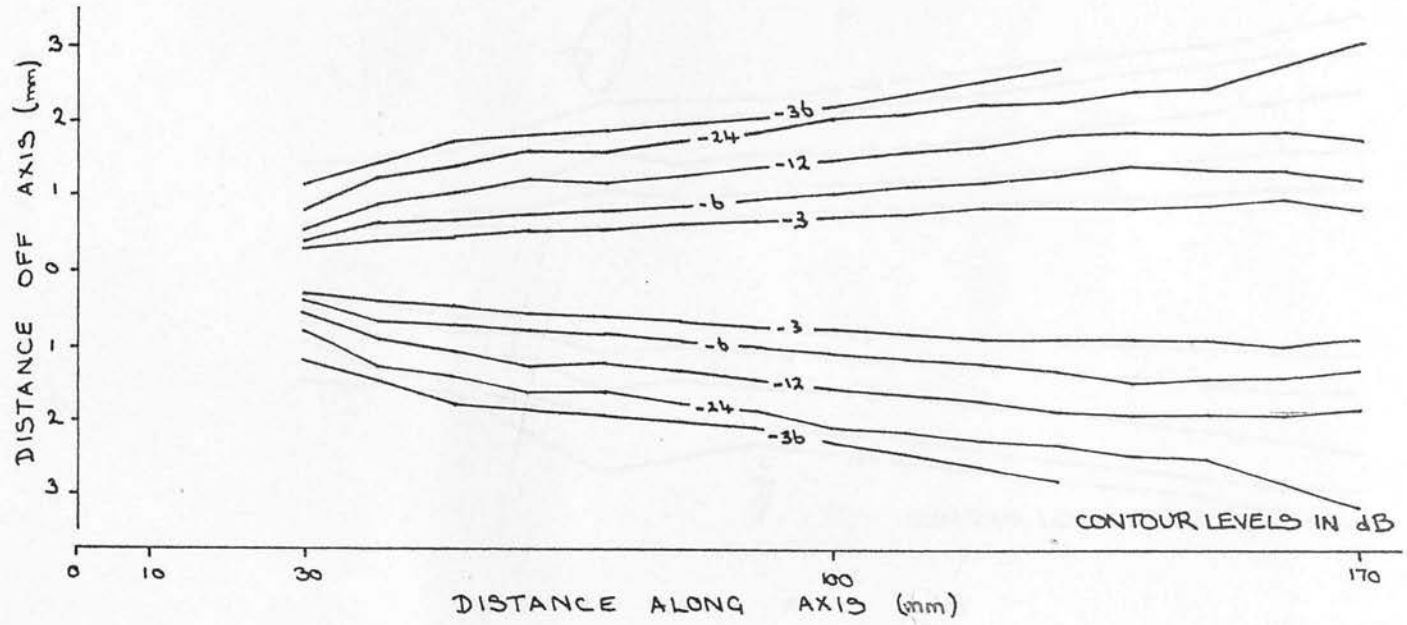

Figure 5.18: Tx.Point focus (130mm): Rx.Swept focus: Iso-echo amplitude contours, simulated time gain compensated array response.

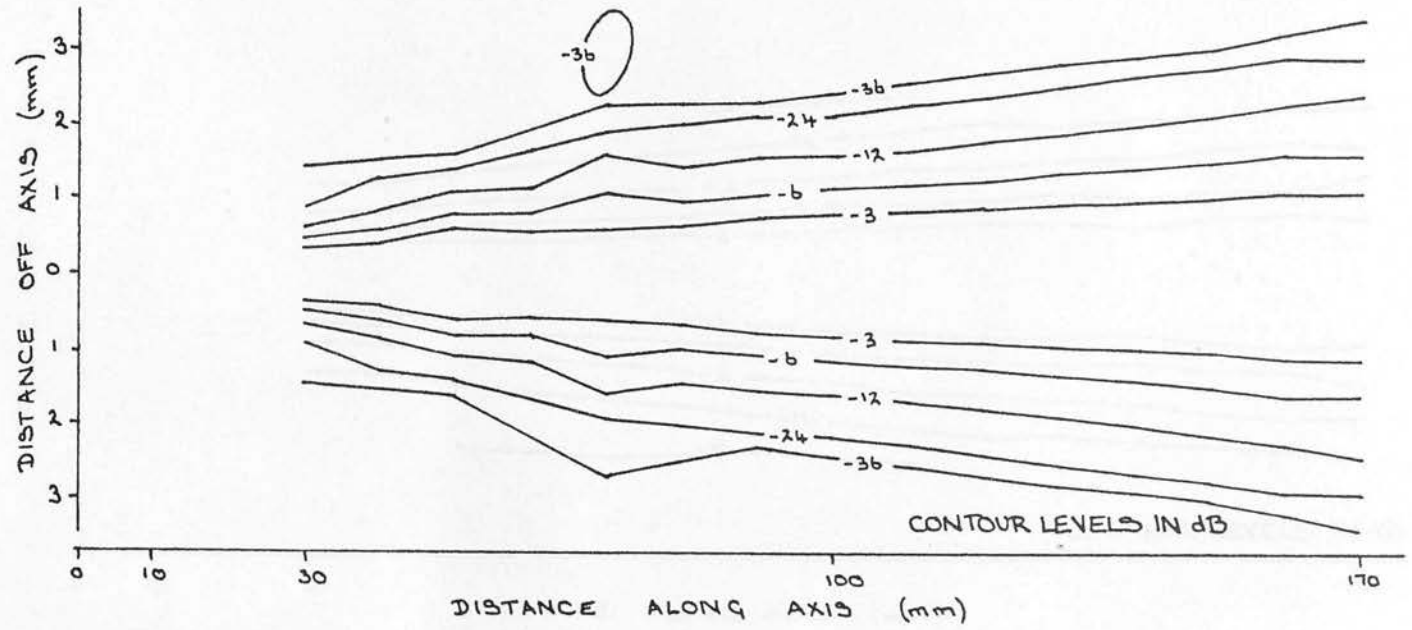

Figure 5.19: Tx.Swept focus: Rx.Swept focus: Iso-echo amplitude contours, simulated time gain compensated response.

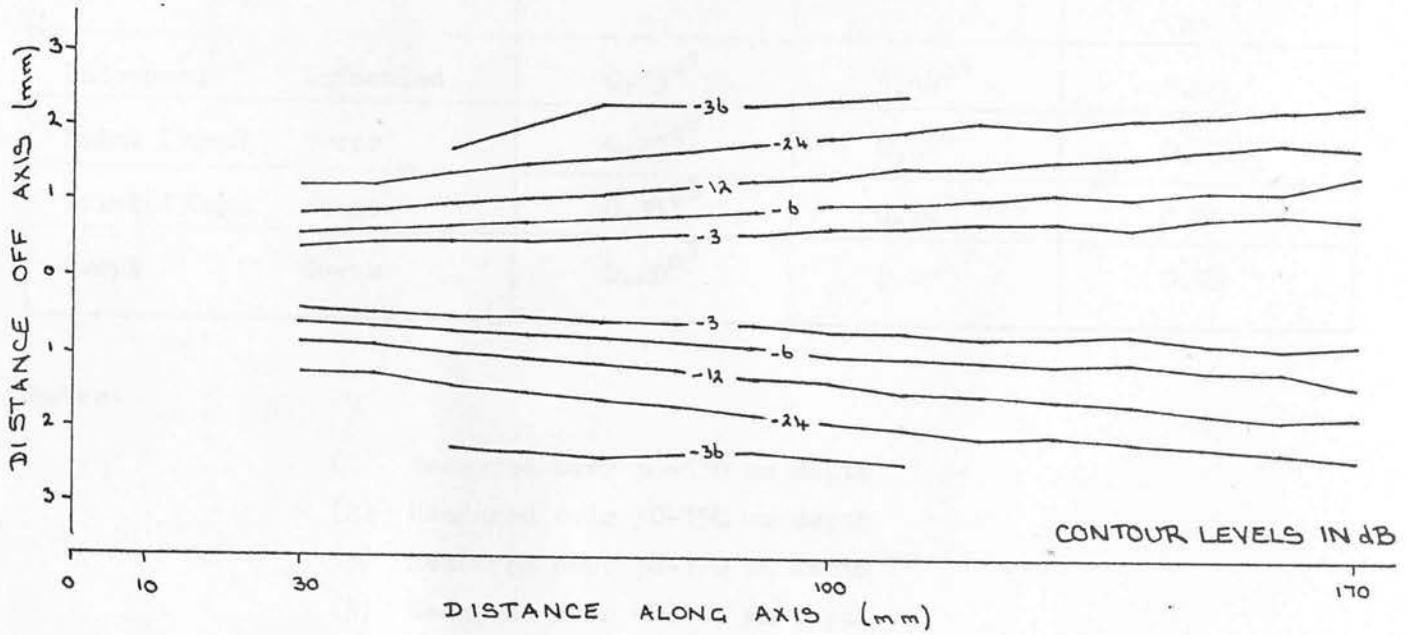

Table 5.4: Summary of iso-echo amplitude contour map features (time gain compensated responses.

Focusing Mode		COLUMN 1	2	3
Transmit	Receive	Divergence of -3dB contour	Divergence of -24dB contour	Width of 50.0mm depth
				mm
Unfocused	Unfocused	0.13^{o1}	1.14^{o4}	0.41
Point (90mm)	Swept*	0.29^{o2}	0.64^{o5}	0.47
Point(130mm)	Swept	0.31^{o3}	0.76^{o3}	0.51
Swept	Swept	0.20^{o3}	0.47^{o3}	0.48

Notes:

(1) Measured over 30-130 mm depth
(2) Measured over 30-150 mm depth
(3) Measured over 30-170 mm depth
(4) Measured over 40-110 mm depth
(5) Measured over 40-150 mm depth

From Table 5.4 it is apparent that all three focusing modes produce a beam of similar width. However, that for the swept-swept mode is more uniform. Its divergence angles are about 30% less than those of the other two focusing modes.

5.7 B-scan Images

The following array focusing modes and commercial transducers have been used to assess the array's performance in the production of actual images, modes (1), (5), (6), (7) and transducers (8), (9) and (10), Table 5.1. The commercial transducers were driven via the swept focusing unit, except in the case of the Fischer 19 mm diameter probe (probe 10) which was driven directly by the Diasonograph.

5.7.1 Test Phantoms

Three different test phantoms were used in assessing the array's imaging ability:

(1) A nylon mono-filament "ladder" phantom immersed in olive oil.

(2) A 100 mm "open wire" AIUM test phantom immersed in water (Hospital Physicists' Association publication).

(3) A "tissue equivalent" test phantom.

The three phantoms are illustrated in figures 5.20 - 5.22. The tissue equivalent phantom is formed from a reticulated plastic foam, saturated with water. This provides a fine matrix of random low level reflectors into which may be introduced anechoic regions (holes) and regions of higher reflectivity (e.g. nylon monofilaments).

Images from the 4201 Diasonograph were recorded on X-ray film via a"Matrix" multiformat imager.

Figure 5.20: Nylon monofilament ladder phantom, immersed in olive oil (courtesy S.Pye).

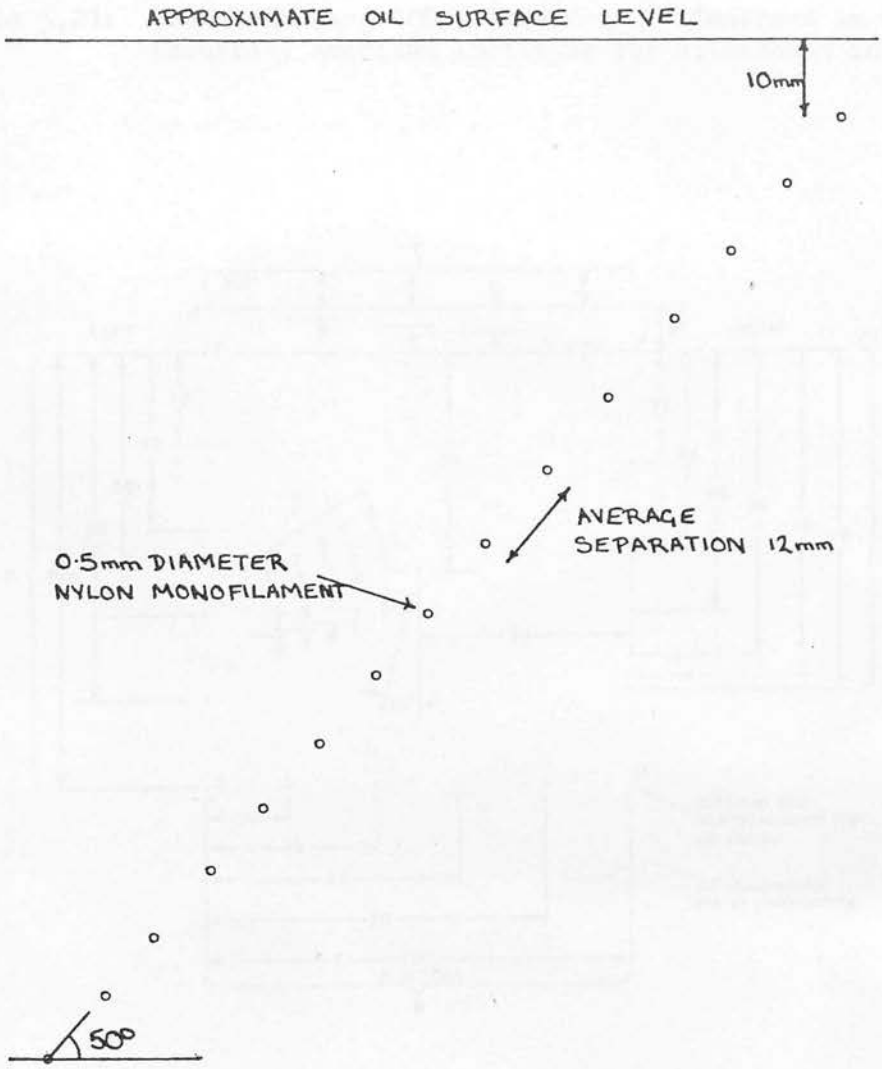

Figure 5.21: AIUM "Standard 100mm Test Object" immersed in water (courtesy American Institute for Ultrasound in Medicine).

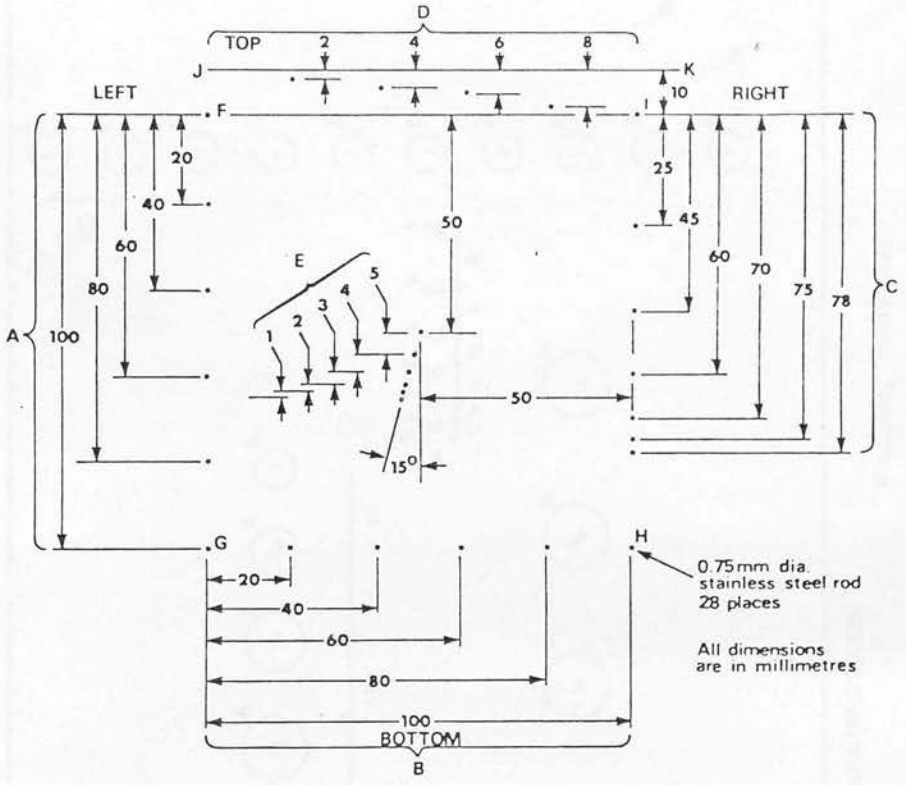

Figure 5.22: Tissue equivalent test phantom.

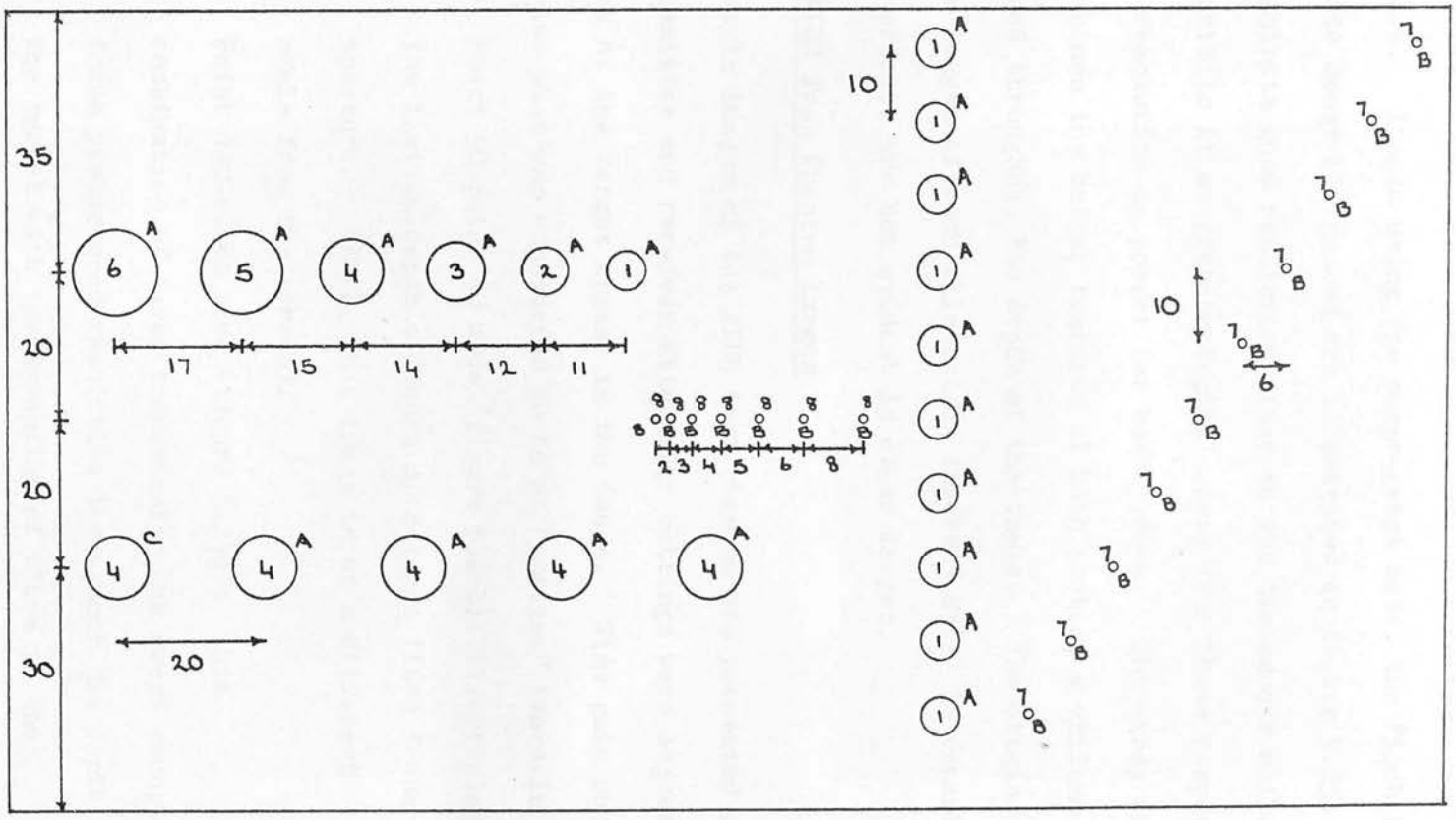

ALL DIMENSIONS IN MILLIMETRES

HOLE DIAMETERS

1 -	4.7	5 -	10.5
2 -	6.0	6 -	11.6
3 -	6.9	7 -	0.8
4 -	8.0	8 -	0.6

FILLING MATERIAL

A - UNFILLED (WATER)

B - 0.016 mm DIAM. NYLON MONOFILAMENT

C - RUBBER COMPOUND

MATRIX MATERIAL IS A RETICULATED PLASTIC FOAM SATURATED WITH WATER

5.7.2 Ladder Phantom Images

These present no further information for the unfocused-unfocused, point 90-swept and point 130-swept modes, than already obtained from the beam plots. Images using the swept-swept mode, the Fischer MIF and the Diagnostic Sonar LIF probes are illustrated in figure 5.23. The MIF probe exhibits good resolution close to the transducer while the LIF probe exhibits it at greater depth. Away from these respective regions lateral resolution is poorer for both probes. The array swept-swept mode combines the better features of both probes, a uniform spot size is maintained throughout the depth of the image. The origin of the multiple images of each filament in figure 5.23(a) is uncertain. Similar effects are not evident in other images.

5.7.3 AIUM Test Phantom Images

Example images of the AIUM test phantom are presented in figure 5.24. The transmitter and receiver attenuator settings were adjusted so that all the wires of the target appear in the image. Time gain compensation was set to give what was considered to be an "optimum" image in each case.

(1) Point 90-point 90 mode (figure 5.24b): illustrates the limited depth of focus of a large fixed focus aperture. (Note, this image is on a different scale from the others).

(2) Point 130-swept mode (figure 5.24c): this combination of fixed transmission and swept reception focus yields good resolution throughout the depth of the target with the exception of close to the transducer. The beam diverges only slowly with depth.

Figure 5.23: Ladder phantom images.

(a) Array, tx. swept focus, rx. swept focus.

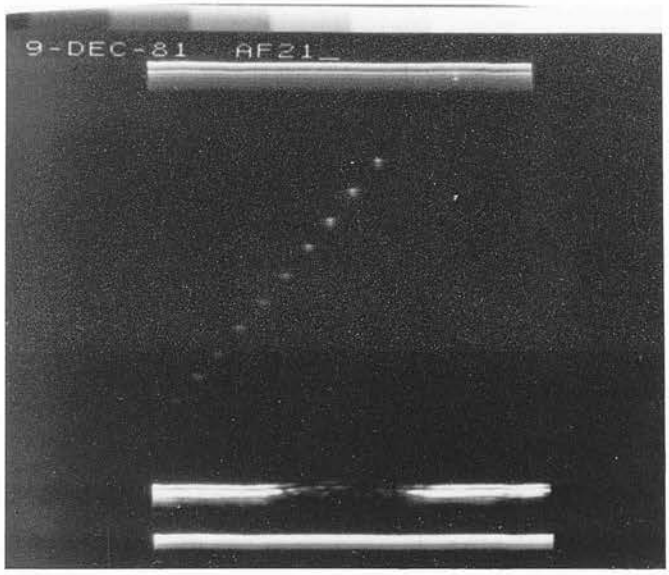

(b) Fischer, 13mm diam. MIF probe.

Figure 5.23: Ladder phantom images.

(c) Diagnostic Sonar, 19mm diam. LIF probe.

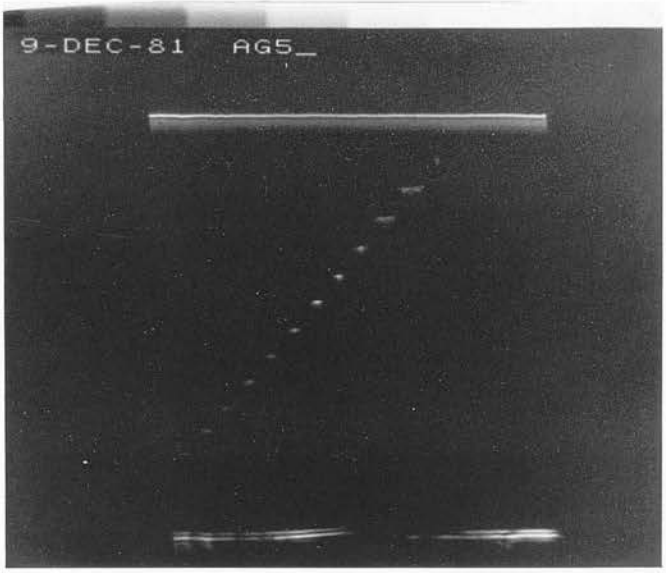

Figure 5.24: AIUM phantom images.

(a) Array, tx. unfocused, rx. unfocused.

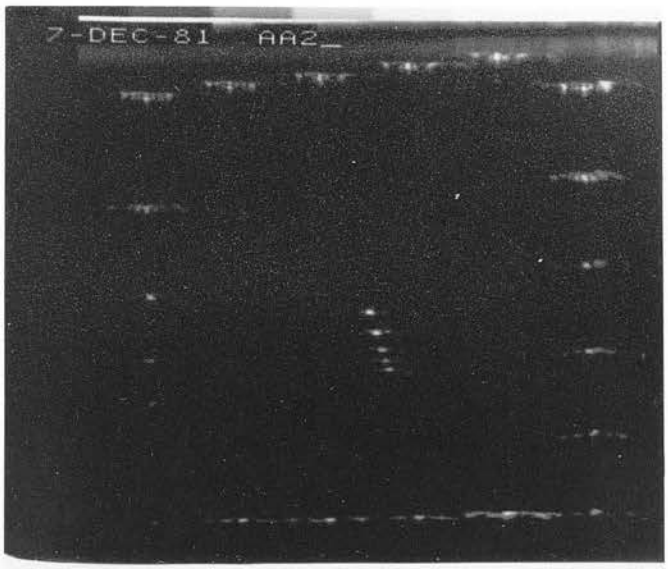

(b) Array, tx. point focus (90mm), rx. point focus (90mm). (Note: different scale).

Figure 5.24: AIUM phantom images.

(c) Array, tx.point focus (130mm), rx. swept focus.

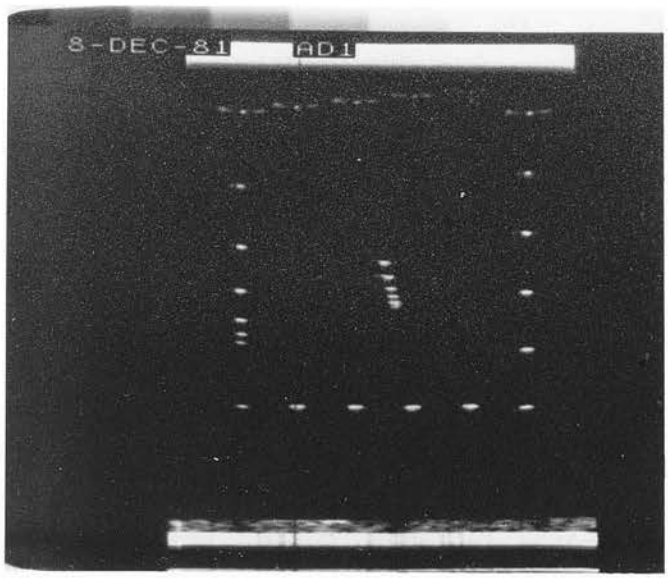

(d) Array, tx. swept focus, rx. swept focus.

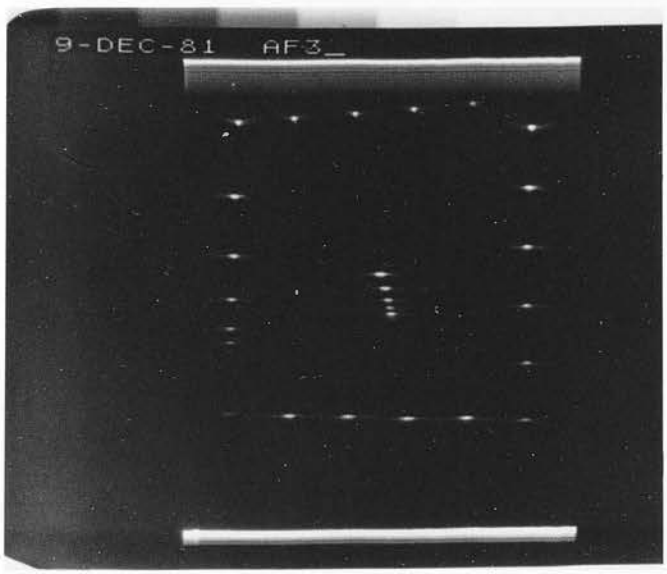

Figure 5.24: AIUM phantom images.

(e) Fischer, 13mm diam. MIF probe.

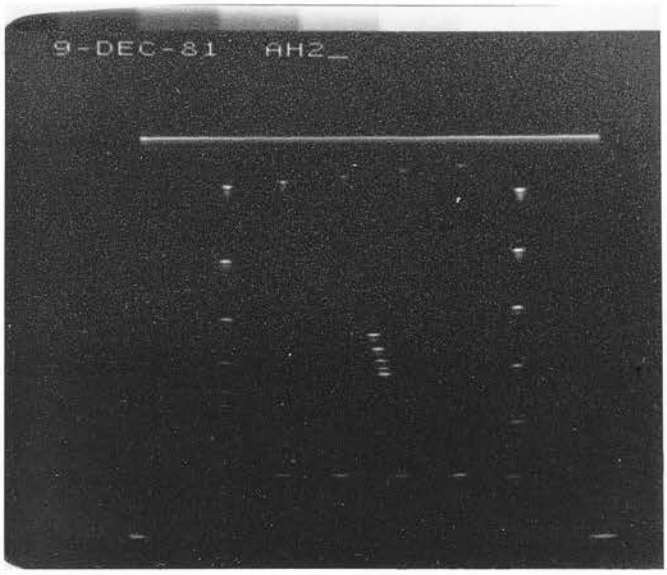

(f) Diagnostic Sonar, 19mm diam. LIF probe.

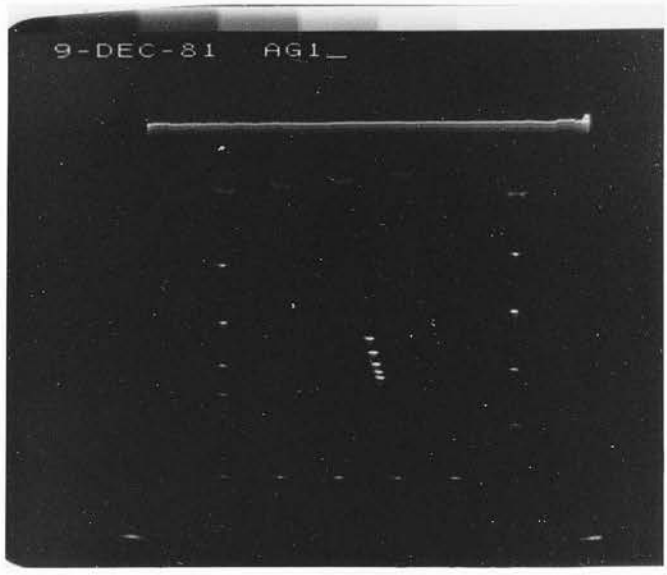

Figure 5.24: AIUM phantom images.

(g) Fischer, 19mm diam. LIF probe (courtesy J. Nicoll).

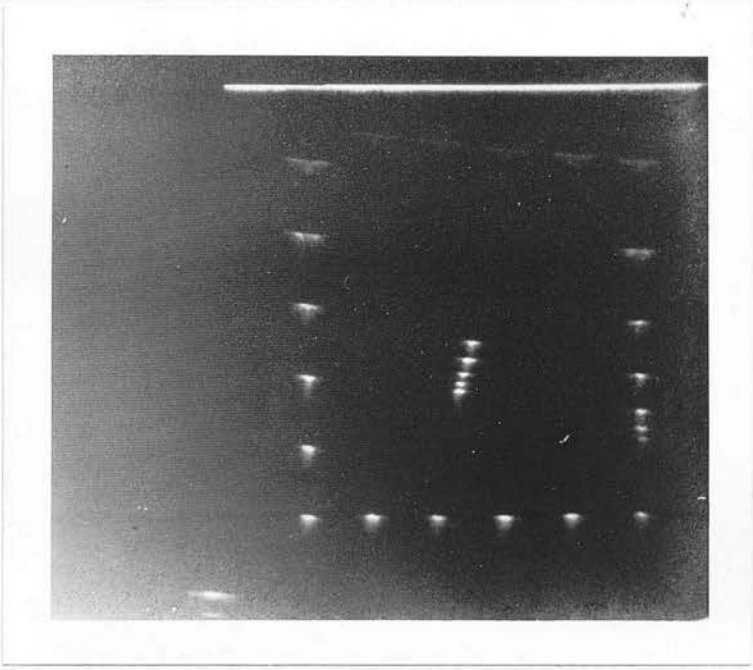

(3) Swept-swept mode (figure 5.24d): very good lateral and axial resolution are maintained throughout the depth of the image. Side lobes are evident because of additional signal compression and saturation of high level echoes not present when beam plotting, but must be below -36 dB, see Table 5.3. These require some further investigation.

(4) Fischer 13 mm probe (figure 5.24e): the small size and medium internal focusing yield quite good resolution close to the transducer, but not towards the bottom of the image.

(5) Diagnostic Sonar 19 mm probe (figure 5.24f): this is a long internal focus probe and exhibits characteristics opposite to those of (4) above, i.e. poor resolution close to the transducer and good resolution at depth.

(6) Fischer 19 mm probe (figure 5.24g): similar to (5), the focus would appear to be located very close to the bottom edge of the image.

In general the array was better able to differentiate the six central wires in the target than were the commercial probes. The images presented reflect very closely the features of the beam plots presented in Section 5.6.

5.7.4 Tissue Equivalent Phantom Images

Images of the tissue equivalent test phantom are presented in figure 5.26. Imaging towards the rear of the phantom was generally difficult. This may be due to entrained air or lack of transmitter power from the swept focusing unit. Artifacts at the edges of the images originate from the walls of the phantom holder.

Figure 5.25: Tissue equivalent test phantom, target groupings.

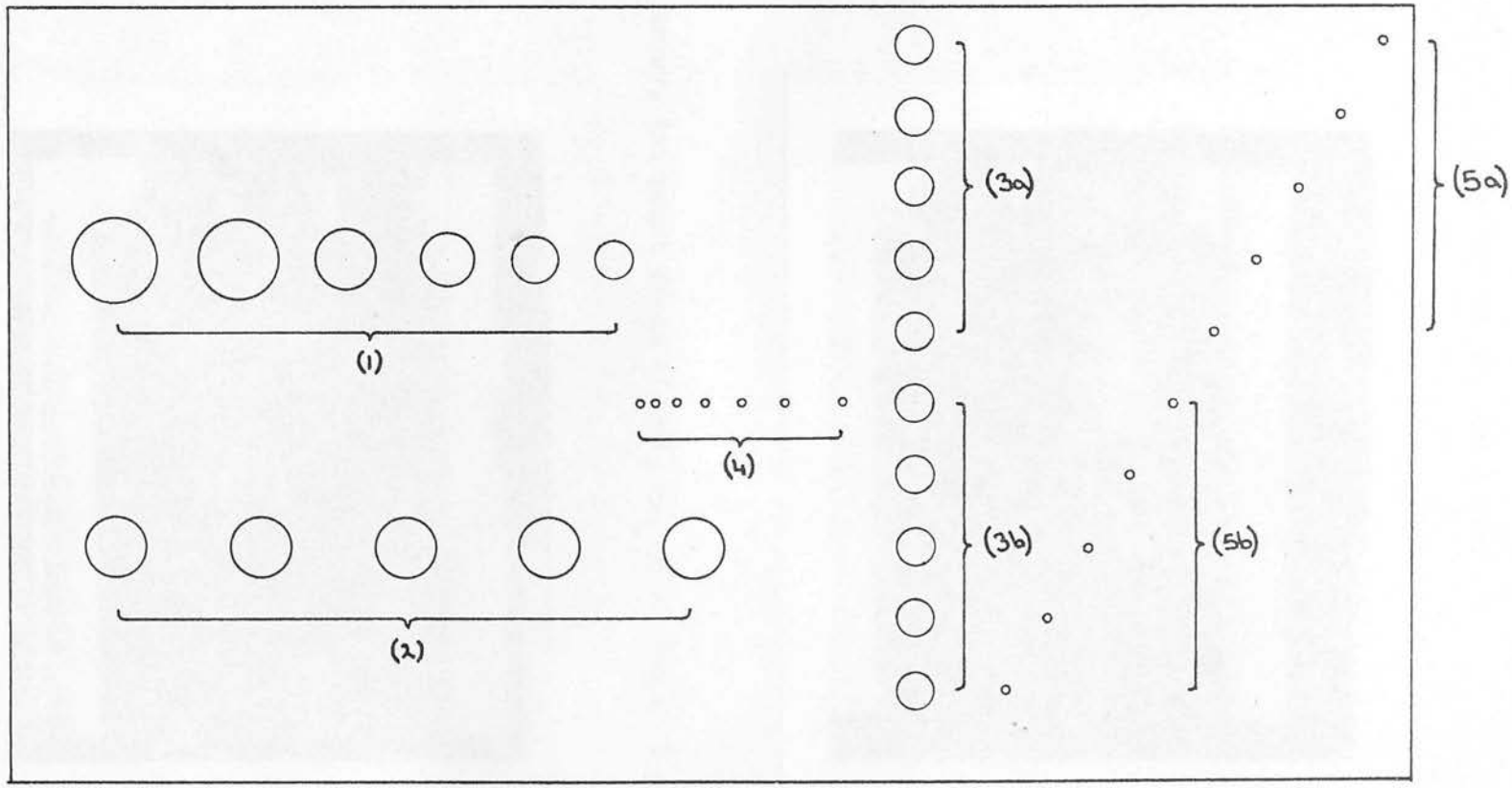

Figure 5.26: Tissue equivalent phantom images.

(a) Array, tx. unfocused, rx. unfocused.

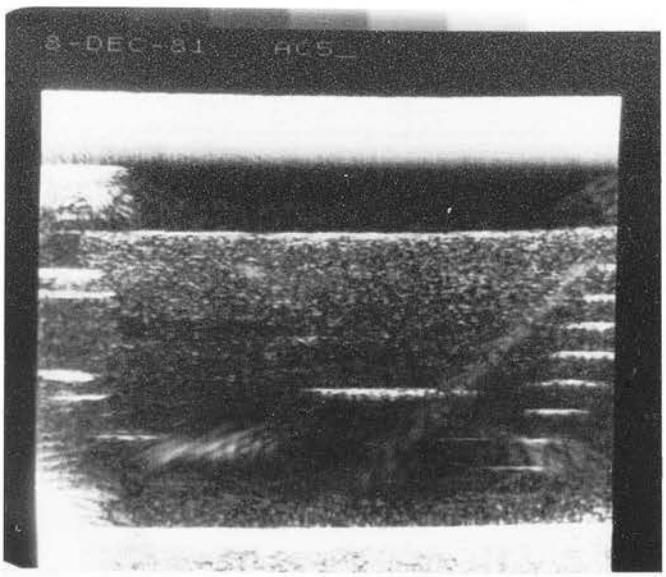

(b) Array, tx. point focus (90mm), rx. point focus (90mm).

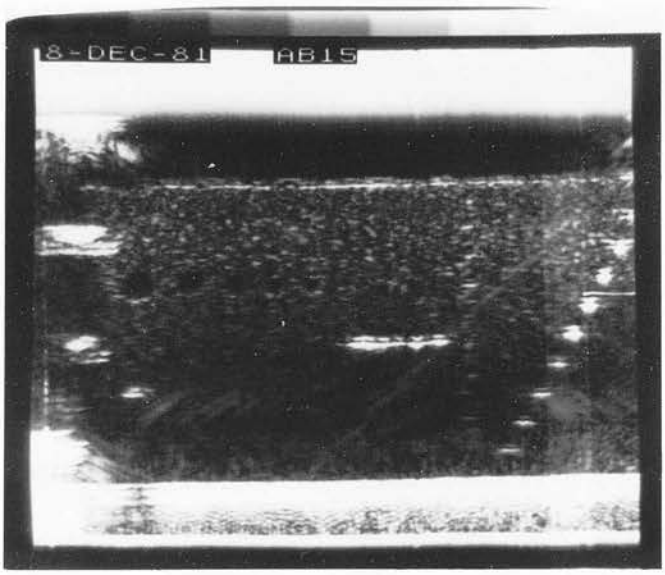

Figure 5.26: Tissue equivalent phantom images.

(c) Array, tx.point focus (130mm), rx. swept focus.

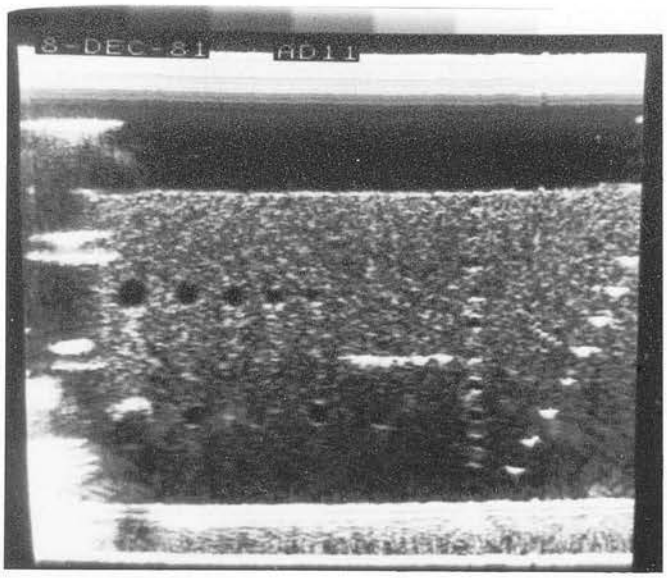

(d) Array, tx.swept focus, rx.swept focus.

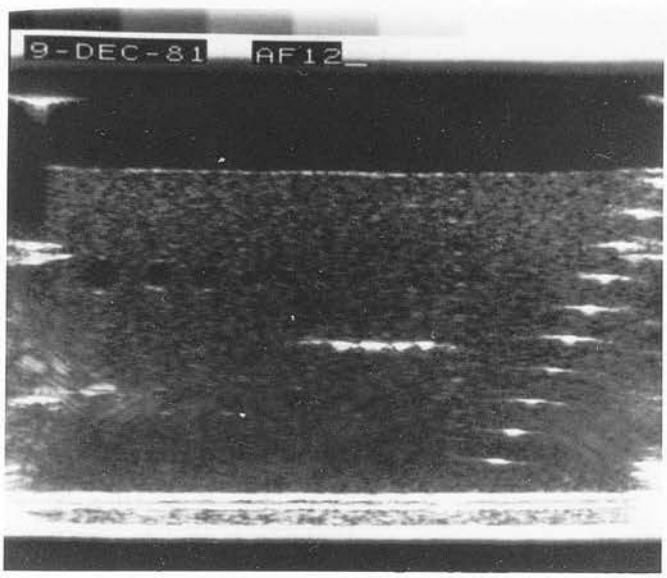

Figure 5.26: Tissue equivalent phantom images.

(e) Fischer, 13mm diam. MIF probe.

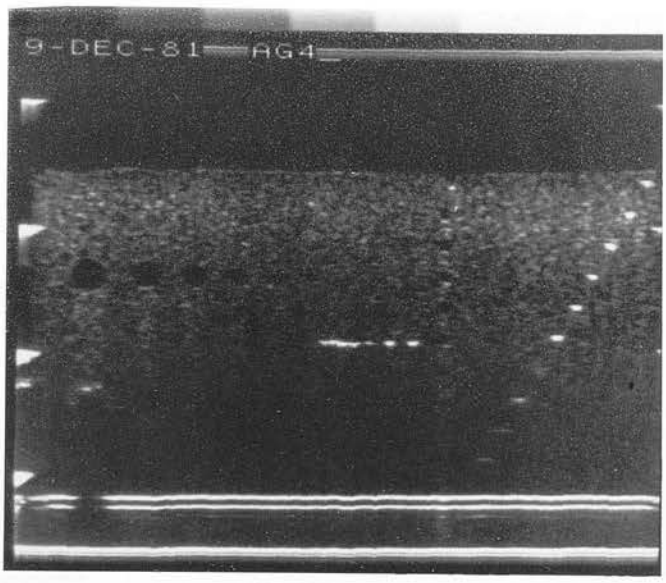

(f) Diagnostic Sonar, 19mm diam. LIF probe.

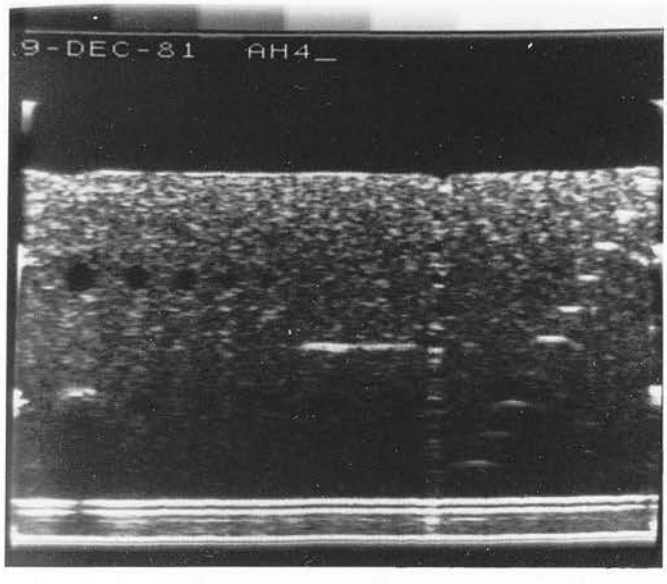

Figure 5.26: Tissue equivalent phantom images.

(g) Fischer, 19mm diam. LIF probe (courtesy J. Nicoll).

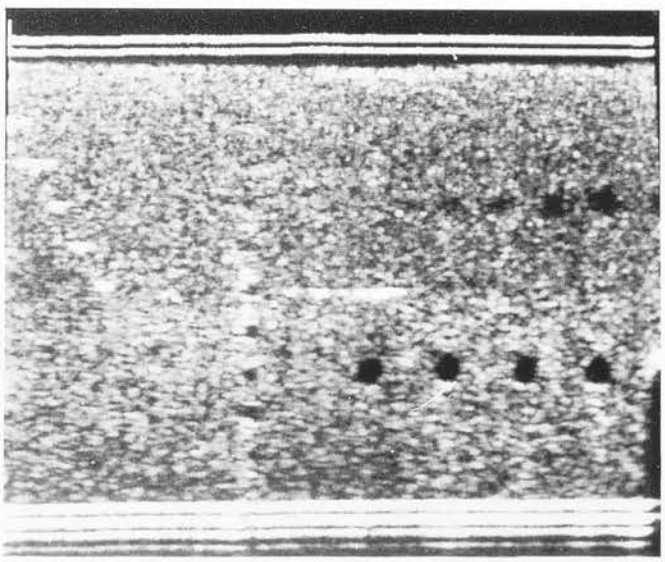

Figure 5.25 illustrates the arrangement of reflectors within the body of the phantom. Each group of reflectors has been numbered and a comparative, qualitative assessment of each is given in Table 5.5. This illustrates the compromise nature of fixed focus probes. These are only able to function well over one part of the image. The swept focusing techniques produce an image of more uniform quality.

5.8 Effects of Tissue Motion

One of the disadvantages of a serial data acquisition system is its sensitivity to tissue motion. Significant tissue movement occurring while a single focused line is being generated will degrade the quality of the focus. Limitations on acceptable tissue motion for the present 4 ring system have been discussed in Section 4.2.1. A tissue velocity of 60 mm sec^{-1} was calculated as the maximum possible before significant degradation of the focus would occur. The maintenance of a reasonable focusing action has been illustrated experimentally.

A calibrated T-M trace of the tissue equivalent phantom in the direction of a well defined echo structure was performed while the phantom was oscillated in the direction of the beam axis (figure 5.27). The maximum velocity of motion is estimated at 56 mm sec^{-1}. Parts of the echo pattern are not distorted relative to each other, merely shifted up and down.

The effects of tissue motion are only really important for the synthetic aperture focus. This relies on serial data acquisition to operate. The other focusing modes could be implemented with a fully parallel acquisition system in which echo information from a reflector is taken in by all rings simultaneously.

Table 5.5: Assessment of image quality of target groupings in the tissue equivalent phantom.

Focusing Mode		Image Assessment						
		Superficial			Deep			
Transmit	Receive	1	3a	5a	2	3b	5b	4
Unfocused	Unfocused	m-g	vp	p	nv	nv	p	p
Point (90mm)	Point (90mm)	vp	nv	vp	nv	nv	vp	vp
Point(130mm)	Swept	g	m-g	m	p-m	m	m	m
Swept	Swept	m-g	m	m-g	p-m	p-m	m-g	m
Fischer 13mm MIF probe		vg	g-vg	g	nv	nv	p	m-g
Diagnostic Sonar 19mm LIF probe		m	p-m	m	vp	p	p	p-m
Fischer 19mm LIF probe		p	nv	m-g	m-g	m	nv	m

Key:

vg - very good
g - good
m - medium
m-g - medium to good
p - poor
vp - very poor
nv - not visible

Figure 5.27: T-M trace of tissue equivalent phantom, oscillated along the array axis.

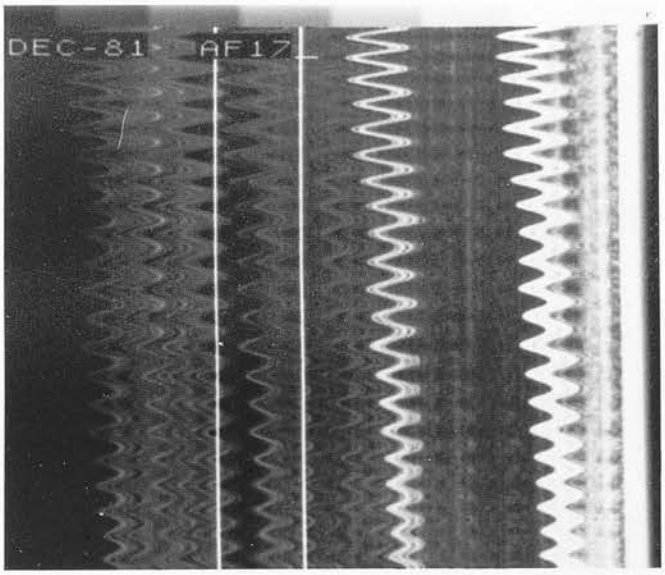

5.9 Summary

The present chapter has described the assessment of an annular array dynamic focusing system. The applicability of the theory used in array design has been investigated and satisfactorily confirmed.

The array used in these investigations is relatively sparse, i.e. only 40% of the available area of the 24 mm aperture is actively used. However, its ability to achieve a focus similar to that of a filled aperture is indicated by the correspondence of the array's normalised beam width (Table 5.3, Column 4) to that of the commercial probe.

Of the focusing modes investigated, three are particularly effective, the point 90-swept*, point 130-swept and swept-swept modes. These exhibit an increased sensitivity of between 7 and 13 dB relative to the unfocused mode; focal zone length is increased by between 36 and 108 %; side lobe levels are reduced by 18 dB. However, there is a corresponding increase in main lobe width of up to 27%.

The use of time gain compensation markedly affects the beam shape. Simulated application of T.G.C. to selected beam plots shows that the synthetic aperture focusing technique produces a significantly more uniform beam than those modes which exhibit a fixed focus transmission process. The beam width at 50 mm remains similar, while the synthetic aperture beam diverges by approximately 30% less than the others.

Both beam plots and phantom images confirm the ability of a dynamically focused probe to overcome the compromise necessarily imposed on fixed focus probes. Further, the use of a novel synthetic aperture technique enables a dynamic focus to be achieved on transmission as well as reception, with a further improvement in beam characteristics.

SUMMARY

The design and implementation of an ultrasonic dynamic focusing annular array system has been described. Theoretical investigation of the behaviour of an annular array transducer has been performed. This used a thin ring continuous wave approach to approximate the actual transient field of a pulse-echo transducer. The applicability of this approach has been discussed. Results from it indicate that a useful array may be formed from four or five rings, evenly spaced within the transducer aperture. Apodisation of the aperture such that the response of each ring is made proportional to its radius improves resolution without seriously raising side lobe levels. Experimental confirmation of the basic theory is available in the literature and in the present work.

Description of an electronic unit to generate and process the signals from the array has been given. Conversion of the analogue echo signal to a digital one, followed by temporary storage in RAM, was identified as the most suitable means of achieving the required variable delays. Delay control functions have been derived. The stability required of the clocks controlling the variable delay process has been considered.

The design of a specific array as a prototype for ones to be introduced into the head of a real-time mechanical scanner has been described, along with a suitable means of fabrication. This array has been evaluated as a contact scanner attached to a static B-scan instrument. Its capability as a dynamic focusing transducer has been confirmed. The novel application of Synthetic Aperture

Imaging to an annular array has been introduced. This overcomes the compromise of dynamic focusing only on reception, with a fixed focus on transmission. A significant improvement in beam shape was observed, at the expense of a lower maximum P.R.F.

Design of annular arrays, based on the present work, and their incorporation into a real-time scanner, has proceeded under Dr. W. N. McDicken (Department of Medical Physics and Medical Engineering, University of Edinburgh) in conjunction with a commercial firm, Diagnostic Sonar Ltd. (Livingstone, Scotland). An illustration of a commercial mechanical real-time scanner incorporating these arrays is given in figure 6.1.

Figure 6.1: A commercial mechanical real-time scanner incorporating annular arrays.

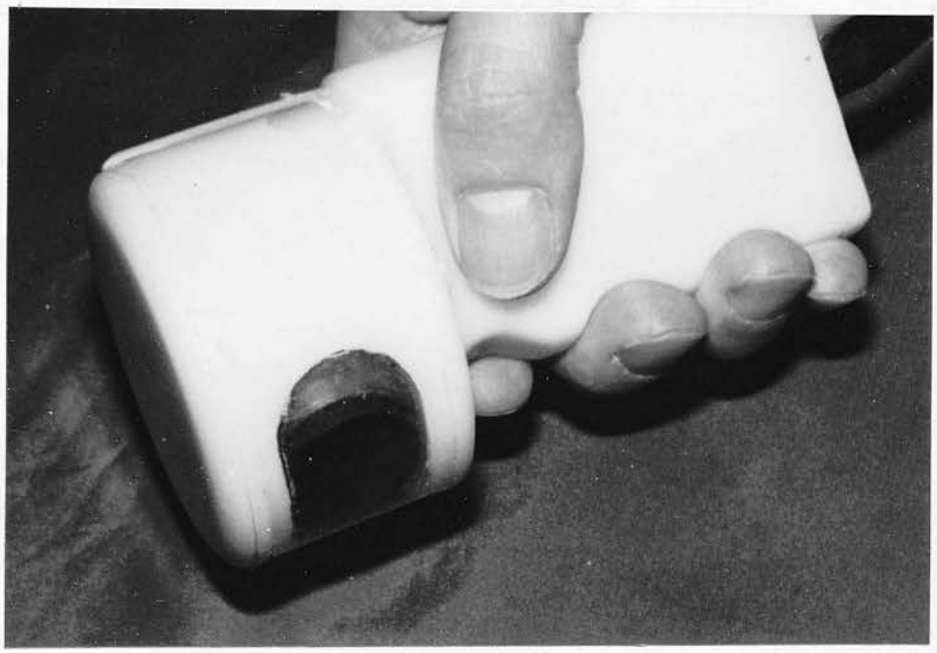

REFERENCES

Archer-Hall J and Gee D (1980); 'A single integral computer method for axisymetric transducers with various boundary conditions'. NDT International, Vol 13, 95-101.

Arditi M, Foster F and Hunt J (1981); 'Transient fields of concave annular arrays'. Ultrasonic Imaging, Vol 3, 37-61.

Beaver W (1974); 'Sonic near fields of a pulsed piston radiator'. J.Acoust.Soc.Am., Vol 56, 1043-1048.

Beaver W, Maginness M, Plummer J and Meindl J (1975); 'Ultrasonic imaging using two-dimensional transducer arrays' in Cardio-Vascular Imaging and Image Processing (edited by Harrison D, Sandler H and Millar H), pp17-24. Proc.Soc. Photo-optical Instrum.Eng., Palos Verdes Estates, C.A.

Bernardi R, Peluso P, O'Connell R, Kellogg S and Shih C (1976); 'A dynamically focused annular array'. I.E.E.E. Ultrasonics Symp. Proc., CH 1120-5SU, 157-159.

Bom N, Lancée C, Honkoop J and Hugenholtz P (1971); 'Ultrasonic viewer for cross-sectional analyses of moving cardiac structures'. Bio-Med.Engng., Vol 6, 500.

Bow C (1979); in Ultrasonic Visualisation of Cardiac Structure and Function. Ph.D. Thesis, Edinburgh University, pp 66-77.

Bow C, McDicken W, Anderson T, Scorgie R and Muir A (1979); 'A rotating transducer real-time scanner for ultrasonic examination of the heart and abdomen'. Br.J.Radiology, Vol 52, 29-33.

Brown T and Haslett R (1963); 'Improvements in flaw detection and like systems using pulsed sonic or ultrasonic waves'. British patent No. 941573.

Burckhardt C, Grandchamp P and Hoffmann H (1975); 'Focusing ultrasound over a large depth with an annular transducer - an alternative method'. I.E.E.E. Trans. on Sonics and Ultrasonics, Vol SU-22, 11-15.

Conner E, Hubelbank M and Lele P (1975); 'Acoustic field patterns of a digitally programmed five-element, concentric ring phased array'. Proc. 3rd New England Bio-Engng.Conf., pp 342-346.

Corl P, Grant P and Kino G (1978); 'A digital synthetic focus acoustic imaging system for NDE'. I.E.E.E. Ultrasonics Symp.Proc., CH 1344-2SU, 395-400.

Dehn J (1960); 'Interference patterns in the near field of a circular piston'. J.Acoust.Soc.Am., Vol 32, 1692-1696.

Dekker D, Piziali R and Dong Jr. E (1974); 'The effect of boundary conditions on the ultrasonic-beam characteristics of circular disks'. J.Acoust.Soc.Am., Vol 56, 87-93.

Dietz D, Norton S and Linzer M (1979); 'Wideband annular array response'. I.E.E.E. Ultrasonic Symp.Proc., Ch 1344-1SU, 206-211.

Dietz D, Parks S and Linzer M (1979); 'Expanding aperture annular array'. Ultrasonic Imaging, Vol 1, 56-75.

Duck F (1981) 'The pulsed ultrasonic field' in Physical Aspects of Medical Imaging (edited by Moores B, Parker R and Pullan B), pp97-108. J. Wiley and Sons, New York.

Eaton M, Melen R and Meindl J (1980); 'A flexible, real-time system for experimentation in phased-array ultrasound imaging' in Acoustical Imaging Vol 8 (edited by Metherell A), pp55-67. Plenum Press, New York.

Evans D and Parton L (1981); 'The directional characteristics of some ultrasonic doppler blood flow probes'. Ultrasound in Med. and Biol., Vol 7, 51-62.

Forsythe G, Malcolm M and Moler C (1977); in Computer Methods for Mathematical Computations, pp92-105. Prentice-Hall Inc., New Jersey.

Foster F and Hunt J (1978); 'The design and characterisation of short pulse ultrasound transducers'. Ultrasonics, Vol 16, 116-122.

Freedman A (1970); 'Transient fields of acoustic radiators'. J.Acoust.Soc.Am., Vol 48, 135-138.

Goodman J (1968); Introduction to Fourier Optics. McGraw-Hill, New York.

Harris G (1981); 'Review of transient field theory for a baffled planar piston'. J.Acoust.Soc.Am., Vol 70, 10-20.

Hospital Physicists' Association (1978); Methods of Monitoring Ultrasonic Scanning Equipment. Topic Group Report 23. Hospital Physicists' Association.

Hubelbank M and Tretiak O (1970); 'Focused ultrasonic transducer design'. Research Laboratory of Electronics, M.I.T.Report No. 98, 169-177.

Kinsler L and Frey A (1962); Fundamentals of Acoustics, 2nd Edition. J. Wiley and Sons, New York.

Kossoff G (1963); 'Design of narrow-beamwidth transducers'. J.Acoust.Soc.Am., Vol 35, 905-912.

Kossoff G (1966); 'The effects of backing and matching on the performance of piezoelectric ceramic transducers'. I.E.E.E. Trans. on Sonics and Ultrasonics, Vol SU-13, 20-30.

Kossoff G (1976); 'Technical procedures and imaging' in Present and Future of Diagnostic Ultrasound (edited by Donald I and Salvator L), pp1-11. Kooyker Scientific Publications, Rotterdam.

Lancée C and Bom N (1977); 'Some signal processing aspects in Medical Ultrasound' in Aspects of Signal Processing, Part 2 (edited by Tacconi G), pp649-657. Reidel Publishing Co., Dordrecht.

Ligtvoet C, Ridder J, Hagemeijer F and Wladimiroff J (1977); 'A dynamically focused ultrasound system'. Ultrasonics International (Brighton) Conf.Proc., pp111-120.

McDicken W, Bruff K and Paton J (1974); 'An ultrasonic instrument for rapid B-scanning of the heart'. Ultrasonics, Vol 12, 269-272.

McDicken W (1981); Diagnostic Ultrasonics - Principles and Use of Instruments, 2nd Edition. J.Wiley and Sons, New York.

McKeighen R and Buchin M (1977); 'New techniques for dynamically variable electronic delays for real-time ultrasonic imaging'. I.E.E.E. Ultrasonics Symp.Proc., CH 1264-1SU, 250-254.

Melen R, Shott J, Lee B and Granger L (1977); 'Charge coupled devices for holographic and beam-steering sonar systems' in Acoustical Holography Vol 7 (edited by Kessler L), pp461-473. Plenum Press, New York.

Melton Jr. H and Thurstone F (1978); 'Annular array design and logarithmic processing for ultrasonic imaging'. Ultrasound in Med. and Biol., Vol 4, 1-12.

Melton Jr. H (1979); 'Annular arrays, dynamic focusing and non-linear processing in manual B-Scanning'. Proc 24th Meeting A.I.U.M. (Montreal), pp69. A.I.U.M., Oklahoma City.

Meire A and Farrant P (1982); in Basic Clinical Ultrasound, pp3-8. British Institute of Radiology.

Morse P and Ingard K (1968); Theoretical Acoustics. McGraw-Hill, New York.

Patterson M and Foster F (1978); 'Acoustic fields of conical radiators'. I.E.E.E. Trans. on Sonics and Ultrasonics, Vol SU-29, 83-92.

Posakony G (1975); 'Engineering aspects of ultrasonic piezoelectric transducer design'. I.E.E.E. Ultrasonics Symp.Proc., CHO-4SU, 1-9.

Schoch A (1941); 'Betrachtungen uber das Schallfeld einer Kolbenmembraan'. Akust.Z., Vol 6, 318-326.

Somer J (1968); 'Electronic sector scanning for ultrasonic diagnosis'. Ultrasonics, Vol 6, 153-159.

Strutt J (Lord Rayleigh) (1945); The Theory of Sound Vol 2, 2nd Revised Edition. Dover, New York.

Vogel J, Bom N and Lancée C (1979); 'Transducer design considerations in dynamic focusing'. Ultrasound in Med. and Biol., Vol 5, 187-193.

Weight J and Hayman A (1978); 'Observations of the propagation of very short ultrasonic pulses and their reflection by small targets'. J.Acoust.Soc.Am., Vol 63, 396-404.

Wells P (1977); Biomedical Ultrasonics. Academic Press, New York.

Woodcock J (1979); Ultrasonics. Adam Hilger Ltd., Bristol.

PUBLICATIONS

The following conference contributions have been presented:-

Pye D, McHugh R and McDicken W (1981); 'Ultrasonic fields from annular array transducers'. Hospital Physicists' Association (Durham) Conference.

Pye D, McHugh R and McDicken W (1982); 'Dynamic focusing of ultrasonic annular array transducers, an experimental and theoretical study of various techniques'. World Ultrasound in Medicine and Biology (Brighton) Conference.

APPENDIX

A1.1 SOLUTION FOR PULSED ARRAY OF FINITE WIDTH RINGS

THE ALGORITHM FOR GENERATION OF PRESSURE DATA AS A FUNCTION OF TIME AND SPACE IS PRESENTED BELOW (PASS 1, SECTION 2.6.2.1). IT REPRESENTS A NUMERICAL SOLUTION OF EQUATION 2.1 (SECTION 2.4.1). THE FUNCTION DEFINING THE INTEGRAND IS GIVEN IN SECTION A1.1.1.

SYMBOLS:

- T - TIME
- X - DISTANCE OFF ARRAY AXIS
- Z - DISTANCE ALONG ARRAY AXIS
- CN - NORMALISED VELOCITY OF SOUND (= VELOCITY / FREQUENCY)
- R11 - MINIMUM DISTANCE FROM FIELD POINT TO INNER RADIUS OF RING
- RMAX1 - MAXIMUM DISTANCE FROM FIELD POINT TO OUTER RADIUS OF RING
- R12 - MINIMUM DISTANCE FROM FIELD POINT TO OUTER RADIUIS OF - RING
- RMAX2 - MAXIMUM DISTANCE FROM FIELD POINT TO OUTER RADIUS OF - RING
- TAUP - PULSE LENGTH ( )
- QUANC8 - IS AN ADAPTIVE QUADRATURE ROUTINE PUBLISHED BY FORSYTHE ET. AL. (1977)

INPUT:

INPUT PARAMETERS SUCH AS FREQUENCY, RING DIMENSIONS, ETC. ARE VIA AN INTERACTIVE SUB-PROGRAM WHICH STORES THEM FOR LATER USE.

LISTING:

```
C
C
C OPTION 3: PRESSURE AS A FUNCTION OF T,X & Z
C ------------------------------------------
        PMINZ=100.0
        PMAXZ=0.0
        IZ=0
3       CONTINUE
C SET 'Z' COUNTER
        IZ=IZ+1
        Z=Z1+FLOAT(IZ-1)*DZ
        PMINX=100.0
        PMAXX=0.0
C
C
C OPTION 2:PRESSURE AS A FUNCTION OF T & X
C ---------------------------------------
C LEAVE SPACE FOR XSECTION HEADER
        CALL WRITE(DATA,5,NSTART,NBLOCK,8,2)
C
        IX=0
2       CONTINUE
C SET 'X' COUNTER
        IX=IX+1
        X=X1+FLOAT(IX-1)*DX
        PMAXT=0.0
C
C
C OPTION 1: PRESSURE AS A FUNCTION OF T
C ------------------------------------
C LEAVE SPACE FOR PULSE HEADER
        CALL WRITE(DATA,5,NSTART,NBLOCK,8,2)
C CHECK FOR EXIT REQUEST
        CALL RSW(1,RS1)
        IF(.NOT.RS1) GOTO 63
        WRITE(4,261)
261     FORMAT(' ARE YOU SURE (Y/N) ?: '$)
        READ(4,160) ANS
        IF(ANS.EQ.'Y') CALL START1(2)
C
63      IT=0
        ITC=0
        R11=SQRT(Z**2+(A(1,NRING)-X)**2)
        RMAX1=SQRT(Z**2+(A(1,NRING)+X)**2)
        R12=SQRT(Z**2+(A(2,NRING)-X)**2)
        RMAX2=SQRT(Z**2+(A(2,NRING)+X)**2)
        T1=Z/CN
        IF(X.LT.A(1,NRING)) T1=R11/CN
        IF(X.GT.A(2,NRING)) T1=R12/CN
        T2=RMAX2/CN+TAUP
        ERROR=0.0
C
1       CONTINUE
C SET 'T' COUNTER AND 'PAGE' POSITION COUNTER
        IT=IT+1
        ITC=ITC+1
        T=T1+FLOAT(IT-1)*DT
        SUM=0.0
        ESTERR=0.0
C
```

```
C
C SET INTEGRATION LIMITS
C ----------------------
C
C SET UPPER AND LOWER BOUNDS ON 'ETA' (OUTSIDE THESE LIMITS
C 'ETA' CORRESPONDS TO POINTS OFF THE XTAL FACE)
C UPPER AND LOWER TIME LIMITS ON 'ETA' ARE 'TAUP' AND 0.0
C DIVIDE INTEGRATION INTERVAL INTO NON-DISCONTINUOUS REGIONS
C
C DISCONTINUITIES OCCUR AT SOME/ALL THE FOLLOWING POINTS
        BNDRY(1)=T-RMAX2/CN
        BNDRY(2)=T-RMAX1/CN
        BNDRY(3)=T-Z/CN
        BNDRY(4)=T-R11/CN
        BNDRY(5)=T-R12/CN
C THERE ARE 4 DISCONTINUITIES EXCEPT FOR A(1,NRING)< X <A(2,NRING)
C SET THE EXTRA BOUNDARY TO BNDRY(1)
        IF(X.LT.A(1,NRING).OR.X.GT.A(2,NRING)) BNDRY(3)=BNDRY(1)
        IF(X.EQ.A(1,NRING)) BNDRY(4)=BNDRY(1)
        IF(X.EQ.A(2,NRING)) BNDRY(5)=BNDRY(1)
C SET ANY BOUNDARIES OUTSIDE THE LIMITS ON 'ETA' BACK ONTO THE LIMIT
        DO 307 I=1,5
        IF(BNDRY(I).LT.0.0)  BNDRY(I)=0.0
307     IF(BNDRY(I).GT.TAUP) BNDRY(I)=TAUP
C SORT INTO ASCENDING ORDER
        DO 300 J=1,4
        DO 301 I=1,4
        K=6-I
        IF(BNDRY(K).GE.BNDRY(K-1)) GOTO 301
        TEMP=BNDRY(K-1)
        BNDRY(K-1)=BNDRY(K)
        BNDRY(K)=TEMP
301     CONTINUE
300     CONTINUE
C
C
C INTEGRATION TO EVALUATE RELATIVE PRESSURE AT (T,X,Z)
C **********************************************
C THE INTEGRAND IS 'FCT' A FUNCTION OF 'ETA'
C THE INTEGRATION VARIABLE IS 'ETA'
C THE LOWER BOUND OF THE INTEGRATION IS 'BNDRY1'
C THE BOUNDARIES OF THE INTEGRATION ARE SET SUCH THAT 'ETA' ONLY TAKES
C ON VALUES CORRESPONDING TO POINTS ON THE TRANSDUCER FACE
C THE INTEGRATION IS PERFORMED USING 'QUANC8'
C
C INTEGRATE OVER EACH "WELL BEHAVED" SECTION SEPARATELY
        DO 302 I=1,4
        BNDRY1=BNDRY(I)
        BNDRY2=BNDRY(I+1)
        IF(BNDRY1.EQ.BNDRY2) GOTO 302
        CALL QUANC8(FCT,P)
        SUM=SUM+P
        ESTERR=ESTERR+ERREST
C HANDLE ERROR CONDITION
        IF(FLAG.NE.0.0) WRITE(4,202) NRING,Z,X,T,IT,FLAG
202     FORMAT(' ALERT: NRING:'G14.6
     ?/'            Z:'G14.6
     ?/'            X:'G14.6
     ?/'            T:'G14.6
     ?/'           IT:'G14.6
     ?/'         FLAG:'G14.6)
302     CONTINUE
        IF(ABS(ESTERR).GT.ABS(ERROR)) ERROR=ESTERR
C
C DATA STORAGE
C ------------
C
C
     DATA PROCESSING:

     THE PULSES FROM EACH RING, AT THE FIELD POINTS SPECIFIED BY THE
USER, ARE STORED SEPARATELY ON DISK FOR LATER COMBINATION AND PROCESSING
BY PASS 2 (SECTION 2.6.2.2).  PASS 2, IS LOADED WITH SUITABLE SUB-
ROUTINES FOR APPLYING PROCESSING OF THE PULSES BEFORE OR AFTER SUMMATION.
THE DESIRED USER DEFINED DELAYS ARE ALSO INCORPORATED.  MOST OF THE
PROGRAM IS SYSTEM DEPENDENT AND IS CONCERNED WITH THE CORRECT TRANSFER
OF DATA BETWEEN DATA FILES.  FOR THIS REASON IT IS NOT ILLUSTRATED.
     DATA DISPLAY IS PERFORMED BY PASS 3 AND IS DISCUSSED AND ILLUSTRATED
IN SECTION 2.6.2.3.
```

A1.2 FUNCTION DEFINING THE INTEGRAND OF EQUATION 2.1

THIS FUNCTION IS SPECIFIED TO QUANC8 AND USED BY IT.

LISTING:

```
C SUBRTN FCT      V1AA   DWP   19-JUN-81
C FILE BMFCT1.FT
C
C INTEGRAND FUNCTION FOR BM1 V2
C
CCCCCCCCCCCCCCCCCCCCCCCCCCCCCCCCCCCCCCCCCCCCCCCCCCCCCCCCCCCCCCCCCCCCCCCC
C
        FUNCTION FCT(ETA)
C
        COMMON /     / RCRD(85)
        COMMON /P101/ COMENT(26),IOPT,SHAPE(170),TAUP
        COMMON /CFCT/ R11,RMAX1,R12,RMAX2,T
        COMMON /RESTRT/ CN,DFREQ,HEAD(8),IDAY,IMNTH,INDEX8,IYEAR,
     ?NBLOCK,NRING,NSTART,PI,PI2,SFREQ
C
        DIMENSION A(2,10)
        EQUIVALENCE (RCRD(11),A(1,1)),(RCRD(50),Z),(RCRD(57),X)
C
C FCT=THETA*DVN/(2*PI)
C 'R' IS THE DISTANCE FROM THE FIELD POINT TO THE POINT ON THE
C XTAL FACE DEFINED BY THIS 'ETA'
        R=CN*(T-ETA)
C
C TREAT ANNULUS AS TWO CONCENTRIC DISCS TO FIND 'THETA'
C EVALUATE 'THETA2'
C TEST IF X > OR < A
        IF(X.GE.A(2,NRING)) GOTO 91
C TEST IF PART/WHOLE OF THE PULSE IS ON THE XTAL FACE AS SEEN
C FROM THE SOUND FIELD POINT
        THETA2=PI2
        IF(R.LE.R12.OR.X.EQ.0.0) GOTO 92
        D=R*R-Z*Z
        ARG=(D+X*X-A(2,NRING)*A(2,NRING))/(2.0*X*SQRT(D))
        IF(ABS(ARG).GT.1.0) ARG=AINT(ARG)
        THETA2=2.0*ACOS(ARG)
        GOTO 92
C
91      D=R*R-Z*Z
        IF(D.EQ.0.0) D=.001*X*X
        ARG=(D+X*X-A(2,NRING)*A(2,NRING))/(2.0*X*SQRT(D))
        IF(ABS(ARG).GT.1.0) ARG=AINT(ARG)
        THETA2=2.0*ACOS(ARG)
C
C EVALUATE 'THETA1'
92      THETA1=0.0
C TEST IF X > OR < A
        IF(X.GE.A(1,NRING)) GOTO 911
C CHECK THIS POINT IS ON THE XTAL FACE
        IF(R.GE.RMAX1) GOTO 912
C TEST IF PART/WHOLE OF THE PULSE IS ON THE XTAL FACE AS SEEN
C FROM THE SOUND FIELD POINT
        THETA1=PI2
        IF(R.LE.R11.OR.X.EQ.0.0) GOTO 912
        D=R*R-Z*Z
        ARG=(D+X*X-A(1,NRING)*A(1,NRING))/(2.0*X*SQRT(D))
        IF(ABS(ARG).GT.1.0) ARG=AINT(ARG)
        THETA1=2.0*ACOS(ARG)
        GOTO 912
C
C CHECK THIS POINT IS ON THE XTAL FACE
911     IF(R.GE.RMAX1.OR.R.LT.R11) GOTO 912
        D=R*R-Z*Z
        IF(D.EQ.0.0) D=.001*X*X
        ARG=(D+X*X-A(1,NRING)*A(1,NRING))/(2.0*X*SQRT(D))
        IF(ABS(ARG).GT.1.0) ARG=AINT(ARG)
        THETA1=2.0*ACOS(ARG)
C
C COMPUTE 'FCT'
912     THETA=THETA2-THETA1
C EXCITATION VELOCITY FUNCTION FOR 0<ETA<TAUP
C A: RECTANGULAR ENVELOPE
C     DVN/DT=A0*SIN(2*PI*ETA)
        DVN=SIN(2.*PI*ETA)
C B: HALF CYCLE SINUSOIDAL ENVELOPE
C     DVN/DT=A0*SIN(PI*ETA/TAUP)*SIN(2*PI*ETA)
C       DVN=-.5*(COS(SFREQ*ETA)-COS(DFREQ*ETA))
        FCT=THETA*DVN/PI2
        RETURN
        END
```

A1.3 SOLUTION FOR A MONOCHROMATIC (CW) RADIATION FOR AN ARRAY OF INFINITESIMALLY NARROW RINGS

THE ALGORITHM PRESENTED BELOW IS A NUMERICAL SOLUTION OF EQUATION 2.7 (SECTION 2.4.2). THE ZERO'TH ORDER BESSEL FUNCTION IS COMPUTED BY A STANDARD LIBRARY ROUTINE.

SYMBOLS:

J0(.) - ZERO'TH ORDER BESSEL FUNCTION
A(I) -I'TH RING RADIUS
W(I) - WIEGHTING FUNCTION FOR I'TH RING
ALPHA - FUNCTION POSSIBLY APPLIED ELECTRONICALLY
ALAMBD - WAVELENGTH

LISTING:

```
C
C
      C=1540.0
      FREQ=3.5
      X1=0.0
      X2=39.0
      DX=0.2
      Z1=100.0
      Z2=100.0
      DZ=0.0
      APSIZ=11.5
C
C NORMALISE TO UNIT FREQUENCY:
C N.B. INTERNAL TO THE PROGRAM, UNITS ARE AS FOLLOWS-
C TIME -CARRIER FREQ.PERIODS
C SPACE-WAVELENGTHS
C HENCE INTERNALLY, FREQ=1. & TAU=1. AND THESE VARIABLES
C DO NOT APPEAR EXPLICITLY IN EXPRESSIONS.
C ALL DATA INPUT & OUTPUT IS IN UNITS OF MM, MHZ, M/SEC, MICRO SEC
C
      CN=C/(1000.0*FREQ)
C WHERE 'CN' IS NORMALISED VELOCITY (GIVES WAVELENGTH = CN)
C
C SET CONSTANTS
      PI=3.1415927
      Z=Z1
      IZ=1
      ALAMBD=CN
      AK=2.*PI/(ALAMBD*Z)
C
C COMPUTE RING RADII (A),WEIGHTS (W) & ELECTRONIC GAIN/ATTENUATION
C FUNCTION (ALPHA), AND THE COEFF (GAMMA)
C
      DO 311 I=1,NR
      A(I)=((FLOAT(I)/FLOAT(NR))**BETA)*APSIZ
      W(I)=A(I)/APSIZ*(-DELTA*A(I)/APSIZ+1.0)
311   CONTINUE
C
C SCAN 'X' :PRESSURE AS A FUNCTION OF X
C
C SCAN EACH XSECTION
      IX=0
20    IX=IX+1
      X=X1+FLOAT(IX-1)*DX
C
C SYNTHESISE FOCAL PLANE RESPONSE OF ARRAY
C
      N=0
      D=.0001
      ABSERR=.0001
      ERREST=0.0
      REAL=0.0
      IMAG=0.0
      AMP=0.0
      CALL CPUOUT
C
      DO 300 NRING=1,NR
C
C COMPUTE J0(ARG)
C
      ARG=AK*A(NRING)*X
      CALL BESJA(ARG,N,BJ,D,ABSERR,AERROR)
C THE COMPUTED VALUE OF J0(ARG) IS BJ
C THE ABSOLUTE UNCERTAINTY IS AERROR
C
      COEFFJ=W(NRING)
      AMP   =AMP+COEFFJ*BJ
      ERREST=ERREST+COEFFJ*AERROR
300   CONTINUE
C
      CALL CPUIN
      DATA(IX)=AMP
      ERR(IX) =ERREST
      IF(X.LE.X2) GOTO 20
C FINISHED THIS XSECTION
```

```
C
C FIND MAX AND MIN PRESSURES
50      PMINX=1000.
        PMAXX=0.0
        DO 301 I=1,IX
        IF(ABS(DATA(I)).LT.ABS(PMINX)) PMINX=ABS(DATA(I))
        IF(ABS(DATA(I)).GT.ABS(PMAXX)) PMAXX=ABS(DATA(I))
301     CONTINUE
        PMINZ=PMINX
        PMAXZ=PMAXX
C
C DATA STORAGE
C ------------
C
C
```

DATA PROCESSING:

THE PROGRAM PERFORMS REPEAT SOLUTIONS FOR CHANGING VALUES OF A(I), W(I), OR ALPHA AS DEFINED IN THE APPROPRIATE LOOP WITTHIN IT. EACH SOLUTION (WHICH IS A CROSS-SECTION OF THE ARRAY RESPONSE AT A PARTICULAR DEPTH) IS STORED SEPARATELY AND THEN INPUT TO PASS 3 FOR DISPLAY.

ACKNOWLEDGEMENTS

This work was carried out in the Department of Medical Physics and Medical Engineering, University of Edinburgh, under the supervision of Dr. W. N. McDicken. I am most grateful to Dr. McDicken for many valuable discussions and for his guidance and encouragement at all stages of the project, and to Professor J. R. Greening for inviting me to work in his Department. The receipt of a University of Edinburgh Medical Faculty Scholarship is gratefully acknowledged.

I should like to thank Mr. R. McHugh for his detailed design and commissioning of the electronic unit I have described and Mr. M. Slessor for much of its construction. Their help was invaluable. I acknowledge the help of Mr. M. Connel and Dr. K. Boardman who provided advice on computing, and Mr. R. Borthwick and Mr. G. Campbell of the Department's mechanical workshop who produced many items which contributed to the success of the project.

I am grateful to Mr. Connel and to all the members of the Ultrasonics Group, particularly Mr. J. Nicoll, for their interest and advice throughout the project. I am indebted to the staff of the Inter-Library Loans Section of the University Medical Library for their patience and efficiency in obtaining for me many papers and journals.

I should like to thank the staff of the Western General Hospital Medical Illustrations Department for reproducing the photographic material presented. I am very grateful to Mrs. L. Rustage for her careful and efficient typing of the final copy of the thesis.

Its preparation and completion is a testimony to my wife Frances' sympathy and support which I greatly appreciate. I am also grateful to her for typing the first draft copy of this text and for help with the illustrations.

My parents and brothers have given me every help and encouragement possible during the project and preparation of this text, and I am very grateful to them.

Lastly, I should like to thank Leslie, Margaret, Elaine, Val, Caroline, and particularly Ian, Christine and Lindsey, who have been my flatmates in various flats during my stay in Edinburgh, for their patience, interest and encouragement.

DECLARATION

I, the undersigned, declare that the work described in this thesis has been carried out by myself and that the thesis has been composed by myself.

(DAVID W. PYE).